Delft University of Technology

Model-based process development for biopharmaceuticals

Pirrung, Silvia

Important note
To cite this publication, please use the final published version (if applicable).
Please check the document version above.

Model-based process development for biopharmaceuticals

Dissertation

for the purpose of obtaining the degree of doctor
at Delft University of Technology
by the authority of the Rector Magnificus prof.dr.ir. T.H.J.J. van der Hagen
chair of the Board for Doctorates
to be defended publicly on
Thursday 25 October 2018 at 10:00 o'clock

by

Silvia Maria PIRRUNG

Master of Science in Industrial Biotechnology, Technical University of Munich, Germany
born in Karlsruhe, Germany

This dissertation has been approved by the promotors.

Composition of the doctoral committee:

Rector Magnificus	chairperson
Prof.dr.ir. L.A.M. van der Wielen	Delft University of Technology, promotor
Dr.ir. M. Ottens	Delft University of Technology, promotor

Independent members:

Prof.dr. J.J. Hubbuch	Karlsruhe Institute of Technology, Germany
Prof.dr. M.H.M. Eppink	Wageningen University
Prof.dr. H.J. Noorman	Delft University of Technology
Prof.dr. W.R. Hagen	Delft University of Technology
Dr. A. Azevedo	Instituto Superior Tecnico, Portugal

Table of Contents

S

Summary & Samenvatting

For a research worker the unforgotten moments of his life are those rare ones which come after years of plodding work, when the veil over natures secret seems suddenly to lift and when what was dark and chaotic appears in a clear and beautiful light and pattern.

Gerty Cori

Contents

S

S.1. Summary

Biopharmaceuticals form a growing share of the global pharmaceutical market. Many new types of biopharmaceuticals are being developed and, thus, need to be produced efficiently. This thesis aims at developing an *in-silico* process development toolbox, which can improve current process development strategies greatly. Here, the focus is set on downstream processing, which is the removal of contaminants from the product.

Chapter 2, thus, gives an overview on the state-of-the-art of process development approaches for biopharmaceuticals. Here it is shown that the biopharmaceutical industry is changing from traditional process development towards high throughput process development. Novel experimental techniques are applied that improve process understanding while using only the small amount of sample available during an early development stage. This increased understanding can also be gained by the use of mechanistic models, which, once calibrated, can efficiently explore the process design space without needing sample material. However, to calibrate these models for accurately predicting a specific case, crucial parameters are needed that describe the adsorption of the product and relevant impurities towards the resins. These parameters can e.g. be determined by high-throughput experimental techniques. The combination of mechanistic modelling and high-throughput experimental techniques is also called hybrid process development.

Mechanistic models are well suited for the optimization of single chromatographic columns regarding their operating conditions including variations in protein load. However, once sequences of columns are to be optimized, speed becomes limiting. Therefore, a new approach is developed that combines fast artificial neural networks in a global optimization with detailed mechanistic models in a local optimization (**Chapter 3**). A simple scheme of the approach as applied here is shown on the right side in Figure 1. These artificial neural networks are trained with data predicted by calibrated mechanistic models. It is shown that these networks can predict chromatographic behaviour inside a trust area reasonably well. However, inaccuracies in their predictions will always occur regardless of the amount of training data. Therefore, they are used in combination with accurate mechanistic models to increase the chance of finding the optimal chromatographic process. Artificial neural networks are used to

assess the purity and yield at certain operating conditions during a preliminary global optimization. The results are used as starting points for a subsequent local optimization, where the mechanistic models are called instead. In this way, the optimization speed can be improved by 70 % compared to an optimization, where only mechanistic models are used.

Chapter 3 uses previously published model input parameters. A new purification problem is the basis of **Chapter 4 and 5**. Here, a monoclonal antibody is to be separated from clarified cell harvest raising the need to determine crucial model input parameters, e.g. adsorption parameters, from a complex mixture.

Previously, a 3D-liquid chromatography method was developed to determine such adsorption parameters with a low standard error using small sample volumes on miniaturized chromatography columns [1]. This method is further extended in this study (**Chapter 4**). A scheme of the three dimensions applied is shown on the left hand side of Figure 1. In this approach, each dimension of liquid chromatography can be based on different separation modes. The first separation dimension is a pH gradient chromatofocusing fractionation step on an ion exchange resin. This step is mainly used to reduce the complexity of the sample, but also to perform a precharacterization based on charge. Fractions created here are carried over to the next separation dimension, which is performed with the resin of interest. Hence, the separation here is based on the mode of separation of the resin of interest, for instance hydrophobicity for a hydrophobic interaction resin. This second dimension is transferred to a robotic liquid handling system to achieve higher parallelization and, thus, faster parameter determination. This is enabled by performing isocratic experiments on RoboColumns® at eight salt concentrations collecting the eluent in 96 well plates. With that and size information from the third dimension, size exclusion chromatography, chromatograms are reconstructed and can be used to determine isotherm parameters in the low protein concentration range by a least-square regression.

Additionally, the approach is extended to obtain parameters describing adsorption at the full range of protein concentrations, at which industrial processes are normally operated. For that, maximal binding capacities of the resin of interest are determined from fractions of the first dimension in batch-uptake experiments in a high throughput format. Moreover, protein-protein interactions are included in the isotherm itself by
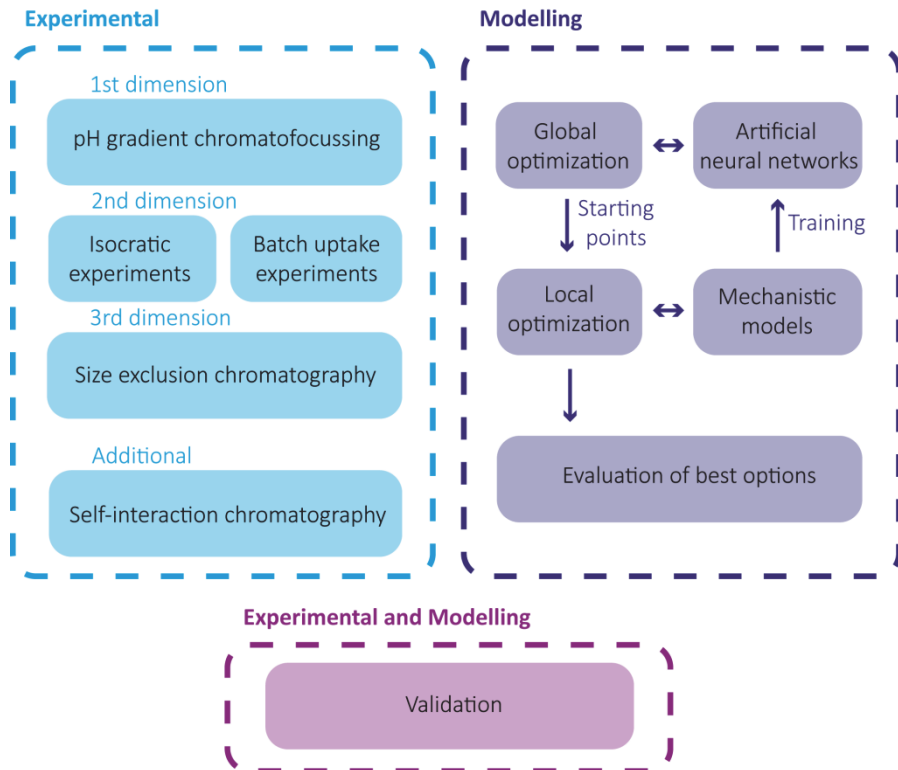
Figure 1: Experimental (left) and modelling (right) methodology including validation (bottom)

using the second virial coefficient, also called the B_{22}. The B_{22} is determined experimentally by self-interaction chromatography. Finally, all determined isotherm parameters are used as input parameters for a mechanistic model. The predictions are validated experimentally showing great agreement between data sets.

Finally, **Chapter 5** applies all parameters determined in **Chapter 4**, together with parameters for an additional resin, in the optimization approach developed in **Chapter 3**. One of the downsides of the approach in **Chapter 3** is that it only includes chromatography units. However, filtration units to e.g. exchange the buffer may actually change the most optimal process. Therefore, a mechanistic model for ultrafiltration/diafiltration steps is developed and needed model parameters such as the sieving curve are experimentally determined. A good agreement is found between predictions of the ultrafiltration/diafiltration process and experimental data. Thus, the ultrafiltration/diafiltration models can be integrated in the process optimization approach. An optimization is then performed, which finds a process option that uses

very little solvent and reaches a high yield of above 95 % while still ensuring a purity of at least 99.9 %.

S.2.   Samenvatting

Biofarmaceutica (waar onder therapeutische eiwitten) vormen een groeiend aandeel in de wereldwijde farmaceutische markt. Veel nieuwe soorten biofarmaceutica worden ontwikkeld en moeten efficiënt worden geproduceerd. Dit proefschrift is gericht op het ontwikkelen van een *in-silico toolbox* voor procesontwikkeling, die de huidige aanpak voor procesontwikkeling aanzienlijk kan verbeteren. De focus ligt op product isolatie en zuivering; het verwijderen van verontreinigingen uit het product.

Hoofdstuk 2 geeft een overzicht van de *state-of-the-art* van procesontwikkeling voor biofarmaceutica. Hierin wordt beschreven dat de biofarmaceutische industrie verandert van een traditionele manier van procesontwikkeling naar *high throughput* procesontwikkeling. Nieuwe experimentele technieken worden toegepast, welke het procesbegrip verbeteren, met minimaal monstervolumegebruik. Dit monstervolume is zeer beperkt beschikbaar tijdens de vroege ontwikkelingsfase van een proces. Een beter begrip van het proces kan ook worden verkregen door het gebruik van mechanistische mathematische modellen. Eenmaal gekalibreerd, kunnen deze modellen de beschikbare procesontwerpruimte efficiënt verkennen zonder gebruik te maken van zeer beperkt beschikbaar monstermateriaal. Voor het kalibreren van deze modellen, die gebruikt kunnen worden voor het nauwkeurig voorspellen van een specifiek geval, zijn echter cruciale parameters nodig. Parameters die de adsorptie van het product en de relevante onzuiverheden aan chromatografische harsen beschrijven. Deze parameters kunnen nu experimenteel bepaald worden door nieuwe *high-throughput* technieken. De combinatie van mechanistische modellering en deze *high-throughput* experimentele technieken wordt nu "hybride procesontwikkeling" genoemd.

Mechanistische modellen zijn uitermate goed geschikt voor de optimalisatie van een enkele chromatografische scheidingskolom met betrekking tot de operatieomstandigheden, inclusief variaties in eiwitbelasting. Wanneer echter sequenties van meerdere scheidingskolommen moeten worden geoptimaliseerd, wordt de simulatiesnelheid een beperkende factor. Daarvoor is een nieuwe aanpak
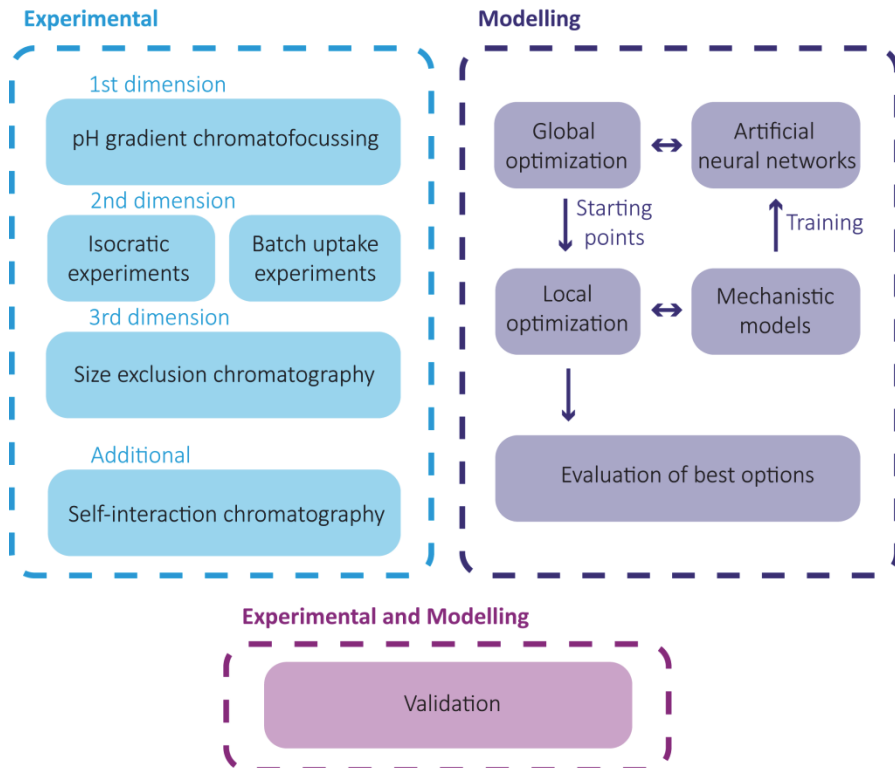
Figure 2: Experimentele (links) en modellering (rechts) benadering met validatie (onderkant)

ontwikkeld die snelle kunstmatige neurale netwerken combineert voor globale optimalisatie met gedetailleerde mechanistische modellen voor een lokale optimalisatie (**Hoofdstuk 3**).

Een eenvoudig schema van de benadering zoals hier toegepast, wordt in figuur 2 rechts weergegeven. De kunstmatige neurale netwerken worden getraind met gegevens die voorspeld zijn door gekalibreerde mechanistische modellen. Er wordt aangetoond dat deze netwerken het chromatografisch gedrag binnen een betrouwbaarheidsgebied redelijk goed kunnen voorspellen. Echter, onnauwkeurigheden in de voorspellingen zullen altijd voorkomen, ongeacht de hoeveelheid trainingsgegevens. Daarom worden ze gebruikt in combinatie met de nauwkeurige mechanistische modellen om de kans op het vinden van het optimale chromatografische proces zoveel mogelijk te vergroten. Kunstmatige neurale netwerken worden gebruikt om de zuiverheid en opbrengst bij bepaalde operatieomstandigheden tijdens een voorlopige globale optimalisatie te berekenen. Deze resultaten werden gebruikt als startpunten voor een latere lokale

optimalisatie, waarbij dan de mechanistische modellen worden gebruikt. Op deze manier kan de snelheid van de optimalisatie met 70% worden verbeterd, in vergelijking met een optimalisatie waarbij alleen mechanistische modellen werden gebruikt.

In **hoofdstuk 3** wordt gebruikgemaakt van eerder gepubliceerde modelparameters. Een nieuw zuiveringsprobleem vormt de basis van **hoofdstuk 4 en 5**. Hier moet een monoklonaal antilichaam worden gescheiden en gezuiverd van een geklaarde cel suspensie. Voor dit systeem dienen ontbrekende cruciale modelparameters, zoals adsorptieparameters van relevante componenten in dit complexe mengsel, te worden bepaald.

Al eerder werd een geminiaturiseerde 3D-vloeistofchromatografiemethode ontwikkeld om dergelijke adsorptieparameters met een lage standaardfout te bepalen, met gebruikmaking van slechts kleine monstervolumes [1]. Deze methode is verder uitgebreid in dit proefschrift (**Hoofdstuk 4**). Een schema van de drie toegepaste scheidingdimensies is weergegeven aan de linkerzijde van figuur 1. In deze benadering kan elke dimensie van vloeistofchromatografie worden gebaseerd op verschillende chromatografische scheidingsmethoden. De eerste scheidingsdimensie is een chromatografische focusseringsstap op een ionenuitwisselingshars. Deze stap wordt gebruikt om de complexiteit van het multicomponent monster te verminderen, maar ook om een voorscheiding uit te voeren op basis van elektrische lading. Fracties hier gemaakt worden getransfereerd naar de volgende scheidingsdimensie, welke wordt uitgevoerd met een ander, van belang zijnde hars. De scheiding is dan gebaseerd op de scheidingwijze behorende bij deze hars, zoals bijvoorbeeld hydrofobiciteit voor een hydrofobe interactiehars. Deze tweede dimensie is nu geïmplementeerd in een robotisch vloeistofhanteringssysteem om een veel hogere parallellisatie en dus snellere parameterbepaling te bewerkstelligen. Dit is uitgevoerd in de vorm van isocratische experimenten op zgn. *RoboColumns*®, bij acht verschillende zoutconcentraties, waarbij het elutievloeistof wordt verzameld in 96 *wells* microtiterplaten. Tezamen met de gegevens over de grootte van de eiwitten, verkregen via de derde scheidingsdimensie (chromatografie op basis van grootte), worden weer chromatogrammen gereconstrueerd. Deze worden dan uiteindelijk gebruikt om de isothermparameters bij lage eiwitconcentraties te bepalen.

Verder is deze nieuwe aanpak uitgebreid met adsorptie parameterbepaling bij hoge eiwitconcentraties, waarbij industriële scheidingprocessen normaal worden uitgevoerd. Daarvoor worden de maximale bindingscapaciteiten van de van belang zijnde hars bepaald uit de fracties van de eerste dimensie in batch-opname experimenten in een *high throughput* formaat. Bovendien worden eiwit-eiwit interacties meegenomen in de mathematische beschrijving van de isotherm zelf, via de zgn. tweede viriaal coëfficiënt, ook wel "B22" genoemd. Deze B22 wordt dan experimenteel bepaald door een speciale vorm van affiniteitschromatografie, nl. "zelfinteractiechromatografie". Ten slotte worden alle isothermparameters gebruikt als invoer voor het ontwikkelde mechanistische model. De uiteindelijk simulaties zijn experimenteel gevalideerd en laten een goede overeenkomst tussen de experimentele- en modelresultaten zien.

Ten slotte worden in **hoofdstuk 5** alle in **hoofdstuk 4** bepaalde parameters toegepast, tezamen met parameters voor een extra hars, in de optimalisatieaanpak ontwikkeld in hoofdstuk 3. Een van de minpunten van de aanpak in hoofdstuk 3 is dat slechts chromatografie wordt beschouwd. Een daadwerkelijk proces bestaat uit meerdere processtappen, bv filtratie. Het meenemen van filtratiestappen voor het aanpassen van buffers in de optimalisatieaanpak, kan een ander optimale proces opleveren. Daarom is een mechanistisch mathematisch model voor ultrafiltratie/diafiltratie ontwikkeld en benodigde modelparameters zijn experimenteel bepaald. Een grote overeenkomst wordt gevonden tussen modelmatige voorspellingen van het ultrafiltratie/diafiltratieproces en de vergaarde experimentele gegevens. De ultrafiltratie/diafiltratiemodellen worden geïntegreerd in de aanpak voor procesoptimalisatie. Als sluitstuk is uiteindelijk een algehele modelmatige procesoptimalisatie uitgevoerd, waarbij een procesoptie is gevonden met minimaal oplosmiddelgebruik en tevens een zeer hoge opbrengst (van meer dan 95%), terwijl toch een zuiverheid van ten minste 99,9% wordt gegarandeerd.

References

1. Hanke AT, Tsintavi E, Ramirez Vazquez MD, et al. 3D-liquid chromatography as a complex mixture characterization tool for knowledge-based downstream process development. *Biotechnol Prog.* 2016;32(5):1283-1291.

1

General Introduction & Thesis Outline

Nothing in life is to be feared, it is only to be understood. Now is the time to understand more, so that we may fear less.

Marie Curie

Contents

1.1. General Introduction

Biopharmaceuticals such as monoclonal antibodies are the main growth drivers in the global pharmaceutical market [1]. Different types of biopharmaceuticals are constantly being developed [2]. With patents for current blockbusters expiring, biosimilars, which are molecules that mimic these blockbusters, are being developed at much lower cost due to decreased research and development costs. Moreover, next-generation biopharmaceuticals are being created, which means that the structure of existing biopharmaceuticals is modified to exhibit e.g. a better half-life or availability. Of course, research effort also goes into finding completely new types of biopharmaceuticals.

Biopharmaceuticals generally need to have a very high purity to prevent unwanted immunological reactions by the patients. Therefore, separating the product from unwanted contaminants can be a great challenge in the production of biopharmaceuticals and, thus, can form the most expensive part of the whole production process; this part is typically called the downstream process. Having cheaper and more efficient downstream processes available would have a large impact on the overall production costs and consequently lead to cheaper pharmaceuticals on the market. Therefore, this thesis focusses on finding better ways to develop downstream processes.
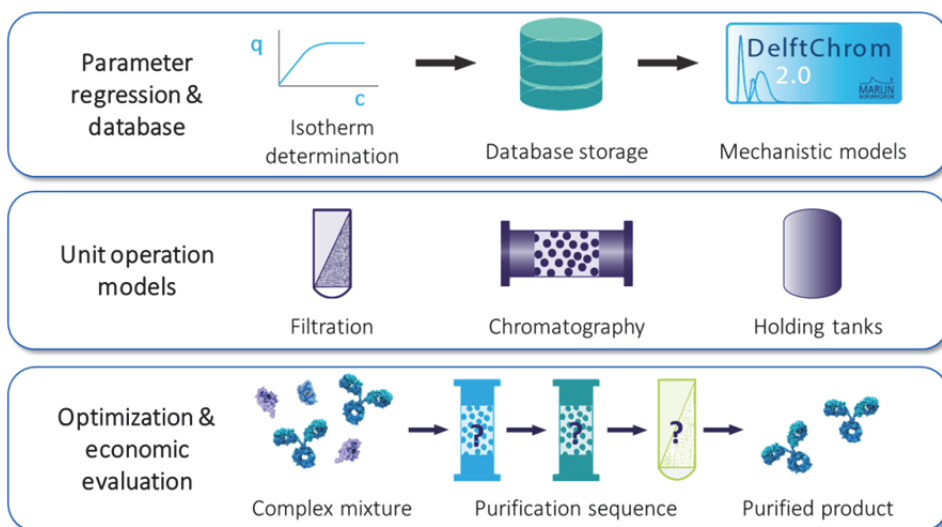

Figure 1: Schematic representation of the *in-silico* process development toolbox
The toolbox consists of three distinct parts, which are described in more detail in the main text below.

The development of such a downstream process is very complex; many possible choices can be made that influence not only the purity but also the costs of the process. For instance, different type of purification units can be used that are based on different separation basics such as hydrophobicity or charge. Additionally, these units can be arranged in different orders. Also the operating conditions applied to each unit have a great influence on the outcome and, therefore, need to be adjusted individually.

Thus, the aim of this thesis is the development of an *in-silico* process development toolbox, which allows to find efficient downstream processes for new biopharmaceutical products quickly. This toolbox is set up of three parts as depicted in Figure 1: The underlying approach is built on the use of mechanistic models, which are based on fundamental or first principles and aim to predict what would happen in the respective purification unit.

First, relevant model input parameters need to be determined. These parameters characterize the purification method. One of the methods applied most is chromatography, which is a column filled with a functionalized resin. Depending on the specific functionalization, the resin can e.g. selectively bind specific components. By subsequent elution, components can be separated from each other. Here for instance, isotherm parameters, which describe the interaction between a chromatographic resin and the product as well as the contaminants during adsorption and elution, are needed at different operating conditions for detailed modelling of the unit. Additionally, characteristics of the resin such as for instance the pore diameter and porosity need to be known.

Once these parameters are determined, they can be used as input parameters in the corresponding mechanistic models. For that, the models need to be developed and implemented first. Moreover, they should be properly validated to guarantee a sufficient predictive ability in the range of interest.

Finally, these models are to be employed in an optimization approach, which is supposed to find the 'best' process based on defined performance metrics. To accomplish that, purification sequences need to be generated by connecting the mechanistic models for each specific unit. Next, the optimization problem needs to be defined, which includes the optimization variables for each unit as well as the objectives and constraints. In biopurification processes, the overall yield is typically

included here due to the high value of the products. Furthermore, purity and cost are important to consider as explained before.

1.2.   Thesis Outline

The state-of-the-art on downstream process development approaches existing at the start of this work is given in **Chapter 2**. After an overview of all possible approaches, it concentrates on one of the newest approaches, the so called hybrid approach. This approach combines detailed mechanistic modelling, which is based on first principles, and high throughput experimental techniques, which allow a fast and automated way to determine input parameters for mechanistic models. Additionally, it shows several cases where this type of approach was applied previously to optimize single downstream processing units as well as several units in sequence.

Chapter 3 then details a novel optimization approach built on the concepts of the previously outlined hybrid approach. The optimization is taken one step further by optimizing connected sequences of different downstream processing units, in this case chromatographic units, simultaneously. Since computational speed can become limiting, when performing such complex optimizations, fast artificial neural networks are evaluated as surrogate for the detailed mechanistic models during the optimization.

In **Chapter 3**, previously published model input parameters are used. **Chapter 4 and 5** now aim to tackle a new purification problem for the purification of a monoclonal antibody from clarified cell harvest.

Chapter 4, thus, introduces an extensive approach to determine such model input parameters reliably using high-throughput experimental techniques. The study combines multiple experimental techniques such as high-throughput isocratic experiments with RoboColumns, batch-uptake experiments and self-interaction chromatography. The validity of the approach is then evaluated by comparing experimental lab scale data with mechanistic model predictions using the determined input parameters.

Chapter 5 then combines the knowledge obtained in both previous chapters; it aims to apply the optimization approach of **Chapter 3** to the crude mixture characterized in **Chapter 4**. Additionally, ultrafiltration/diafiltration units, which perform a size-based

separation, are added to e.g. adjust buffer conditions. Disregarding them might lead to a suboptimal process.

Finally, the overall work is summarized and an outlook is given in **Chapter 6**.

References

1. Schmidt M, Patel S, Veiby P, Liu Q, Buckley M. Forty Years of Innovation in Biopharmaceuticals–Will the Next 40 Years Be as Revolutionary? *Value Creation in the Pharmaceutical Industry: The Critical Path to Innovation.* 2016:244-275.

2. Moorkens E, Meuwissen N, Huys I, Declerck P, Vulto AG, Simoens S. The Market of Biopharmaceutical Medicines: A Snapshot of a Diverse Industrial Landscape. *Frontiers in Pharmacology.* 2017;8(314).

2

High Throughput Process Development

State of the Art

Contents

2.1. Introduction to High Throughput Process Development

The increasingly large quantities, in which some of the industrial proteins are needed, together with advances in for instance molecular engineering lead to higher titers produced during upstream processing. As a result, the bottleneck in bio pharmaceutical protein production is being shifted towards downstream processing. In order to purify this increased amount of product, larger facilities are needed which implies higher investment and operating costs due to an increased consumption of buffers and other consumables [1]. Another challenge for the development of purification processes resulting from the optimization towards high titers in upstream processing is a modification of the broth composition regarding type and concentration of impurities [2].

Furthermore, the regulatory initiative quality by design (QbD) asks for a systematic and efficient approach during process development to explore the design space, which is defined by QbD as the permissible range of operating conditions assuring product quality, on the basis of critical process parameters (CPP), key process parameters (KPP) and critical quality attributes (CQA) as can be seen in Figure 1. An extensive description of QbD principles and how they can be applied to biopharmaceuticals can be found elsewhere [3]. In order to do so, a comprehensive knowledge about the underlying mechanisms would be beneficial.

As a result, simple trial and error approaches cannot be applied anymore which forces
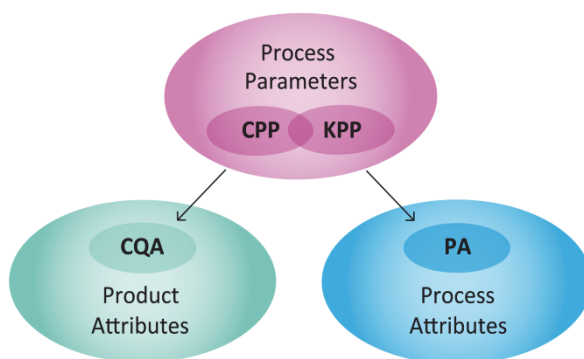
Figure 1: Scheme showing the relationship between different QbD parameters

Here, CQA that define the needed product quality are identified, an example could for instance be viral clearance or product aggregation. Subsequently, process parameters, CPP, whose variation could have an effect on these CQA leading to a high risk of falling outside the design space, are determined. Additionally, other process parameters, KPP, that are not influencing the CQA but do influence the process attributes, PA which is for instance yield, have to be determined as well for a full description of the QbD design space.

the biopharmaceutical industry to look into new strategies for improving purification processes. One of these strategies that is being used more and more during the last 10 years is high throughput process development (HTPD) [4]. These techniques can be seen as combinations of high throughput experimentation (HTE), which is characterized by miniaturization, automation and parallelization, and mechanistic modelling of the chromatographic separations.

In a recent survey regarding process development in bio manufacturing, most respondents thought that the most important prerequisite for an easier process development is having a *sufficient understanding of performance driving parameters* and *having applicable scale down models available* [5]. This clearly shows that the industry is aware of the need for high throughput techniques in process development and is adopting this in their practices as showcased for instance in the academic-industrial conference series on HTPD [6].

The efforts here are mainly focused on chromatographic purification steps, since these are still the most important steps during bio purification [7] which can be underlined by the fact, that downstream processes in large-scale bio manufacturing use an average of three chromatographic steps [5]. Optimization via HTPD can be done on different aspects of the chromatography unit. The optimal resin out of the huge amount available in the market today differing from each other in particle size, ligand type and pressure flow characteristics among others has to be found while ensuring suitability for scale-up and reusability. Another aspect to be optimized is the binding of the protein to the resin where often design of experiment (DoE) approaches are used to find buffer conditions that allow optimal binding. Finding the optimal elution conditions is another important aspect considered during optimization of a chromatographic step. Finally, the robustness of the process has to be good enough for manufacturing [8].

2.2. Process Development Approaches

The process design space in chromatographic operations is rather big, choices between a vast number of media, operating conditions, chromatography modes and their order have to be made. The optimum in this design space where the cost is at its minimum has to be found by still satisfying all constraints such as purity, quality, yield etc. This challenging task has been tackled with many different approaches which are described

below [9]. Which part of the design space some of these approaches can cover is visualized in Figure 2. However, one has to keep in mind that the more process design space is to be covered, the more information and resources are needed for developing a bio purification process.

2.2.1. Trial and Error Approach

In traditional purification development, due to heavy feed material demands only a few column experiments can be used to investigate different operating parameters in the process design space which results in a process with technically and economically sub optimal conditions [10].

One Factor at a Time (OFAT)

One method often used in trial and error approaches, is the OFAT. Like the name implies, the OFAT method just changes one factor at a time while other factors are kept constant and thereafter, draws conclusion from the resulting effects. This method can lead to a suboptimal solution since dependencies between variables are being neglected as can be seen in Figure 3. Additionally, it is a material consuming and time intensive method since many experiments have to be performed to investigate several
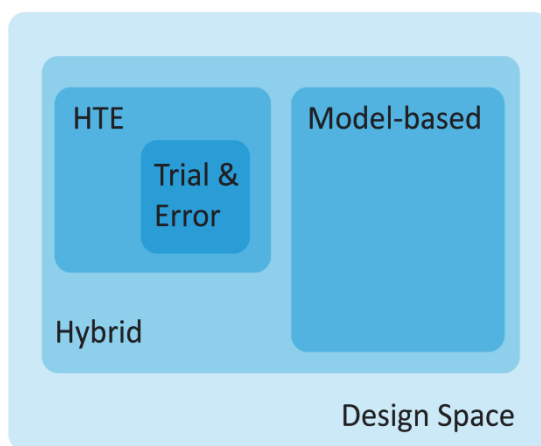
Figure 2: Coverage of the process design space by different approaches

Using the trial and error approach, just a small part of the process design space can be explored due to the inefficient nature and the high consumption of resources during this approach. HTE allows the investigation of a bigger part of the design space while utilizing the same amount of resources due to its miniaturized experiments. Having a trustworthy mechanistic model available, enables investigation of the design space by mere *in silico* simulation and, thus, eliminates the limitation due to resources. Combining mechanistic models with HTE techniques, the so-called hybrid approach, makes it possible to tailor your model to your experimental system and, hence, to cover an even bigger part of the design space.

factors.

DoE

A more efficient method is DoE since different factors are considered simultaneously as shown in Figure 3. Therefore, less resources are needed to explore a bigger part of the process design space compared to OFAT.

Additionally, results obtained are more accurate since more observations are being made to describe one effect [11]. How multivariate techniques can be applied to chromatographic separations is extensively described in a review [12].
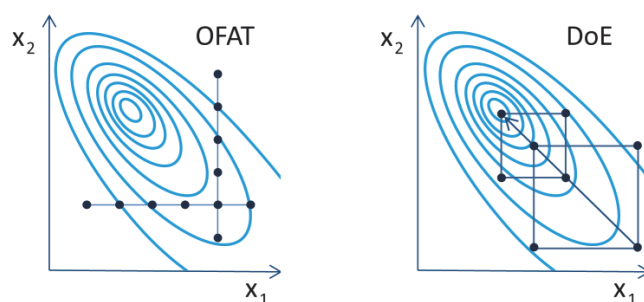
Figure 3: Comparison of OFAT and DoE

In the OFAT approach, one variable (x1 or x2) is changed at a time which neglects all interactions between these variables and can thus lead to a suboptimal point. In the DoE approach on the other hand, x1 and x2 are varied simultaneously which allows to capture dependencies between the two and hence enables finding the direction of the true optimum. Based on [13].

2.2.2.   Expert Knowledge-Based Process Development

Asenjo et al use an approach to select a purification step in a rational manner. Their approach relies on the application of expert knowledge based on large scale production in a system which contains hundreds of different logical rules and methods. These rules are supposed to imitate an expert's reasoning. This system then uses data of the main contaminant proteins out of databases. In this way, the whole sequence of downstream process operations can be selected [14-16]. The disadvantage in this approach is that data about each protein contaminant has to be available in one of the databases used. Subsequently, they used different models to simulate the chromatographic unit operations and, thus, further optimize their entire process [17,18].

2.2.3. High Throughput Experimentation

In the beginning of developing a protein purification process, there is usually little information available about the proteins and the contaminants inside the crude protein mixture, hence, finding the optimal conditions for a process requires many experiments for instance in order to characterize the mixture or to screen for suitable chromatographic media. To accelerate this time-consuming process, high throughput techniques are being commonly applied for their high level of miniaturization, automation and parallelization.

Therefore, the main advantage of using this kind of system is that it allows a fast investigation of many chromatographic conditions while just using a small amount of material. By additionally taking into account accurate mass transfer and kinetic models, the column performance can be quantitatively foreseen [19]. As a net result, the time for having a functioning process is shortened and other issues concerning the process can be addressed. Another advantage is that, if a product fails during late clinical trials, at that moment, comparably less money has been spent as would have been spent in a traditional process development approach [10]. A review on different formats used in HTE such as miniature columns or 96 well plates and their applications can be found elsewhere [20].

In a purely experimental approach, optimization is usually achieved by DoE and subsequent empirical modelling by response surface analysis. This has been shown to be significantly inferior to an approach based on mechanistic modelling [21]. Additionally, using just high throughput experimentation during process development does not guarantee that the optimal process is being selected in the end [9]. However, HTE can perfectly be used in industrial process development as a screening tool prior to further optimizing to assess the operating space as shown for instance in research at Biogen Idec and Merck [22,23]. Furthermore, isotherm and kinetic parameters can be determined in a fully automated manner [24]. A reported downside of HTE is that in some applications just solutions of pure proteins can be applied to generate an accurate result. Additionally the small working volume may limit further analytics [25]. Often the analytics used themselves are low throughput techniques. Thus, analytics may become the bottleneck in HTE. A strategy that addresses this issue has been proposed [26]. An example for a detailed protocol on how to build an HTPD platform can be found in [8].

2.2.4. Model-based Approaches

Models can be used to aid process development especially by reducing the time and material consumption involved. Instead of real experiments different conditions can be tested by mere *in silico* simulation and thus, a much wider range of operating conditions can be investigated. Another advantage is that mechanistic models are built on fundamental understanding of the process which has been made necessary to obtain by the QbD initiative.

Current modelling approaches on different aspects - the column, process parameters, the process - are outlined in the following.

Modelling of a Chromatography Column

In the modelling of a chromatography column, there are several levels of complexity [27]. Often one dimensional models such as the equilibrium transport dispersive model are used for their speed in computing and often sufficient ability of predicting chromatograms [28,29]. Another advantage here is that fewer parameters are needed. This model can describe the chromatographic behavior of components in the liquid phase by the following balance based partial differential equation [30]:

$$\frac{\partial c_{p,i}}{\partial t} + F\frac{\partial q_{p,i}}{\partial t} = -v\frac{\partial c_{p,i}}{\partial x} + D_{L,i}\frac{\partial^2 c_{p,i}}{\partial x^2} \tag{1}$$

where $c_{p,i}$ is the protein concentration in the bulk phase, $q_{p,i}$ is the protein concentration in the stationary phase, v is the interstitial velocity of the mobile phase calculated as $v = u/\varepsilon_b$ where u is the superficial velocity and ε_b the bed porosity, and $D_{L,i}$ is the axial dispersion coefficient. F is the phase ratio, defined as $F = (1 - \varepsilon_t)/\varepsilon_t$ in adsorption chromatography and $F = (\varepsilon_t - \varepsilon_b)/\varepsilon_b$ in size exclusion chromatography with the total porosity ε_t. The total porosity is calculated as $\varepsilon_t = \varepsilon_b + (1 - \varepsilon_b)\varepsilon$. Figure 4 clarifies the definitions of different types of porosities and velocities inside a chromatographic column.

In the equilibrium transport dispersive model, the mass transfer can be quantified by the liquid-film linear driving force approximation where a linear concentration profile in the boundary layer, a stagnant film surrounding the particle, can be assumed. Therefore, the external mass transfer can be expressed as:

$$\frac{\partial q_{p,i}}{\partial t} = k_{ov,i}\left(c_{p,i} - c_{p,i}^*\right) \tag{2}$$

Here, $c_{p,i}^*$ is the equilibrium concentration in the liquid phase which can be calculated using an appropriate isotherm description such as for instance the mixed mode isotherm by Nfor et al [30]. The overall mass transfer coefficient $k_{ov,i}$ is defined as the series connection of the mass transfer resistance inside the stagnant film and the mass transfer resistance inside the pore. The effects occurring in a chromatography column as described by the equilibrium transport dispersive model are depicted in Figure 4.
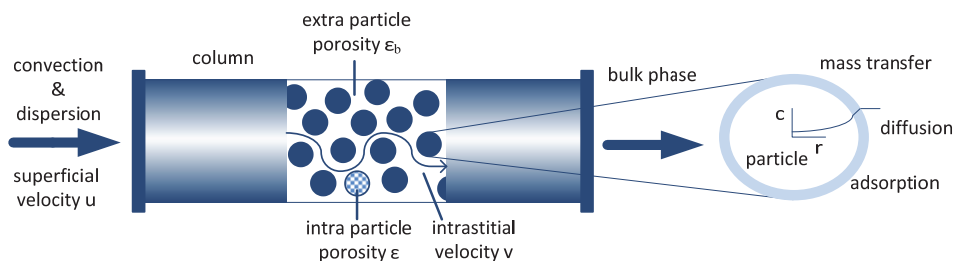
Figure 4: Schematic drawing of the different porosities, velocities and effects inside a column as captured by the equilibrium transport dispersive model including the mass transfer approximated via the liquid-film linear driving force.

Also two dimensional models are being used. The most common one is the general rate model, which shows a high predictability [31-35]. This model is a detailed chromatography model taking radial mass transport inside the particle pores into account. Additionally some attempts have been made to model a chromatographic column in three dimensions, thereby accounting for cross sectional flow conditions and concentration distributions. An issue here is the large amount of beads inside a column (even in case of a micro column), that could not yet be reproduced in the modelling software [36]. A more detailed overview on models used for chromatography modelling can be found in relevant literature [37,38] and elsewhere in the book, where this chapter is published [39].

These chromatographic models can for example be used for model based resin selection [40], or to investigate control strategies and to evaluate the robustness of a process [29,35,41]. Models were also successfully applied for risk analysis of coupled process steps [42]. As well, aggregate removal has been successfully predicted by mechanistic models [43], and model-based single chromatographic unit operation optimization [44], as well as cascaded chromatographic process operation optimization has been realized [45].

Parameter Estimation

While using a mechanistic model to predict column performance, specific process parameters need to be determined beforehand in order to use them as input parameters for modelling. In bioprocesses, this can be an issue due to the ill-defined and complex nature of the cell broth. If the composition of the feed regarding at least the product and the main contaminants are known, some of these process parameters can be approximated by using engineering correlations such as the correlation by Young to determine the free diffusivity of globular proteins [46] or the extended Ogston model for the distribution coefficient in size exclusion chromatography [47]. Of course, parameters predicted by simple engineering correlations are not as accurate as the ones experimentally determined or predicted by a more advanced model but in some cases they can help to predict the column performance sufficiently.

In adsorptive chromatography techniques, it is difficult to predict all the parameters involved describing the binding in between protein and resin. There is quite some scientific effort focused on developing models that can predict these without using any experiments. One fully atomistic approach is to predict the resin-protein colloidal interactions based on the full three dimensional protein structure using molecular dynamics simulations, which is a computationally rather expensive approach for large proteins [48]. Another noteworthy approach is based on quantitative structure-property relationships (QSPR). In this approach, properties of proteins such as pH dependent atomic partial charges, here called descriptors, are calculated using their crystal structures and protein sequence. This allows to model the effect of protein surface properties on protein adsorption and, hence, the prediction of protein retention behavior in chromatographic columns [49-51].

Another promising approach utilizes a protein charge model that enables the simulation of resin-protein interaction while having the amino acid sequence of the proteins available and therefore, the prediction of the retention factor [52]. However, detailed information about the investigated proteins, its amino acid sequence or even crystal structure, has to be known. Therefore, strictly model-based and at the same time accurate process development in adsorption chromatography is just possible while investigating the process for a well-known and defined feed.

Computational prediction of protein ligand interaction is not only of interest in academic research but also in industrial research as shown by the Research Laboratories located at Merck. Their work applied for instance an atomistic modelling approach to the separation of variants of Glargine from the desired insulin for guiding the selection of ligands used in process development [53].

Modelling of a Chromatographic Process

Another area of chromatography modelling research focuses on not optimizing just the chromatographic column but instead on optimizing the whole sequence of chromatographic unit operations. Simple mathematical correlations describing two chromatography modes, ion exchange and hydrophobic interaction, which are based on charge densities and hydrophobicities of the proteins respectively are used to describe retention times in a chromatographic unit operation [54,55]. Based on these, optimization models for different objectives such as purity and cost have been formulated [56,57]. However, since very simple models that are based on triangles instead of actual peak shapes are used to describe the chromatographic behavior it can be questionable how accurate the simulations describe the real process and hence, how optimal the resulting process really is.

2.2.5. Hybrid Methods

A quickly emerging field in process development approaches are hybrid methods, they seem to be more and more recognized in academia and industry. A hybrid method is a combination of the before outlined methods of HTE and detailed mechanistic modelling and therefore, it is combining the advantages of both approaches. One advantage here is for example, that scaling effects can be implemented in the mechanistic model and, thus, ensure scalability of the data obtained in HTE [58].

One concept on how high throughput experimental data can be combined nicely with a model-based approach in order to optimize a single chromatographic step has been presented by Osberghaus et al [59]. First, parameters on column scale such as the porosity and dispersion are being determined experimentally on a high throughput robotic platform. Secondly, parameters on the particle level concerning the adsorption to the resin are estimated [60]. At the same time, the model is being calibrated with experimental results and, thereafter as last step, the model is used to predict conditions for optimal elution experiments. Additionally, upscale predictive ability

could be verified. However, the case study this approach was applied to consisted just of three model proteins and not of a crude unknown protein mixture.

More detailed examples, where the workflow in hybrid approaches is described, can be found below.

Parameter Estimation

A lot of research focusses on parameter estimation as already outlined in the modelling part since feed materials in bioprocessing are complex and ill defined. By using hybrid methods, the parameters can either be acquired via HTE, via modelling or most likely via a combination of both depending on the type of parameter. A popular way of estimating model parameters is the inverse method. Here, the difference between experimentally determined elution profiles and simulated elution profiles is optimized with typically a least square minimization technique. The result are parameters which give the best fit of experimental to simulated data [61]. However, it has to be kept in mind that these parameters bear an uncertainty and that in case the experimental conditions are not accurately determined they can still be erroneous even if they result in a low residual [62].

Additionally, new HTE methods to determine model parameters by adapting mechanistic models to the specific experimental setup utilized in a robot arise as for instance shown by Traylor et al. in case of pore diffusivity [63]. Another nice example for parameter estimation describes how model input parameters for a complex lysate can be obtained via HTE and used for prediction of protein retention behavior can be found by Kroner et al.. However, low throughput analytics still seem to be an issue in this otherwise high throughput approach [64,65]. An overview of possible combinations between process design tools and the required sources for input data can be found in a review by Hanke and Ottens [58].

Process optimization

Similarly to the mere modelling approach, the hybrid approach is also being applied to look at the complete process. However, approaches here are built on very detailed unit operation models which lead to other limitations during modelling such as the high computational cost. Recently, the hybrid approach has been used to simulate and optimize a multiple step chromatographic separation. Such an optimization can either

be done sequentially or simultaneously. Sequentially has the advantage that a large computational problem can be solved as a sequence of several smaller sub problems and thus, the problem becomes more manageable. In a recent approach sequential modelling and optimization of chromatographic unit operations was successfully achieved, using parameters obtained from crude feedstocks, while taking into account the HCPs [45]. This approach is described in detail below during the second example.

A simultaneous hybrid approach has been applied only to a two-step ion exchange chromatographic process using model proteins [66]. Here it was shown that the concerted approach can be superior to the sequential one which is reasonable since in a simultaneous approach possible trade-offs can all be taken into account at the same time which increases the chance of finding the optimal solution. However, in this sort of approach computational costs are highly increased.

2.3. Case descriptions

2.3.1. Optimization of a Single Chromatographic Purification Step

An application of an hybrid approach was shown to work in an industrial case for the separation of whey proteins in order to optimize a chromatographic unit operation [44]. A schematic overview on this approach can be seen in Figure 5.

The first step is to decide on which chromatographic unit operations to investigate for the separation. In this case, the choice was made to focus on ion exchange chromatography (IEX) and hydrophobic interaction chromatography (HIC), but these could be expanded at will. As a next step, the operating window has to be established. Here, the crude mixture, which is in this case a milk serum, has been analyzed by
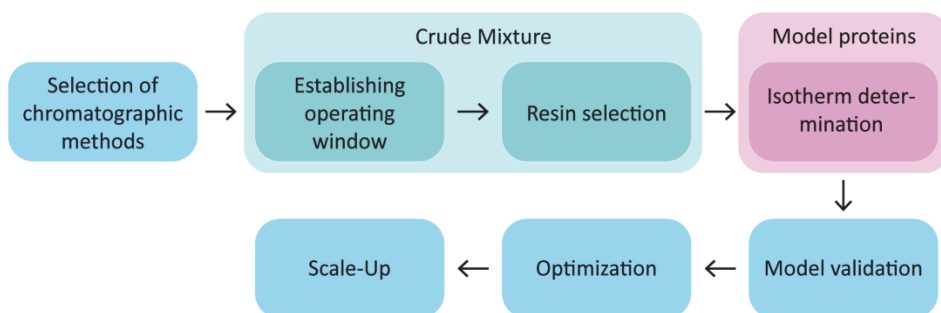

Figure 5: Workflow for applying the hybrid approach to a chromatographic separation

different methods. In order to determine the protein composition of the crude mixture and the elution pH of the target protein, which is known to be a reliable indicator for protein retention, a pH gradient fractionation and subsequent analysis via gel electrophoresis and mass spectrometry was performed [67]. A scheme on this step is presented in Figure 6.

Additionally, protein precipitation behavior was studied to ensure stability of the product during operation. In this case, the precipitation results showed that cation exchange chromatography (CEX) was not a reasonable option for this separation. For further experiments, multiple industrial grade resins for anion exchange (AEX) and hydrophobic interaction chromatography (HIC) were selected and evaluated using high throughput batch uptake experiments based on a strategy considering various performance metrics such as selectivity and resin capacity as described by Nfor et. al [40]. Possible 96 well plate configurations to be carried out during this type of resin screening are shown in Figure 7.
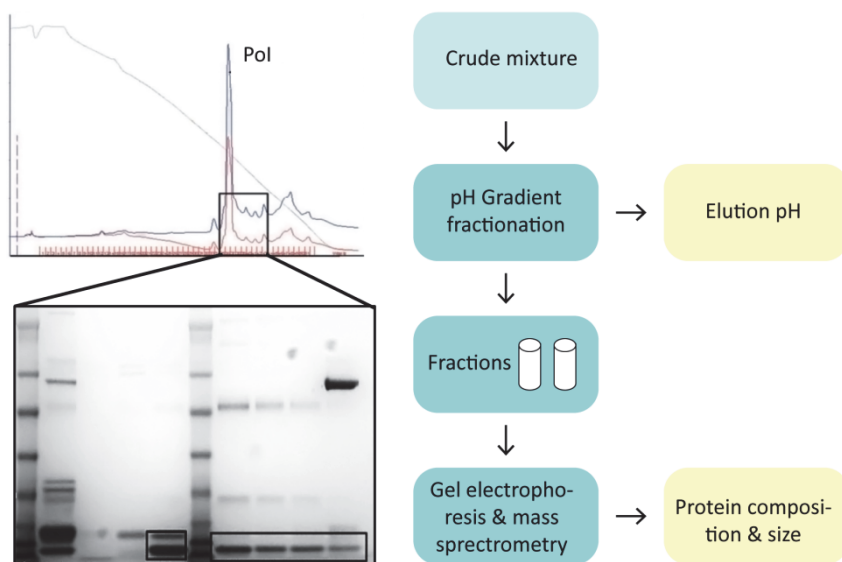

Figure 6: Scheme on the establishment of an operating window allowing pH selection;

Upper part: pH gradient fractionation to determine elution pH of protein of interest (PoI), fractions for gel electrophoresis are marked with a black box; Lower part: Gel electrophoresis of the fractions retrieved from the pH gradient fractionation, PoI marked with a black box. Based on [44].

These remaining and selected resins and operating conditions were then used to determine adsorption isotherms over a wide range of salt, pH and protein concentrations by HTE using pure protein solutions of the main proteins present in the milk serum. Subsequently, these isotherm parameters are used as input parameters for the column model to predict chromatograms. These predictions for AEX and HIC are compared to experimental runs in order to validate the model as can be seen in Figure 8 (A) and (B). After validation, the predictions generated by the model can be assumed to be accurate enough and the model can subsequently be used to optimize the chromatographic step regarding variables such as column loading and cut points of the product pool.

Finally, it could be shown that the optimization produced for lab scale could easily be scaled up to preparatory scale using the chromatography model by keeping the optimized operating variables constant and only changing the column dimensions (Figure 8 (C) and (D)). In both cases, the simulation results showed very similar elution profiles with components eluting at around the same column volume (CV) during gradient elution. Moreover, peak resolution is significantly improved which is expected by using a wider column diameter. Therefore a higher purity and yield of the chromatographic step can be achieved, which shows that column optimization should be done considering larger scale columns to obtain accurate results regarding the highest available column loading and other variables without violating yield and purity constraints. Finally optimal conditions were found via *in-silico* process design of this chromatographic purification using step elution at preparative scale (data not shown).
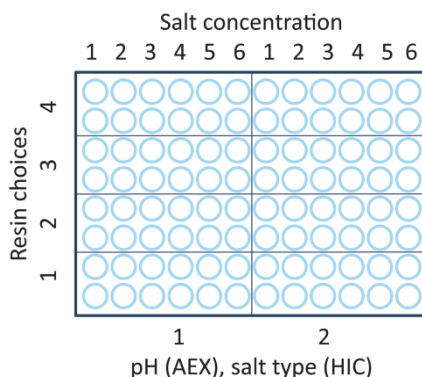

Figure 7: Possible plate configurations for HTE resin screening in batch uptake experiments;

Tested resins, salt concentrations, pH values in case of AEX and salt type in case of HIC are varied.
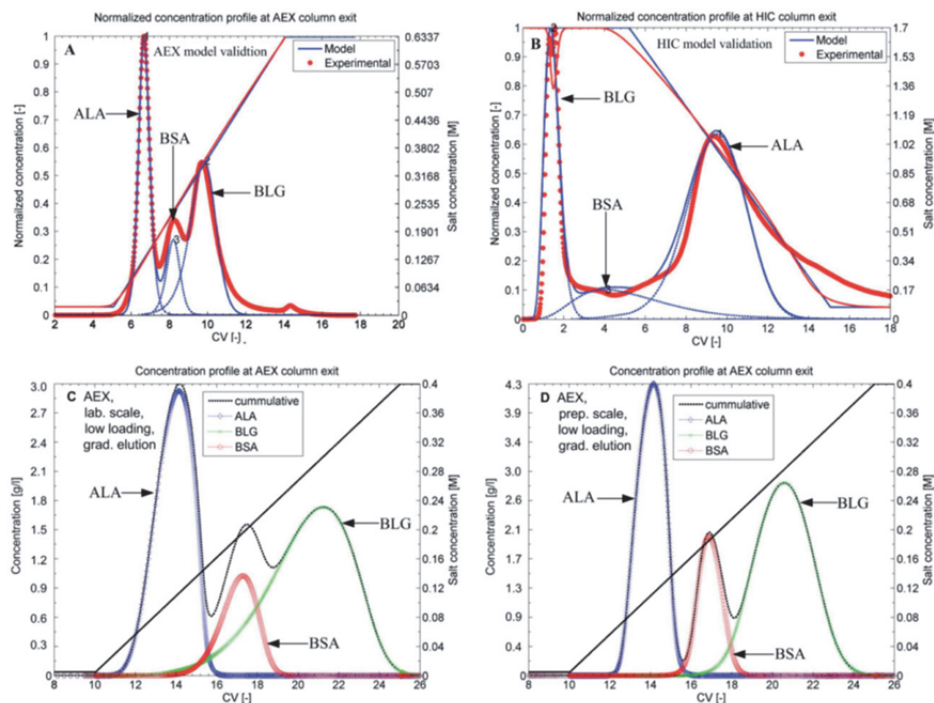
Figure 8: (A) and (B) Column model validation showing overlaid experimental and simulated elution profiles of serum proteins in AEX and HIC. (C) and (D) Optimized column profiles.

(A) and (B) Feed composition-1.5, 3.5 and 0.6 mg/mL of ALA, BLG, and BSA, respectively, ALA: molecular mass (Mw = 14.2 kDa, pI = 4.2-5.1; BLG: Mw = 18.3 kDa; pI = 5.2-5.4; BSA- Mw = 66-69 kDa pI = 4.9-5.1) (C) Lab. scale AEX: column volume = 1.0 mL; pH = 7.5; resin = Capto Q. Optimized conditions: gradient length = 15 CV; linear velocity = 400.7 cm/h, sample load = 5.0 CV (8% binding capacity); lower cut point = 11.7 CV, upper cut point = 15 7 CV (D) Prep, scale AEX (column volume = 35.3 L; column length = 50 cm; internal diameter = 30 cm) in linear gradient elution The pH sample load and all other optimized conditions are the same as in (C). Adapted from [44].

2.3.2. Multiple Column Process Design

A comprehensive example where a hybrid HTPD approach is nicely implemented in order to design and further optimize a downstream process for purification of an antibody without a protein A capture step, considering several chromatographic unit operations and starting from a ***crude*** protein mixture produced by a Hybridoma cell culture, has been published by Ottens and co-workers [45]. The workflow in this approach is presented in Figure 9.

First, the purification task is being defined which means that the CQA, such as host cell protein (HCP) level and product stability, and PA, such as recovery yield, for the case have to be identified. Next, the best resin for each chromatography mode (in this case,
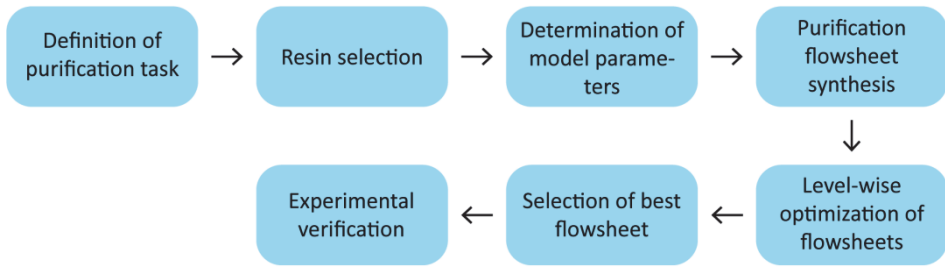
Figure 9: Workflow for applying the hybrid approach to cascaded process optimization

ion exchange, hydrophobic interaction as well as size exclusion chromatography (SEC) have been investigated) according to data and recommendations by the supplier is being selected. After that, the crude protein mixture is being characterized by a multi-dimensional fractionation and characterization scheme by means of different chromatographic fractionation steps in combination with analytical methods such as mass spectrometry as depicted in Figure 10. In this way, crucial model parameters as for instance the physicochemical and thermodynamic properties of the protein product and the main contaminants required for the modelling of several chromatography modes are being determined in a fast and efficient manner [61].
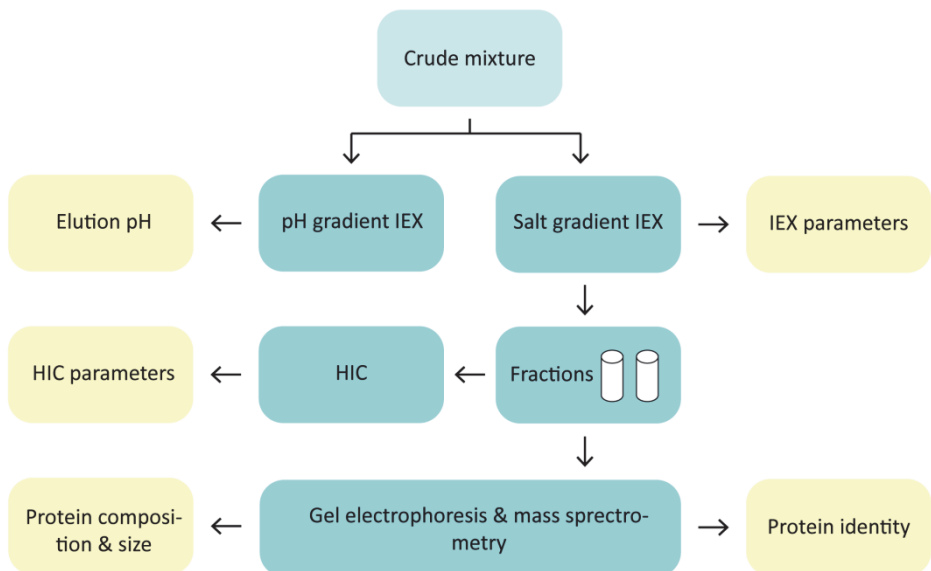
Figure 10: Complex fractionation and characterization scheme to determine important model parameters for crude protein mixtures. Based on [45].

These parameters can then be stored in a database together with the parameters describing the auxiliary materials such as the chromatographic media to enable utilization in future process development. As a next step, validated unit operation models as described in the section on modelling a chromatography column can use these parameters to simulate different process alternatives.

These process alternatives consist of cascaded chromatographic unit operations and can for instance be shown in a tree diagram (Figure 11). For simplification, just a two level graphic has been chosen. The least promising of these alternatives are being discarded based on expert knowledge to simplify the optimization process. A mathematical algorithm is then applied to find the optimum process out of all these alternatives based on the selected objectives such as purity or operating cost. The optimization is executed by considering one level at a time, hence, it constitutes a sequential optimization.
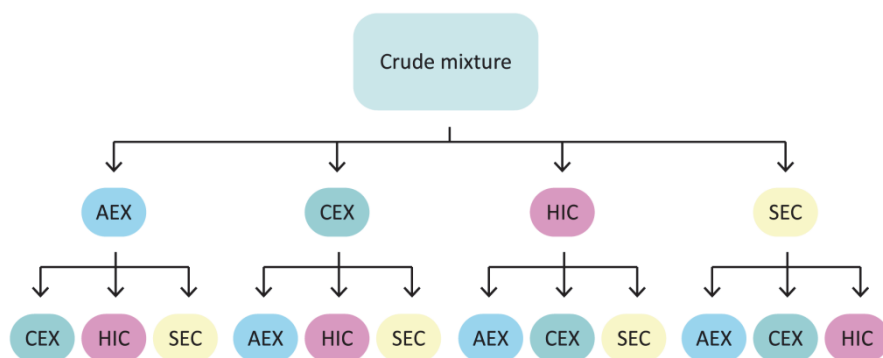
Figure 11: Tree Diagram showing all possible combinations of different chromatographic operations (AEX: anion exchange, CEX: cation exchange, HIC: hydrophobic interaction, SEC: size exclusion) up to a level of two sequential units.

2.4.   Future Directions

Current downstream processing practices applied in the biopharmaceutical industry need to advance to be able to face the challenges resulting from higher cell culture titers and recent regulatory initiatives [68]. Applying high throughput techniques and mechanistic modelling approaches during process development are a promising way to address some of these challenges.

Nonetheless, one part that still needs improvement in high through put techniques is the common usage of low throughput analytics, which are then becoming the bottleneck regarding speed of development. Another issue is the huge amount of data that is being created which requires good data handling structures. Therefore, finding ways of achieving faster analysis and the handling of the produced results are still important areas for future research [4,58].

One obvious trend is a higher degree of integration between different approaches as can be seen in the increasingly more applied hybrid approach. Another aspect where integration is becoming more relevant is the cascading of the chromatographic unit with other unit operations in the downstream process, which is likely to be taken even further by integrating the upstream process as well which would allow for an overall optimization of the entire bio production process. Optimization software tools based on accurate and complex mechanistic models using a flow sheeting approach for bio process development are fruitful ground for future research and development.

References

1. Low D, O'Leary R, Pujar NS. Future of antibody purification. *J Chromatogr B Analyt Technol Biomed Life Sci.* 2007;848(1):48-63.

2. Gronemeyer P, Ditz R, Strube J. Trends in Upstream and Downstream Process Development for Antibody Manufacturing. *Bioengineering.* 2014;1(4):188-212.

3. Rathore AS, Winkle H. Quality by design for biopharmaceuticals. *Nat Biotech.* 2009;27(1):26-34.

4. Łącki KM. High throughput process development in biomanufacturing. *Curr Opin Chem Eng.* 2014;6(0):25-32.

5. Tran R, Lacki K, Davidson A, Sharma B, Titchener-Hooker N. Changing manufacturing paradigms in downstream processing and the role of alternative bioseparation technologies. *J Chem Technol Biot.* 2014;89(10):1534-1544.

6. Hansen SK, Oelmeier SA. Meeting report: High-throughput process development--HTPD 2012: June 4-7, 2012, Avignon, France. *Biotechnol J.* 2012;7(10):1189-1191.

7. Bhambure R, Rathore AS. Chromatography process development in the quality by design paradigm I: Establishing a high-throughput process development platform as a tool for estimating "characterization space" for an ion exchange chromatography step. *Biotechnol Prog.* 2013;29(2):403-414.

8. Rathore AS, Bhambure R. High-throughput process development: I. Process chromatography. *Methods Mol Biol.* 2014;1129:29-37.

9. Nfor BK, Ahamed T, van Dedem GWK, et al. Design strategies for integrated protein purification processes: challenges, progress and outlook. *J Chem Technol Biotechnol.* 2008;83(2):124-132.

10. Titchener-Hooker NJ, Dunnill P, Hoare M. Micro biochemical engineering to accelerate the design of industrial-scale downstream processes for biopharmaceutical proteins. *Biotechnol Bioeng.* 2008;100(3):473-487.

11. Czitrom V. One-factor-at-a-time versus designed experiments. *Am Stat.* 1999;53(2):126-131.

12. Ferreira SL, Bruns RE, da Silva EG, et al. Statistical designs and response surface techniques for the optimization of chromatographic systems. *J Chromatogr A.* 2007;1158(1-2):2-14.

13. Mandenius CF, Brundin A. Bioprocess optimization using design-of-experiments methodology. *Biotechnol Prog.* 2008;24(6):1191-1203.

14. Leser EW, Lienqueo ME, Asenjo JA. Implementation in an expert system of a selection rationale for purification processes for recombinant proteins. *Ann N Y Acad Sci.* 1996;782:441-455.

15. Asenjo J, Andrews B. Is there a rational method to purify proteins? From expert systems to proteomics. *J Mol Recognit.* 2004;17(3):236-247.

16. Lienqueo ME, Asenjo JA. Use of expert systems for the synthesis of downstream protein processes. *Comput Chem Eng.* 2000;24(9-10):2339-2350.

17. Asenjo JA, Andrews BA. Protein purification using chromatography: selection of type, modelling and optimization of operating conditions. *J Mol Recognit.* 2009;22(2):65-76.

18. Sandoval G, Shene C, Andrews BA, Asenjo JA. Extension of the selection of protein chromatography and the rate model to affinity chromatography. *J Mol Recognit.* 2010;23(6):609-617.

19. Coffman JL, Kramarczyk JF, Kelley BD. High-throughput screening of chromatographic separations: I. Method development and column modeling. *Biotechnol Bioeng.* 2008;100(4):605-618.

20. Lacki KM. High-throughput process development of chromatography steps: advantages and limitations of different formats used. *Biotechnol J.* 2012;7(10):1192-1202.

21. Osberghaus A, Hepbildikler S, Nath S, Haindl M, von Lieres E, Hubbuch J. Optimizing a chromatographic three component separation: a comparison of mechanistic and empiric modeling approaches. *J Chromatogr A.* 2012;1237:86-95.

22. Sanaie N, Cecchini D, Pieracci J. Applying high-throughput methods to develop a purification process for a highly glycosylated protein. *Biotechnol J.* 2012;7(10):1242-1255.

23. Welsh JP, Petroff MG, Rowicki P, et al. A practical strategy for using miniature chromatography columns in a standardized high-throughput workflow for purification development of monoclonal antibodies. *Biotechnol Prog.* 2014;30(3):626-635.

24. Schuldt S, Schembecker G. A Fully Automated Ad- and Desorption Method for Resin and Solvent Screening. *Chem Eng Technol.* 2013;36(7):1157-1164.

25. Yoshimoto N, Minakuchi K, Itoh D, Isakari Y, Yamamoto S. High-throughput process development methods for chromatography and precipitation of proteins: Advantages and precautions. *Eng Life Sci.* 2013;13(5):446-455.

26. Konstantinidis S, Kong S, Chhatre S, Velayudhan A, Heldin E, Titchener-Hooker N. Strategic Assay Selection for analytics in high-throughput process development: case studies for downstream processing of monoclonal antibodies. *Biotechnol J.* 2012;7(10):1256-1268.

27. Nilsson B. Aspects of Modeling a preparative ion-exchange step for antibody purification. *Chem Eng Technol.* 2005;28(11):1367-1374.

28. Javeed S, Qamar S, Seidel-Morgenstern A, Warnecke G. Efficient and accurate numerical simulation of nonlinear chromatographic processes. *Comput Chem Eng.* 2011;35(11):2294-2305.

29. Close EJ, Salm JR, Bracewell DG, Sorensen E. A model based approach for identifying robust operating conditions for industrial chromatography with process variability. *Chem Eng Sci.* 2014;116(0):284-295.

30. Nfor BK, Noverraz M, Chilamkurthi S, Verhaert PD, van der Wielen LA, Ottens M. High-throughput isotherm determination and thermodynamic modeling of protein adsorption on mixed mode adsorbents. *J Chromatogr A.* 2010;1217(44):6829-6850.

31. von Lieres E, Andersson J. A fast and accurate solver for the general rate model of column liquid chromatography. *Comput Chem Eng.* 2010;34(8):1180-1191.

32. Gu TY, Iyer G, Cheng KSC. Parameter estimation and rate model simulation of partial breakthrough of bovine serum albumin on a column packed with large Q Sepharose anion-exchange particles. *Sep Purif Technol.* 2013;116(0):319-326.

33. Li ZG, Gu YS, Gu TY. Mathematical modeling and scale-up of size-exclusion chromatography. *Biochem Eng J.* 1998;2(2):145-155.

34. Nagrath D, Messac A, Bequette BW, Cramer SM. A hybrid model framework for the optimization of preparative chromatographic processes. *Biotechnol Prog.* 2004;20(1):162-178.

35. Borg N, Brodsky Y, Moscariello J, et al. Modeling and robust pooling design of a preparative cation-exchange chromatography step for purification of monoclonal antibody monomer from aggregates. *J Chromatogr A.* 2014;1359(0):170-181.

36. Schnittert S, Winz R, von Lieres E. Development of a 3D Model for Packed Bed Liquid Chromatography in Micro-columns. Paper presented at: Computer Modeling and Simulation, 2009. EMS '09. Third UKSim European Symposium on; 25-27 Nov. 2009, 2009.

37. Guiochon G, Felinger A, Shirazi DG, Katti AM. *Fundamentals of Preparative and Nonlinear Chromatography.* Elsevier Inc.; 2006.

38. Schmidt-Traub H, Schulte M, Seidel-Morgenstern A. *Preparative chromatography.* John Wiley & Sons; 2012.

39. Staby A, Rathore AS, Ahuja S. *Preparative Chromatography for Separation of Proteins.* Wiley; 2017.

40. Nfor BK, Zuluaga DS, Verheijen PJT, Verhaert PDEM, van der Wielen LAM, Ottens aM. Model-based rational strategy for chromatographic resin selection. *Biotechnol Prog.* 2011;27(6):1629-1643.

41. Westerberg K, Borg N, Andersson N, Nilsson B. Supporting Design and Control of a Reversed-Phase Chromatography Step by Mechanistic Modeling. *Chem Eng Technol.* 2012;35(1):169-175.

42. Westerberg K, Broberg-Hansen E, Sejergaard L, Nilsson B. Model-based risk analysis of coupled process steps. *Biotechnol Bioeng.* 2013;110(9):2462-2470.

43. Sejergaard L, Karkov HS, Krarup JK, Hagel AB, Cramer SM. Model-based process development for the purification of a modified human growth hormone using multimodal chromatography. *Biotechnol Prog.* 2014;30(5):1057-1064.

44. Nfor BK, Ripic J, van der Padt A, Jacobs M, Ottens M. Model-based high-throughput process development for chromatographic whey proteins separation. *Biotechnol J.* 2012;7(10):1221-1232.

45. Nfor BK, Ahamed T, van Dedem GWK, et al. Model-based rational methodology for protein purification process synthesis. *Chem Eng Sci.* 2013;89(0):185-195.

46. Young ME, Carroad PA, Bell RL. Estimation of diffusion coefficients of proteins. *Biotechnology and Bioengineering.* 1980;22(5):947-955.

47. Bosma JC, Wesselingh JA. Partitioning and diffusion of large molecules in fibrous structures. *J Chromatogr B Biomed Sci Appl.* 2000;743(1-2):169-180.

48. Dismer F, Hubbuch J. 3D structure-based protein retention prediction for ion-exchange chromatography. *J Chromatogr A.* 2010;1217(8):1343-1353.

49. Ladiwala A, Rege K, Breneman CM, Cramer SM. A priori prediction of adsorption isotherm parameters and chromatographic behavior in ion-exchange systems. *Proc Natl Acad Sci U S A.* 2005;102(33):11710-11715.

50. Hou Y, Cramer SM. Evaluation of selectivity in multimodal anion exchange systems: a priori prediction of protein retention and examination of mobile phase modifier effects. *J Chromatogr A.* 2011;1218(43):7813-7820.

51. Chung WK, Hou Y, Freed A, Holstein M, Makhatadze GI, Cramer SM. Investigation of protein binding affinity and preferred orientations in ion exchange systems using a homologous protein library. *Biotechnol Bioeng.* 2009;102(3):869-881.

52. Guelat B, Delegrange L, Valax P, Morbidelli M. Model-based prediction of monoclonal antibody retention in ion-exchange chromatography. *J Chromatogr A.* 2013;1298:17-25.

53. Insaidoo FK, Rauscher MA, Smithline SJ, et al. Targeted purification development enabled by computational biophysical modeling. *Biotechnol Prog.* 2015;31(1):154-164.

54. Lienqueo ME, Mahn A, Asenjo JA. Mathematical correlations for predicting protein retention times in

hydrophobic interaction chromatography. *J Chromatogr A.* 2002;978(1-2):71-79.

55. Alvarez EV, Lienqueo ME, Pinto JM. Optimal synthesis of multistep protein purification processes. *Lat Am Appl Res.* 2001;31(4):373-381.

56. Polykarpou EM, Dalby PA, Papageorgiou LG. A novel efficient optimisation system for purification process synthesis. *Biochem Eng J.* 2012;67(0):186-193.

57. Liu SS, Simaria AS, Farid SS, Papageorgiou LG. Optimising chromatography strategies of antibody purification processes by mixed integer fractional programming techniques. *Comput Chem Eng.* 2014;68(0):151-164.

58. Hanke AT, Ottens M. Purifying biopharmaceuticals: knowledge-based chromatographic process development. *Trends Biotechnol.* 2014;32(4):210-220.

59. Osberghaus A, Drechsel K, Hansen S, et al. Model-integrated process development demonstrated on the optimization of a robotic cation exchange step. *Chem Eng Sci.* 2012;76:129-139.

60. Osberghaus A, Hepbildikler S, Nath S, Haindl M, von Lieres E, Hubbuch J. Determination of parameters for the steric mass action model--a comparison between two approaches. *J Chromatogr A.* 2012;1233(0):54-65.

61. Nfor BK, Ahamed T, Pinkse MW, et al. Multi-dimensional fractionation and characterization of crude protein mixtures: toward establishment of a database of protein purification process development parameters. *Biotechnol Bioeng.* 2012;109(12):3070-3083.

62. Borg N, Westerberg K, Andersson N, von Lieres E, Nilsson B. Effects of uncertainties in experimental conditions on the estimation of adsorption model parameters in preparative chromatography. *Comput Chem Eng.* 2013;55:148-157.

63. Traylor SJ, Xu X, Li Y, Jin M, Li ZJ. Adaptation of the pore diffusion model to describe multi-addition batch uptake high-throughput screening experiments. *J Chromatogr A.* 2014;1368:100-106.

64. Kroner F, Elsasser D, Hubbuch J. A high-throughput 2D-analytical technique to obtain single protein parameters from complex cell lysates for in silico process development of ion exchange chromatography. *J Chromatogr A.* 2013;1318:84-91.

65. Kroner F, Hanke AT, Nfor BK, et al. Analytical characterization of complex, biotechnological feedstocks by pH gradient ion exchange chromatography for purification process development. *J Chromatogr A.* 2013;1311(0):55-64.

66. Huuk TC, Hahn T, Osberghaus A, Hubbuch J. Model-based integrated optimization and evaluation of a multi-step ion exchange chromatography. *Sep Purif Technol.* 2014;136(0):207-222.

67. Ahamed T, Chilamkurthi S, Nfor BK, et al. Selection of pH-related parameters in ion-exchange chromatography using pH-gradient operations. *J Chromatogr A.* 2008;1194(1):22-29.

68. Liu HF, Ma J, Winter C, Bayer R. Recovery and purification process development for monoclonal antibody production. *MAbs.* 2010;2(5):480-499.

Optimization of biopharmaceutical downstream processes supported by mechanistic models and artificial neural networks

Abstract

Downstream process development is a major area of importance within the field of bioengineering. During the design of such a downstream process, important decisions have to be made regarding the type of unit operations as well as their sequence and their operating conditions. Current computational approaches addressing these issues either show a high level of simplification or struggle with computational speed. Therefore, this article presents a new approach that combines detailed mechanistic models and speed-enhancing artificial neural networks. This approach was able to simultaneously optimize a process with three different chromatographic columns towards yield with a minimum purity of 99.9 %. The addition of artificial neural networks greatly accelerated this optimization. Due to high computational speed, the approach is easily extendable to include more unit operations. Therefore, it can be of great help in the acceleration of downstream process development.

Keywords: chromatography, purification process synthesis, downstream processing, model-based process development approach

Contents

3.1. Introduction

Developing a process for the purification of biopharmaceuticals is a highly complex task, due to the vast amount of choices which have to be made. These choices include for instance the type of unit operation, their order and their operating conditions. With such ample possibilities, the problem arises to find the best one among these.

Current approaches tackling this problem are mainly focused on chromatographic techniques [1]. These approaches are either mostly computational [2-7], mostly experimental [8] or a true combination of computational and experimental techniques, also called the hybrid approach [9,10]. Since mechanistic models built on first principles need many process parameters that usually require experimental determination, computational approaches are often based on non-mechanistic models such as simple economic models or the approximation of chromatograms as triangles. However, these simple models do not help in gaining additional process understanding, an increasingly important concept as put forward by the Quality by Design framework [11]. Experimental techniques, even if they apply multivariate data analysis to link process parameters, can only reach a causal understanding, which explains what causes what. If a higher process understanding explaining how or why is desired to predict performance, mechanistic models are needed [12]. In the hybrid approach, the use of mechanistic models yields more understanding of the process itself and the mechanisms occurring inside the respective purification units. In addition, the use of high throughput experimental techniques speeds up the time to determine parameters needed as input for the mechanistic models.

In recent studies, the hybrid approach has been applied successfully despite still showing certain limitations. Nfor et al. optimized the sequence of chromatographic unit operations sequentially rather than simultaneously, which reduces the complexity of the combinatorial problem since possible unit operation sequences increase drastically with an increasing number of unit operations [13]. Nevertheless, sequential optimization may lead to a suboptimal overall process [9,14,15]. Moreover, several process options were excluded which seemed to be not competitive based on prior knowledge about the process [13]. However, such knowledge might not always be available or be false in a specific case. Additionally, this approach has been applied to the simultaneous optimization of a short process sequence consisting of only two purification units [9]. One

of the key issues why this approach has not yet been applied to more complex cases is the computational expense to find the optimal process. Together, these studies show the need for a computationally cheap approach based on mechanistic models that can easily be extended to include more unit operations while at the same time being able to optimize all resulting process options simultaneously.

This article proposes a new approach to optimize biopurification processes based on the hybrid approach which aims to consider all process options possible with a certain set of unit operations. This means that mechanistic models (MMs) describing each relevant unit operation are linked in every possible order and simultaneously optimized regarding their operating conditions. So-called metamodels are commonly used instead of slow mechanistic models for optimizations in engineering [16,17] and process engineering [18] to bypass speed limitations. Therefore, the approach is further extended by the application of metamodels, more specifically artificial neural networks (ANNs), which were previously applied to chromatography [19].

3.2. Materials & Methods

3.2.1. Methodology

Figure 1 schematically shows the proposed optimization approach. First, a superstructure including all possible process alternatives was generated [20,21]. As depicted in Figure 2, the superstructure includes three distinct chromatographic modes namely anion exchange chromatography (AEX), cation exchange chromatography (CEX), and hydrophobic interaction chromatography (HIC). By definition, this superstructure contains the most optimal process that can be designed with this defined set of unit operations. The simplest option would be a process without a chromatographic unit, which would mean that no purification is required. More importantly, all process options consisting of one, two or three chromatographic units in any possible sequence are included.
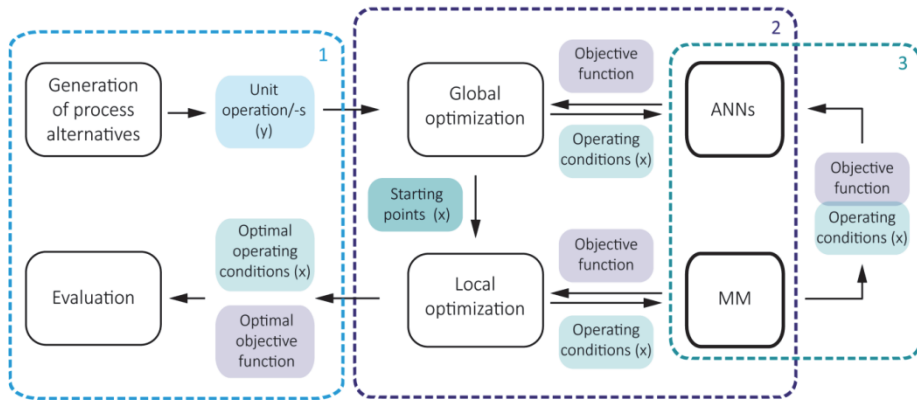
Figure 1: Scheme of the proposed optimization approach

The blue box (1) shows the master problem, the purple box (2) the sub problems, and the green box (3) the creation of ANNs.

To simulate a sequence of several chromatographic units, the product pool of the previous unit was concentrated two times and used as a feed for the subsequent unit. Additionally, a buffer exchange step to reach the pH and salt concentration required for the subsequent unit was assumed. It was assumed that each unit can be used just once, since different purification units should be based on different separation principles, which is also called the 'orthogonality principle'. As a result, 16 possible process options were evaluated.

Secondly, the process optimization problem was formulated as a mathematical problem. In its general form, a constrained optimization problem can be written as the following:
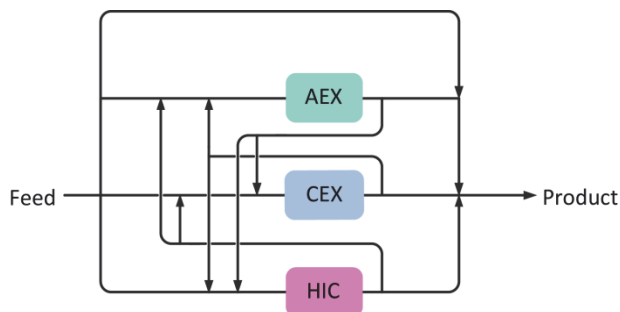
Figure 2: Superstructure showing all process options possible with three different chromatographic columns (AEX, CEX, HIC)

max $f(x, y)$ (1a)

$s.t.$ $h(x) = 0$

        $g(x, y) \leq 0$ (1b)

        $\text{lb} \leq x \leq \text{ub}, \; y \in \{0, 1\}$

where $f(x, y)$ is the objective function to be optimized depending on the binary variables y and the continuous variables x. The objective in this study was yield. The binary variables y are the linking variables. These variables determine which unit operations are in the investigated sequence. The continuous variables x can be operating or design parameters such as flowrates or sizing parameters. Here, they were chosen to be the initial and final salt concentration, which was applied during isocratic or gradient elution, as well as both cut points, which define the product pool that is being fed from one chromatographic column to the next. The lower boundaries (lb) and upper boundaries (ub) are, respectively, 0 and 1, since all variables x were normalized. These continuous variables must obey the equality equations $h(x)$, which are for example mass balances and equilibrium relations. Both have to satisfy design specifications such as physical operating limits and logical constraints. These can be expressed in the inequalities $g(x, y)$. A logical constraint was applied so that each distinct chromatographic mode cannot be used more than once in the process sequence. Additionally, the purity was defined to be at least above 99.9 %.

For simplification of the problem, it was divided into a master problem, represented by the blue box in Figure 1, and several sub problems, represented by the purple box in Figure 1. This process is called hierarchical decomposition [22]. The master problem contains all linking variables y:

max $f(y_{m,s})$ (2a)

s.t. $\sum_m y_{m,s} \leq 1$

        $\sum_s y_{m,s} \leq 1$

        $1 - \sum_m y_{m,2} + \sum_m y_{m,1} \geq 1$ (2b)

        $1 - \sum_m y_{m,3} + \sum_m y_{m,2} \geq 1$

        $y_{m,s} \in \{0,1\}$

where subscript m indicates the mode used, $m \in \{1, 2, 3\}$ meaning AEX, CEX and HIC, and s the number of purification steps, $s \in \{1, 2, 3\}$. The first constraint only allows the choice of maximal one chromatography unit per purification step, while the second

3

constraint only allows the use of each distinct chromatography mode maximally once. The third and the fourth constraint mean that a chromatography unit has to be chosen for all earlier occurring purification steps. These y variables were then fed into the sub problems, which were solved for the local variables x. If, for instance, the y variables are [0 1 0; 1 0 0; 0 0 0], the sequence consisting of CEX as the first and AEX as the second unit operation form the sub problem. Next, the results of all sub problems were collected and evaluated.

Still, each sub problem forms a complex optimization problem. Therefore, a global optimization technique was applied to avoid a suboptimal solution. However, these techniques usually have a poor convergence performance. Hence, global optimization techniques are commonly combined with faster, local search techniques [23,24]. When these local search techniques are used, the optimum solution depends heavily on the starting points investigated [25]. Consequently, a global optimization algorithm was used in each sub problem to find good initial starting points for a subsequent local search.

The global optimization problem was defined as a multi-objective optimization problem without nonlinear constraints, since such a problem can be solved easier than the one described above:

$$\max \quad yield(x), \, purity(x) \tag{3a}$$

$$s.t. \quad \begin{aligned} h(x) &= 0 \\ 0 &\leq x \leq 1 \end{aligned} \tag{3b}$$

When a sequence of several chromatographic units was optimized with the mechanistic model (MM), the subsequent unit was only evaluated if the yield of the one before was above 5 %. This prevents that the solver fails due to very low feed concentrations. Thus, the objective had to be formulated slightly differently if any subsequent units could not be evaluated. Otherwise the solver could get stuck at a minimum with just evaluating one unit in the sequence. This could happen for instance if the first unit has a yield of 50 %, which means the subsequent unit can be evaluated. If the yield of the subsequent unit now would be 3 %, the overall yield of both units would be 1.5 %, which would be much lower than the 5 % threshold. The solver could then end up with only the first unit at 4.9 % yield as the maximum, although an optimization of a sequence with several units was desired. To overcome this, penalties were introduced if not all units in

the to-be-optimized sequence could be simulated. Since only the purity of the last unit operation is of concern, purity was only included in the objective function if all prior units could be evaluated. Additionally, purity was multiplied with a weight factor of two to increase the importance of purity over yield during the global search. The range of the objective function values were normalized from zero to one; one means the maximum value of 100 % yield and 100 % purity.

A similar approach was chosen during the local search; then, however, purity was not considered an objective but a constraint. The best points found during the global search were used as initial starting points for the local search. The local search problem being solved subsequently was defined with a nonlinear constraint on purity:

$$\max \quad yield(x) \tag{4a}$$

$$
\begin{aligned}
s.t. \quad & h(x) = 0 \\
& purity(x) > 99.9\,\% \\
& 0 \le x \le 1
\end{aligned}
\tag{4b}
$$

Thirdly, artficial neural networks (ANNs) were built that can speed up the optimization. They were used instead of the MM to evaluate the objective function during the global optimization since at that point accuracy is not as important and speed is limiting. For the local search, only MMs were used to avoid the influence of any inaccuracies in the ANNs to the final result. The building, training and evaluation of the ANNs is shown in detail in the next section.

3.2.2. Numerical methods

Ten well distributed starting points were created for the global search with the MATLAB function *lhsdesign*. This function generates a latin hypercube sample which is optimized towards a reduced correlation between data points, when the criterion is set to correlation. As optimization algorithm for the global optimization, MATLAB's *pattern search* solver from the Global Optimization Toolbox[TM] was chosen, since direct search algorithms are generally suitable for problems with fewer variables and have a high efficiency [26]. Here, an additional search step with a latin hypercube search was performed, which randomly generates points at each iteration. All of these points were than evaluated and the one with the highest objective function was chosen. This enables the search of the entire search space resulting in globally good initial points for

the local search. The maximum amount of function evaluations were set to 250 and the tolerance in the change of the objective function to 0.01 to force an early stopping of the optimization. Additionally, an output function was added that stops the optimization if an objective function of more than 0.99 was reached; the maximum value of the objective function was one. During the global optimization, the objective function was evaluated with ANNs or with the MM as explained in section 3.3.2. The local search was done using the *fmincon* function by MATLAB which uses a sequential quadratic programming method. The objective and constraint function during the local optimization were evaluated with the MM.

All computations have been done on an Intel® Xeon® Processor E5-1620 v2 with 3.7 GHz. Evaluation of the sample points for the ANN, training the ANN's and the optimization for multiple starting points have been computed in parallel on four cores using MATLAB's Parallel Computing Toolbox™.

Mechanistic model

The chosen mechanistic model (MM), which was used to explain the effects inside a chromatographic column, was the equilibrium transport dispersive model for its computational speed. The solver takes around 2.3 s to calculate one chromatographic separation for 2 components on 100 axial grid points without any parallelization of tasks. If the more accurate general rate model is solved in a very efficient manner although with a less powerful CPU (2.4 GHz), the solver takes for the same task 6.3 to 135.3 depending on the amount of radial grip points (10 to 160) used [27]. Clearly, a tradeoff has to be made between speed and accuracy. For the applications considered here, previous validation studies showed a sufficiently high accuracy between model and experimental results [13].

The equilibrium transport dispersive model can be formulated as:

$$\frac{\partial c_{p,i}}{\partial t} + F\frac{\partial q_{p,i}}{\partial t} = -v\frac{\partial c_{p,i}}{\partial x} + D_{L,i}\frac{\partial^2 c_{p,i}}{\partial x^2} \tag{5}$$

where $c_{p,i}$ is the concentration in the bulk phase and $q_{p,i}$ the concentration in the stationary phase of protein i. The interstitial velocity of the mobile phase, v, was calculated as $v = u/\varepsilon_b$ where u is the superficial velocity and ε_b the bed porosity. $D_{L,i}$ is the axial dispersion coefficient and F is the phase ratio, which was defined as $F = (1 - \varepsilon_t)/\varepsilon_t$ with the total porosity, ε_t.

The mass transfer was taken into account by the liquid-film linear driving force approximation:

$$\frac{\partial q_{p,i}}{\partial t} = k_{ov,i}\left(c_{p,i} - c_{p,i}^*\right) \tag{6}$$

where $k_{ov,i}$ is the overall mass transfer coefficient and $c_{p,i}^*$ is the equilibrium concentration in the liquid phase which can be calculated using an appropriate isotherm. The isotherms used for describing the adsorption of the proteins towards the resin material were developed within Mollerup's thermodynamic framework [28] as shown in [29]. The general form of the isotherm valid for multicomponent systems in ion exchange, hydrophobic interaction and mixed mode chromatography is:

$$\frac{q_{p,i}}{c_{p,i}^*} = A_i \left(1 - \sum_{j=1}^{m} \frac{q_{p,j}}{q_{p,j}^{max}}\right)^{v_i + n_i} \tag{7}$$

where the term $1 - \sum_{j=1}^{m} \frac{q_{p,j}}{q_{p,j}^{max}}$ represents the fraction of free ligands with the maximum binding capacity q_p^{max}, the number of proteins m and protein species j. v_i and n_i are stoichiometric coefficients for ion exchange chromatography and hydrophobic interaction chromatography, respectively. v_i can be calculated as z_p/z_s, where z_p is the effective binding charge of the protein and z_s the charge on the salt counter ion. A_i, the initial slope of the isotherm, can be calculated by:

$$A_i = K_{eq,i}\Lambda^{(v_i+n_i)}(z_s c_s)^{-v_i} c_v^{-n_i}\gamma_i \tag{8}$$

where K_{eq} is the thermodynamic equilibrium constant, Λ the ligand density, c_s the salt concentration and c_v the molarity of the solution in the pore volume. The activity coefficient can be calculated at low protein concentrations as $\gamma_i = e^{K_{s,i}c_s}$ given K_s the salt-protein interaction coefficient.

The mechanistic model and its solution was described in full detail previously [30]. The only change was the correlation used to calculate the axial dispersion coefficient $D_{L,i}$. In this paper, an empirical correlation found by Athalye [31] based on data of Miller and King [32] was used as done in [33]. The mechanistic model was used to predict the value of the objective function and the nonlinear constraints, which were the yield and purity, under varying operating conditions, which were defined by changes in the variables x.
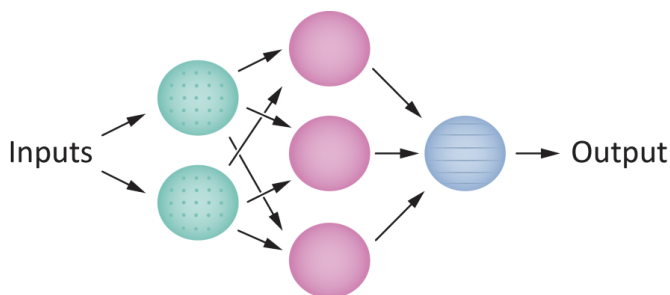
Figure 3: Schematic of an artifical neural network consisting of several hidden layers (green dots and pink even fill) and an output layer (blue lines)

3

Artificial neural networks

Artificial neural networks were designed to mimic the brains behavior in a very simplified manner. They consist of many interconnected neurons, which are organized in several layers as can be seen in Figure 3. ANNs comprise at least one layer of hidden neurons connecting inputs to a layer of output neurons. A single neuron is shown in Figure 4. The input given to the neuron is first multiplied by a weight, then a bias or offset is added. This forms the input for the so-called transfer or activation function, which delivers the output of the neuron [34]. The output of neurons in the hidden layer was calculated by means of hyperbolic tangent sigmoid transfer functions, while the output of output neurons was calculated by linear transfer functions.

The ANNs were generated and trained with the Neural Network Toolbox[TM] by MATLAB. First, datasets showing input-output relationships were generated with the mechanistic model. To create a well distributed input dataset for training the ANN, the MATLAB function *lhsdesign* was used. Each of these input data points, which correspond to the variables x, was evaluated with the mechanistic model to obtain the corresponding output (yield of the product and protein concentrations of all components). General practice is the division of the data into three subsets: 70 % of the data points are used for training, 15 % for validation, and 15 % for testing.
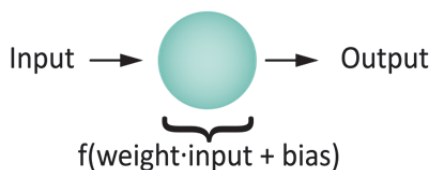

Figure 4: Schematic of a single neuron showing how the input is being transformed to obtain the output

Next, the neural network structure was defined. A single hidden layer of neurons was chosen, which is known to be sufficient in most cases; this is especially true when dealing with the approximation of continuous functions [35]. The ideal number of neurons in this layer was determined.

Then, the ANN was trained to mimic the behavior predicted by the mechanistic model, which means that the weights and biases were adjusted to best translate the input-output relationship. The Levenberg-Marquardt algorithm was chosen as a training algorithm. However, each time an ANN is being trained different initial weights and biases are applied, which leads to ANNs with varying accuracy. Therefore, 20 different ANNs were trained to determine a single, best ANN.

Finally, the ANNs were validated to ensure sufficient predictive abilities. One way to measure the accuracy of an ANN is the R^2 value, which compares the output predicted by the ANN, $\hat{o}_i$, with the output observed by the mechanistic model, o_i, at test data points, defined below

$$R^2 = 1 - \frac{\sum_{i=1}^{m}(o_i - \hat{o}_i)^2}{\sum_{i=1}^{m}(o_i - \bar{o})^2} \tag{9}$$

where $\bar{o}$ is the mean of observed values and m the number of additional sample points [17]. Consequently, the best ANN was chosen based on the R^2 value calculated for each of the ANNs.

3.2.3. Materials

Isotherm data for five proteins as shown in Table 1 were taken from a previously published study [36]. As a product, the monoclonal antibody (1) was picked. A total number of four impurities having similar properties as the product were chosen to represent most impurities present. For the simulation, the initial protein concentrations (C_{feed}) were 1 g/L for each impurity and 2 g/L for the product.

Table 1: Summary of all isotherm parameters taken from [36]

Mode	Protein	C_{feed} [g/L]	MW [kDa]	K_{eq} [-]	z_p [-]	n [-]	q_{max} [mM]	K_s [-]
AEX	product	2,0	145,6	0,5	4,0	-	10,2	-
AEX	impurity 1	1,0	68,0	0,5	4,0	-	10,2	-
AEX	impurity 2	1,0	51,5	0,9	1,7	-	145,5	-
AEX	impurity 3	1,0	56,2	3,9	2,9	-	13,1	-
AEX	impurity 4	1,0	54,5	3,9	2,9	-	13,1	-
CEX	product	2,0	145,6	8,5	2,6	-	32,1	-
CEX	impurity 1	1,0	68,0	500,8	2,5	-	27,0	-
CEX	impurity 2	1,0	51,5	604,2	2,6	-	24,1	-
CEX	impurity 3	1,0	56,2	0,0	0,0	-	0,0	-
CEX	impurity 4	1,0	54,5	8,5	2,6	-	32,1	-
HIC	product	2,0	145,6	9,3	-	9,3	12,7	0,0860
HIC	impurity 1	1,0	68,0	1,6	-	1,6	15,8	0,0030
HIC	impurity 2	1,0	51,5	10,4	-	10,4	2,4	1,00
HIC	impurity 3	1,0	56,2	9,3	-	9,3	12,7	0,09
HIC	impurity 4	1,0	54,5	1,6	-	1,6	15,8	0,0030

Proteins: product: mAB, impurity 1: Moesin, impurity 2: Chitotrisidase, impurity 3: Legumain, impurity 4: Thioredoxin reductase; MW: molecular weight; K_{eq}: equilibrium constant; z_p: effective charge in ion exchange; n: stoichiometric coefficient in HIC; q_{max}: maximum binding capacity; K_s: salt interaction parameter in HIC

The data for each resin is summarized in Table 2 and was taken from a previous paper [13]. All resins are from GE HealthCare Life Sciences. Additionally, Table 2 shows the salt type used in each mode for the elution as well as the concentration range that was investigated. In the simulations, the linear velocity was 150 cm/h. The column dimensions were 7 x 25 mm. The bed and total porosity were assumed to be 0.27 and 0.95, respectively. The loading factor of a single column/ the first column in a sequence was 0.1. In case of a sequence of columns, the load on the subsequent columns was defined by the product pool collected in the earlier column, which was concentrated two times. The gradient length was 8.6 column volumes (CV).

Table 2: Summary of all resin specific parameters and information about the salt type used for the elution as well as the investigated range of salt concentrations for the gradient

Mode	Resin	dp [µm]	dpore [nm]	Λ [mM]	salt type	salt range [mM]
AEX	Source Q	30	40	320	NaCl	0-500
CEX	Source S	30	40	135	NaCl	0-500

d_p: mean particle diameter; d_{pore}: mean pore diameter; Λ: ligand density

3.3. Results & Discussion

3.3.1. Artificial Neural Network

Structure

First, ANNs had to be generated which can predict the yield and the concentrations of all proteins at certain operating conditions accurately enough. Hence, it was investigated how many sample points are needed to train such ANNs. Figure 5a shows the accuracy of networks trained with different numbers of sample points for the prediction of the product concentration on the CEX resin. The accuracy is represented by the correlation coefficient (R^2), which was determined at unseen test data points

<center>(a)   (b)</center>
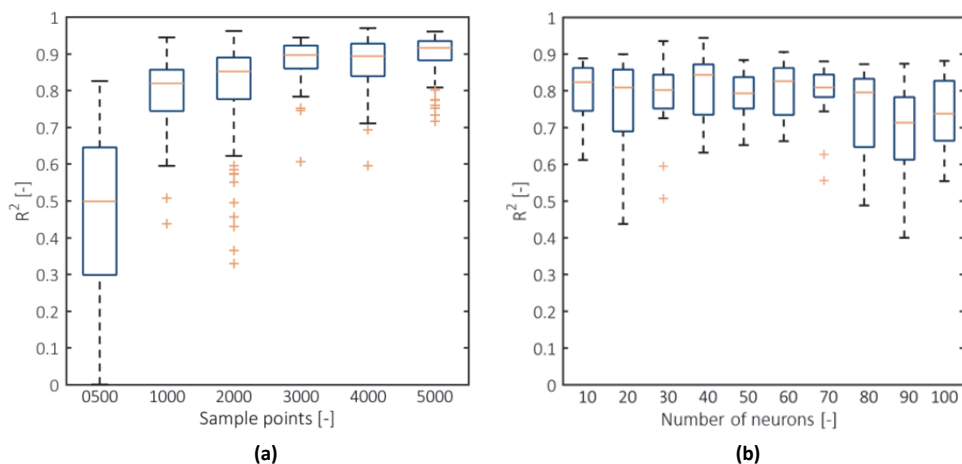
Figure 5: Boxplots showing the accuracy of trained networks regarding the number of sample points (a) and the number of neurons per layer at 1000 sample points (b).

The blue box marks the interquartile range (IQR) with the 25th percentile, the lower corner of the box, and the 75th percentile, the upper corner of the box. The median is shown in orange, while the minimum and maximum values are in black. The orange crosses mark the outliers.

using equation 9. The number of neurons was varied from 10 to 50. 500 sample points resulted in a high variation of accuracy between the trained networks, which can be seen by the wide interquartile range (IQR). Increasing the number of sample points increased in turn the accuracy, although a plateau was reached from 3000 to 5000 sample points. For all further calculations, 1000 sample points were chosen as a compromise between accuracy and speed. Data sets with at least 3000 sample points should be generated, if more accurate networks are needed. This could be the case if the entire optimization would be based on neural networks.

Additionally, the best number of neurons was determined as can be seen in Figure 5b. On the one hand, if too few neurons are chosen, the output cannot be approximated accurately enough. On the other hand, if too many neurons are chosen, over-fitting might occur. This means that the fit will be very good for the training data set but not sufficient regarding unseen test data [35]. Overfitting was observed when the number of neurons was increased to 50 and above and is especially visible at 90 and 100 sample points. The median here is quite decreased in comparison to lower numbers of neurons. As 40 neurons seemed to result in the best fitting ANNs with the highest median, this amount was chosen for generating all other ANNs.

Quantitative evaluation

As summarized in Table 3, the correlation coefficients (R^2) calculated for the different resins are quite high with a minimal value of 0.87. Generally, a metamodel with an R^2 above 0.8 indicates good predictive abilities [16]. The ANNs created here surpass this and, thus, were deemed to be sufficient for the optimization.

Table 3: R^2 values showing the correlation between protein concentrations predicted by ANNs and MM for all investigated resins

	yield	product	impurity 1	impurity 2	impurity 3	impurity 4
CEX	0.96	0.94	0.99	0.99	0.99	0.91
AEX	0.93	0.90	0.87	0.94	0.94	0.95
HIC	0.94	0.91	1	0.96	0.87	1

However, the R^2 only informs about the correlation between data sets; it does not indicate, however, if the prediction results in the correct values. Therefore, 100 random, previously unseen data points were evaluated with both type of models, the ANNs and the MM, for CEX. The protein concentrations predicted by both models were very similar; the plot can be seen in Figure 6a. Additionally, the residual between values predicted by MM and ANN was of interest to see if the ANNs show a random error in their predictions or if they under/overestimate in certain areas (Figure 6b). Since the residuals in the scatter plot appear to be randomly distributed, the error in prediction
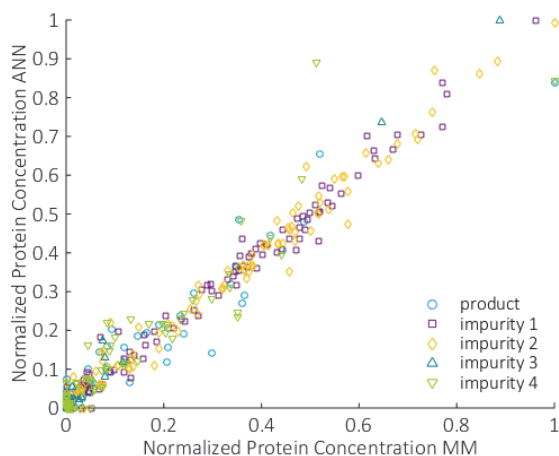
(a)
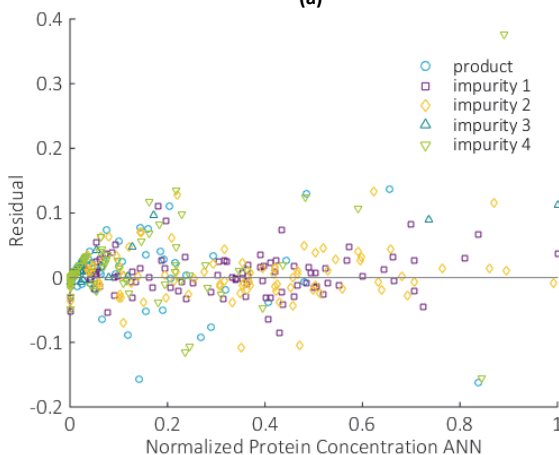
(b)

Figure 6: Quantitative evaluation of the predictive abilities of the ANNs

a) 100 random data points were evaluated and plotted with both models for the product and all impurities; **b**) Residuals of the values predicted by ANN and MM

was assumed to be random as well. Therefore, protein concentrations predicted by the ANNs can be trusted. This also means that protein concentrations predicted in the product pool of one column can be used as an input for the subsequent column.

Qualitative evaluation

Figure 7 compares the behavior of a trained ANN to the MM on a CEX resin. In Figure 7 a, a chromatogram, which was generated with the MM, is shown at fixed salt gradient concentrations. For these concentrations, the ANN simulated the expected product
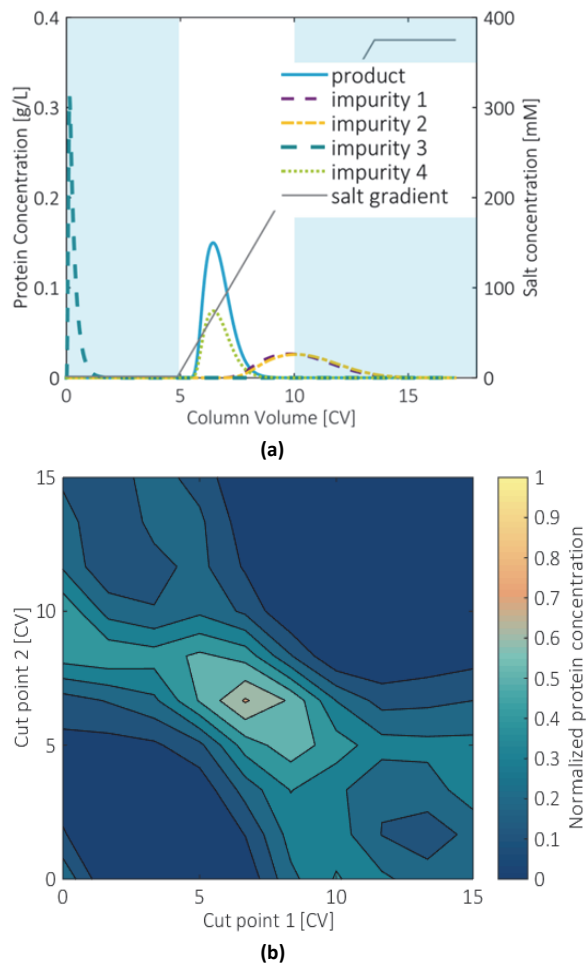

(a)

(b)

Figure 7: Qualitative evaluation of the predictive abilities of the ANNs

a) Simulated Chromatogram at initial salt concentration of almost 0 and final salt concentration of 300 mM on CEX; b) Predictions of protein concentrations for impurity 1 with ANN at varying cut points at identical salt concentrations as in a.

concentrations with varying product pool cut points depicted in Figure 7 b. The output of the ANN is reasonable: Low cut points (0-5 CV) show that the product is not present in the product pool while cut points around the eluting salt concentration (around 6.5 CV) result in increasingly higher concentrations of the product. If both cut points are above 10 CV, no product will be present in the product pool.

Contour plots in Figure 8 compare the output of ANN and MM over most of the investigated parameter range. The location of maximal protein concentrations is almost identical. At lower concentrations, however, the contour lines vary noticeably. This stems from the way neural networks function; they pick up general trends in a data set
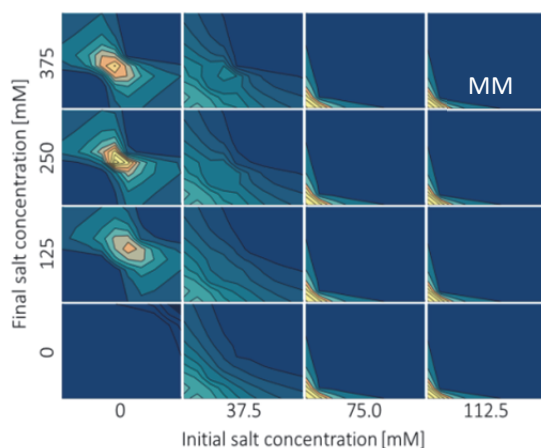
(a)
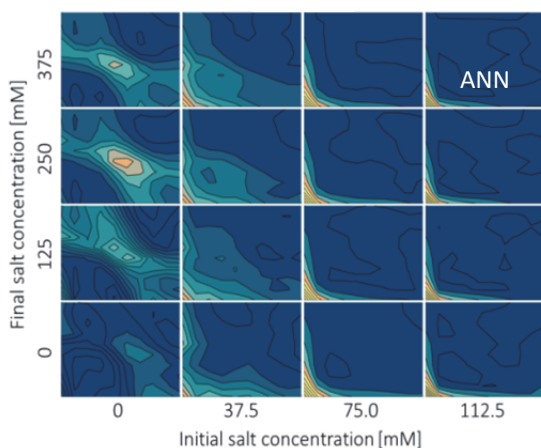
(b)

Figure 8: Predictions of protein concentrations for impurity 1 over investigated parameter range with MM (a) and with ANN (b)

but fail to mimic slight tendencies. In the global optimization, this behavior is anyways preferable since the search for good global starting points should not be hindered by small concentration changes. In the final local search, the 'true' optimum is desired, which includes exact operating conditions. Consequently, the MM was used here.

3.3.2. Process Optimization

Global Optimization

The solution of the global optimization problem differed noticeably when ANNs were used instead of MMs. To demonstrate that, the objective values were compared. Histograms show the distribution of the objective function values that were obtained by global optimizations of all sequences with one chromatographic unit (Figure 9a), two sequential units (Figure 9b) and three sequential units (Figure 9c).

When the ANNs were used to optimize the process sequence, the best objective function values and the respective operating variables could be obtained; one means that purity as well as yield were equal to 100 %. However, once these optimal operating variables were evaluated with the MM, which is denoted as ANN-MM in Figure 9, considerably lower objective function values could be observed. The reasons for this are inaccuracies in the ANNs; optimal points are found that do not exist when evaluated with the MM. These findings show the necessity of an extra verification step or the need of more accurate ANNs if only ANNs are used for the entire optimization. This is not the case in the approach proposed here with its subsequent optimization step with the MM. Comparing these ANN-MM values with the MM values, similar optimal results could be obtained for a sequence of one or two unit operations. For three unit operations, objective values found with the ANNs were considerably lower. Therefore, the number of maximum function evaluations was increased to 500, which improved the quality of the starting points for the subsequent local search. Another way to increase the quality of starting points would be to use more initial starting points in the global search. Then, only the ones resulting in high objective function values after evaluation with the MM could be used further. Since global optimizations with the ANN are much faster than with the MM, this would still result in a much higher overall speed.

(a)

(b)
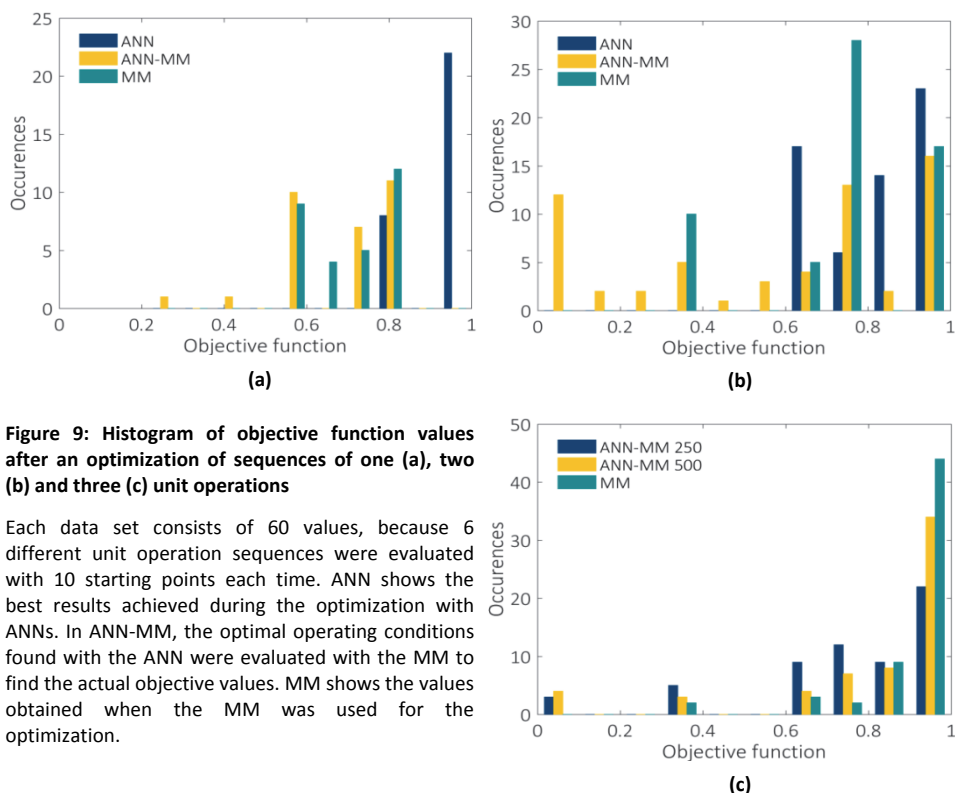
Figure 9: Histogram of objective function values after an optimization of sequences of one (a), two (b) and three (c) unit operations

Each data set consists of 60 values, because 6 different unit operation sequences were evaluated with 10 starting points each time. ANN shows the best results achieved during the optimization with ANNs. In ANN-MM, the optimal operating conditions found with the ANN were evaluated with the MM to find the actual objective values. MM shows the values obtained when the MM was used for the optimization.

(c)

Local Optimization

The subsequent local optimization was carried out identically regardless if ANNs or MM were used during the global optimization. In this local optimization, a purity of 99.9 % was set as a hard constraint leaving yield as the sole objective. Optimization results are presented in Figure 10 for all investigated process sequences. Overall, the results obtained are very similar; only sequences containing CEX and HIC were able to reach a purity and yield of around 100%. In other options, a tradeoff between yield and purity was necessary. Since the purity was a hard constraint and not a second objective, yield was also not optimized further if the constraint could not be fulfilled.
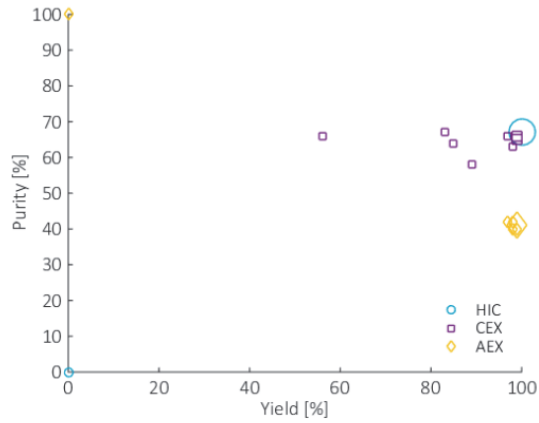
(a)
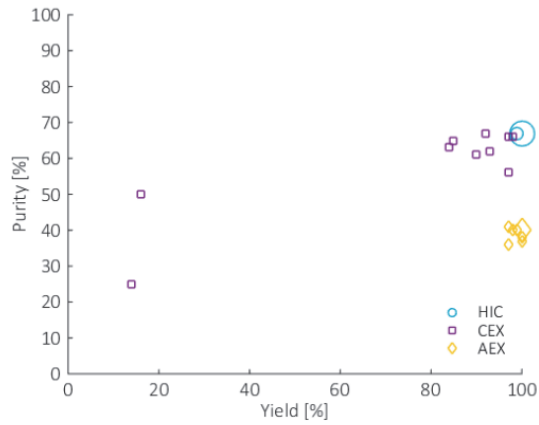
(b)
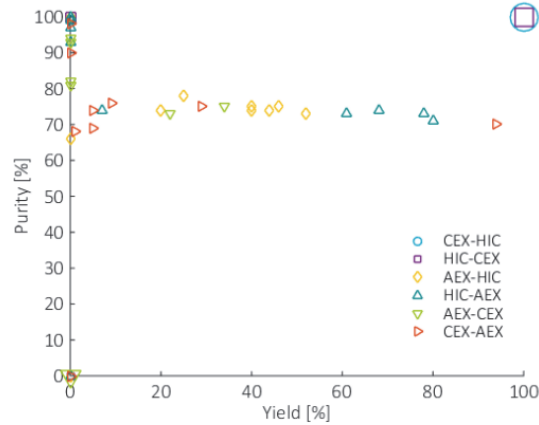
(c)

Figure 10: Optimization results for all sequences with one (a, b), two (c, d) and three (e, f) chromatographic units.
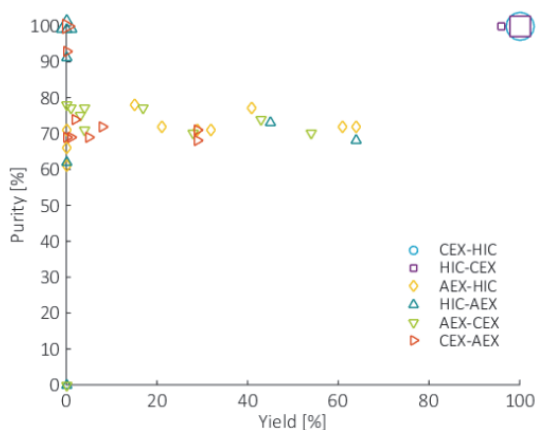
(d)
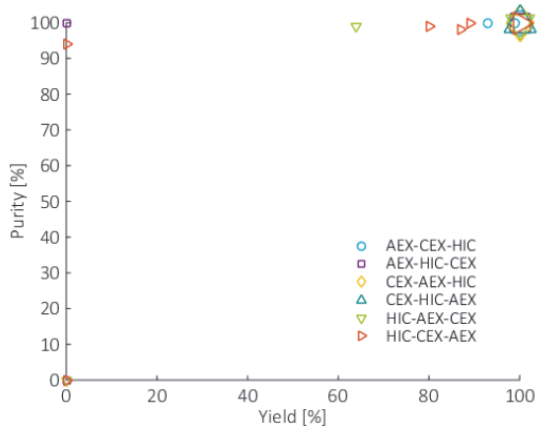
(e)

(f)
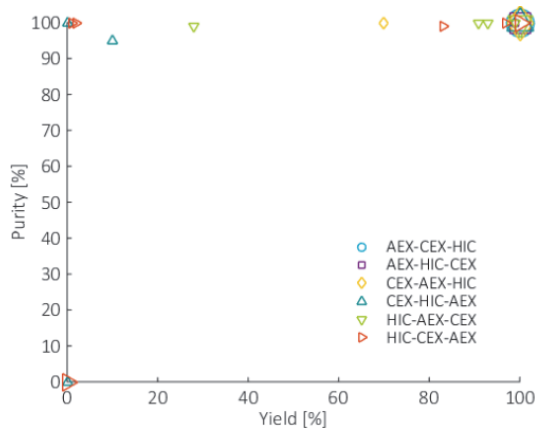
The starting points were retrieved with the MM (a, c, e) and the ANN (b, d, f). The size of the markers indicates the amount of points in one type of sequence with identical yield and purity.

This resulted in the points with varying yields around 70 % purity. All sequences with three units include CEX and HIC. Therefore, most optimizations could reach optimal values. Normally, however, process sequences with less units are preferred. Therefore, the optimal process here would be HIC-CEX or CEX-HIC, which is shown in Figure 11. This differs from the optimal process determined by Nfor et al., since a different subset of impurities at increased protein concentrations as well as different objectives and constraints were chosen in this study [13]. In conclusion, the optimization approach is able to find the most optimal operating points for each sequence regardless if ANNs or MMs were used to identify good starting points.
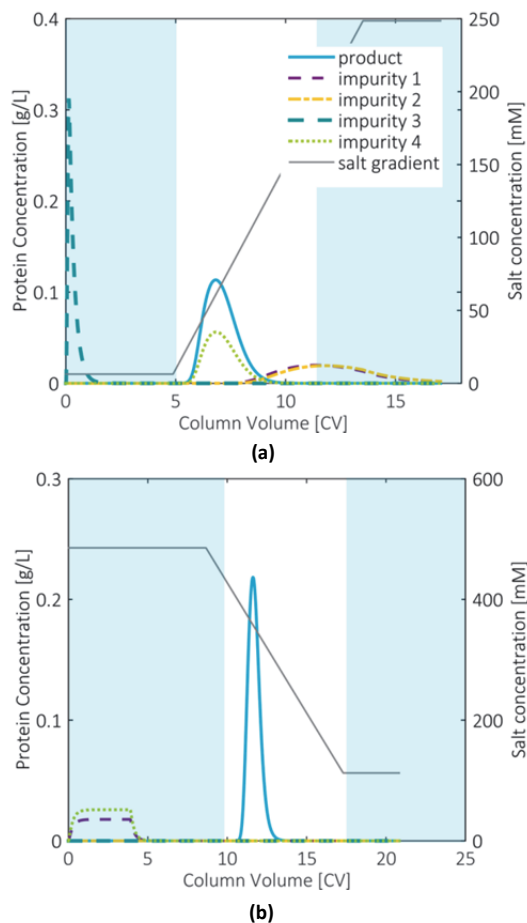
Figure 11: Optimized process sequence of CEX (a) and HIC (b)

Note that impurity 2 cannot be eluted in HIC under the elution conditions proposed.

Computational Speed

The advantage in using ANNs is clearly the saved computational time. A single function evaluation for all five proteins with an ANN takes 0.04 s compared to 3 s with the MM with 50 axial grid points. Times for the complete evaluation of all possible process sequences are given in Table 4. The global optimization is around 30 times faster, if ANNs are used. However, the time to generate sample points and to train the ANNs has to be added to compare the computational time fairly (1 h). Including that, the total computational time was decreased by around 50 % when ANNs were used. This speed decrease gets increasingly important the more unit operations are to be simulated in sequence, since the optimization of three sequential units already takes about two thirds of the overall computational time.

The local optimizations took generally longer with the starting points provided by the ANNs due to inaccuracies in the ANNs as shown in section 3.3.1. This was improved by including an extra evaluation step, where these starting points are first checked with the MM before they are fed to the local optimizer. In this way, only points with an objective function value above 0.6 were investigated further. This did not considerably influence the results, as can be seen in Figure 12. Since now starting points at global optima that only exist due to discrepancies in the ANNs are discarded, the overall time for local optimizations was decreased by at least 40 % leading to a total time of 6.5 h. Including the time for training the networks, this is only 30 % of the time needed to optimize all chromatographic units with the MM.

Table 4: Computational times in hours for an optimization supported by MMs (left side) and by ANNs and MMs (right side); times with an extra evaluation step are shown in italic

	1 UO			2 UO			3 UO			Total		
	MM	ANN - MM		MM	ANN - MM		MM	ANN - MM		MM	ANN - MM	
Global	0.58	0.02		5.25	0.14		10.66	0.32				
Local	0.99	1.10	*0.28*	2.17	3.35	*1.67*	5.01	6.8	*4.03*			
Total	1.57	1.12	*0.3*	7.42	3.49	*1.81*	15.67	7.08	*4.35*	24.67	11.69	*6.46*

UO: Unit operation

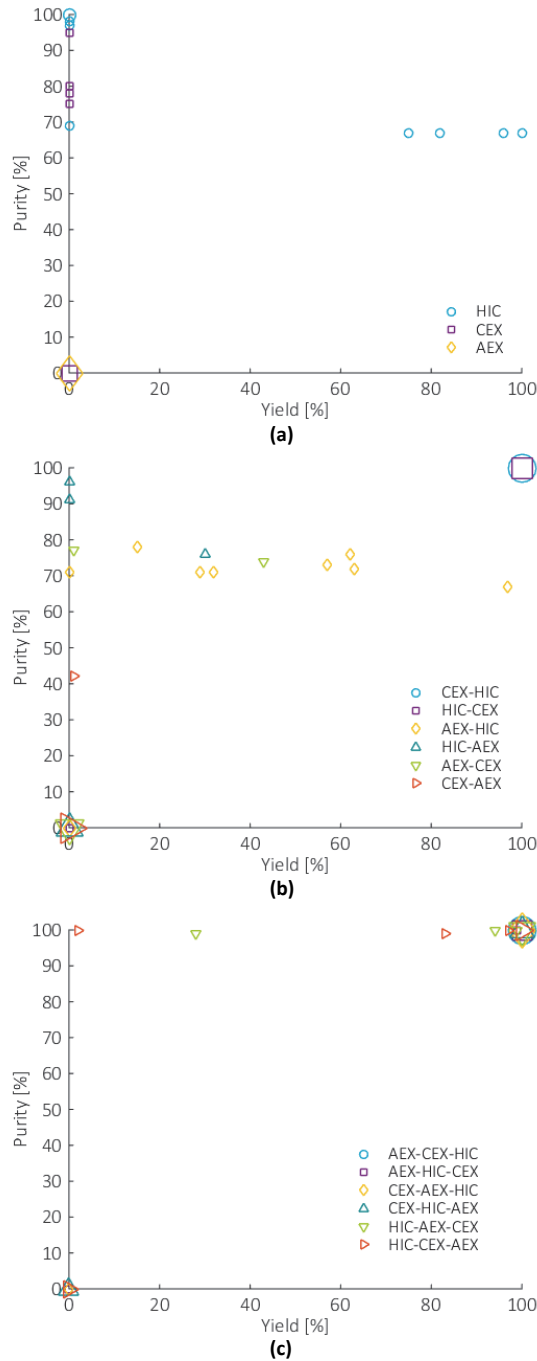**Figure 12: Optimization results for all sequences with one (a), two (b) and three (c) chromatographic units**
Starting points were found with the ANN, only starting points with an objective function value above 0.6 were locally optimized. The size of the markers indicates the amount of points in one type of sequence with identical yield and purity.

Of course, also here the number of starting points could be reduced by discarding poor initial points, which would result in a faster local optimization. Another way to improve the computational time further could be the use of ANNs for the local optimization as well. In that case, however, regular evaluation steps with the MM would have to be included in the optimization routine. More accurate ANNs would be beneficial then, which could be created for instance by increasing the number of sample points as shown in Section 3.3.1.

3.4. Conclusion

This study has introduced an optimization approach for the purification of biopharmaceuticals by means of different forms of chromatography, which is based on detailed mechanistic models as well as fast artificial neural networks. First, the accuracy of predictions by ANNs was shown to be sufficient (R^2 above 0.8). Next, a purification process was globally optimized with the help of ANNs to supply good starting points for a subsequent local search with mechanistic models. With that, the best sequence of chromatographic units and their optimal operating conditions could be found. The full optimization including the creation of ANNs took 12.7 h. A comparison with the same approach without ANNs showed no difference in results but a major increase in overall speed by around 50 % (24.7 h). A small other change resulted in a total time of 7.5 h including training of the networks, which is an additional speed improvement of 40 % (total improvement of 70 %).

Overall, the approach is very flexible; it could be easily extended to include more unit operations. Moreover, any design or operating condition that is included in the mechanistic model could be used as a variable. Additionally, economical aspects could be introduced either in the objective function or as constraints.

Once a more complex problem is tackled, the speed improvement due to ANNs becomes crucial. For instance, for a purification with maximal three chromatographic columns, the average amount in current large scale purification trains [37], and eight possible chromatographic modes, a total of 400 flowsheets, calculated as in [13], would be possible. Evaluating and optimizing these flowsheets is computationally very expensive. ANNs were shown to be good candidates in reducing this expense.

However, certain limitations remain. For instance, interstage conditioning such as filtration was not yet considered but could potentially alter the choice of the best purification process. ANNs are commonly used in filtration processes, which suggests an easy implementation in this approach [38]. Additionally, an experimental validation of the proposed best process is desirable. Therefore, future research is needed.

Notwithstanding these current limitations, this study can be seen as a next step towards a model-based approach that can deliver the best possible bio-purification process. Such a model-based approach has great advantages to traditional downstream process development. Material, time and overall costs are reduced, because experiments are mainly needed for parameter determination and model validation. With only few further experiments, it could easily be assessed which process sequence and operating conditions would result in the best process.

Acknowledgements

References

1. Hanke AT, Ottens M. Purifying biopharmaceuticals: knowledge-based chromatographic process development. *Trends Biotechnol.* 2014;32(4):210-220.

2. Liu SS, Simaria AS, Farid SS, Papageorgiou LG. Optimising chromatography strategies of antibody purification processes by mixed integer fractional programming techniques. *Comput Chem Eng.* 2014;68(0):151-164.

3. Polykarpou EM, Dalby PA, Papageorgiou LG. Optimal synthesis of chromatographic trains for downstream protein processing. *Biotechnol Prog.* 2011;27(6):1653-1660.

4. Polykarpou EM, Dalby PA, Papageorgiou LG. A novel efficient optimisation system for purification process synthesis. *Biochemical Engineering Journal.* 2012;67(0):186-193.

5. Vasquez-Alvarez E, Pinto JM. Efficient MILP formulations for the optimal synthesis of chromatographic protein purification processes. *J Biotechnol.* 2004;110(3):295-311.

6. Allmendinger R, Simaria AS, Turner R, Farid SS. Closed-loop optimization of chromatography column sizing strategies in biopharmaceutical manufacture. *J Chem Technol Biotechnol.* 2014;89(10):1481-1490.

7. Allmendinger R, Farid SS. A Multiobjective Evolutionary Optimization Framework for Protein Purification Process Design. Paper

presented at: Parallel Problem Solving from Nature – PPSN XIII: 13th International Conference; September 13-17, 2014; Ljubljana, Slovenia.

8. Winkelnkemper T, Schuldt S, Schembecker G. Systematic downstream process development for purification of baccatin III with key performance indicators. *Sep Purif Technol.* 2011;77(3):355-366.

9. Huuk TC, Hahn T, Osberghaus A, Hubbuch J. Model-based integrated optimization and evaluation of a multi-step ion exchange chromatography. *Sep Purif Technol.* 2014;136(0):207-222.

10. Nfor BK, Ahamed T, van Dedem GWK, et al. Design strategies for integrated protein purification processes: challenges, progress and outlook. *J Chem Technol Biotechnol.* 2008;83(2):124-132.

11. Yu LX. Pharmaceutical quality by design: product and process development, understanding, and control. *Pharm Res.* 2008;25(4):781-791.

12. Julien C, Whitford W. A new era for bioprocess design and control, part 1: the basic concepts. *BioProcess Int.* 2008;6:16.

13. Nfor BK, Ahamed T, van Dedem GWK, et al. Model-based rational methodology for protein purification process synthesis. *Chem Eng Sci.* 2013;89(0):185-195.

14. Otero B, Degerman M, Hansen TB, Hansen EB, Nilsson B. Model-based design and integration of a two-step biopharmaceutical production process. *Bioprocess Biosyst Eng.* 2014;37(10):1989-1996.

15. Helling C, Borrmann C, Strube J. Optimal Integration of Directly Combined Hydrophobic Interaction and Ion Exchange Chromatography Purification Processes. *Chem Eng Technol.* 2012;35(10):1786-1796.

16. Forrester A, Sobester A, Keane A. *Engineering design via surrogate modelling: a practical guide.* Chichester: John Wiley & Sons; 2008.

17. Wang GG, Shan S. Review of metamodeling techniques in support of engineering design optimization. *J Mech Des N Y.* 2007;129(4):370-380.

18. Caballero JA, Grossmann IE. An algorithm for the use of surrogate models in modular flowsheet optimization. *AIChE J.* 2008;54(10):2633-2650.

19. Nagrath D, Messac A, Bequette BW, Cramer SM. A hybrid model framework for the optimization of preparative chromatographic processes. *Biotechnol Prog.* 2004;20(1):162-178.

20. Biegler LT, Grossmann IE, Westerberg AW. *Systematic methods of chemical process design.* Upper Saddle River, New Jersey: PTR Prentice-Hall; 1997.

21. Yeomans H, Grossmann IE. A systematic modeling framework of superstructure optimization in process synthesis. *Comput Chem Eng.* 1998:709–731.

22. Papalambros PY, Michelena NF. Model-based partitioning in optimal design of large engineering systems. Paper presented at: ICASE/NASA Langley Workshop on Multidisciplinary Design Optimization; March 13-16, 1997; Hampton, Virginia.

3

23. El-Mihoub TA, Hopgood AA, Nolle L, Battersby A. Hybrid Genetic Algorithms: A Review. *Engineering Letters.* 2006;13(2):124-137.

24. Kelner V, Capitanescu F, Uonard O, Wehenkel L. A hybrid optimization technique coupling an evolutionary and a local search algorithm. *J Comput Appl Math.* 2008;215(2):448-456.

25. Chong EKP, Zak SH. *An Introduction to Optimization.* Vol 76. Hoboken, New Jersey: John Wiley & Sons; 2013.

26. Kolda TG, Lewis RM, Torczon V. Optimization by direct search: New perspectives on some classical and modern methods. *Siam Review.* 2003;45(3):385-482.

27. von Lieres E, Andersson J. A fast and accurate solver for the general rate model of column liquid chromatography. *Comput Chem Eng.* 2010;34(8):1180-1191.

28. Mollerup JM, Hansen TB, Kidal S, Staby A. Quality by design--thermodynamic modelling of chromatographic separation of proteins. *J Chromatogr A.* 2008;1177(2):200-206.

29. Nfor BK, Noverraz M, Chilamkurthi S, Verhaert PD, van der Wielen LA, Ottens M. High-throughput isotherm determination and thermodynamic modeling of protein adsorption on mixed mode adsorbents. *J Chromatogr A.* 2010;1217(44):6829-6850.

30. Nfor BK, Zuluaga DS, Verheijen PJ, Verhaert PD, van der Wielen LA, Ottens M. Model-based rational strategy for chromatographic resin selection. *Biotechnol Prog.* 2011;27(6):1629-1643.

31. Athalye AM, Gibbs SJ, Lightfoot EN. Predictability of Chromatographic Protein Separations - Study of Size-Exclusion Media with Narrow Particle-Size Distributions. *J Chromatogr.* 1992;589(1-2):71-85.

32. Miller SF, King CJ. Axial Dispersion in Liquid Flow through Packed Beds. *AIChE J.* 1966;12(4):767-&.

33. Langford JF, Schure MR, Yao Y, Maloney SF, Lenhoff AM. Effects of pore structure and molecular size on diffusion in chromatographic adsorbents. *Journal of Chromatography A.* 2006;1126(1–2):95-106.

34. Hagan MT, Demuth HB, Beale MH, De Jesús O. *Neural network design.* Vol 20. Boston, Massachusetts: PWS publishing company Boston; 1996.

35. Rafiq MY, Bugmann G, Easterbrook DJ. Neural network design for engineering applications. *Comput Struct.* 2001;79(17):1541-1552.

36. Nfor BK, Ahamed T, Pinkse MW, et al. Multi-dimensional fractionation and characterization of crude protein mixtures: toward establishment of a database of protein purification process development parameters. *Biotechnol Bioeng.* 2012;109(12):3070-3083.

37. Tran R, Lacki K, Davidson A, Sharma B, Titchener-Hooker N. Changing manufacturing paradigms in downstream processing and the role of alternative bioseparation technologies. *Journal of Chemical Technology and Biotechnology.* 2014;89(10):1534-1544.

38. Soleimani R, Shoushtari NA, Mirza B, Salahi A. Experimental investigation, modeling and optimization of membrane separation using artificial

neural network and multi-objective optimization using genetic algorithm. *Chemical Engineering Research & Design.* 2013;91(5):883-903.

4

Chromatographic parameter determination for complex biological feedstocks

Abstract

The application of mechanistic models for chromatography requires accurate model parameters. Especially for complex feedstocks such as a clarified cell harvest, this can still be an obstacle limiting the use of mechanistic models. Another commonly encountered obstacle is a limited amount of sample material and time to determine all needed parameters. Therefore, this study aimed at implementing an approach on a robotic liquid handling system that starts directly with a complex feedstock containing a monoclonal antibody. The approach was tested by comparing independent experimental data sets with predictions generated by the mechanistic model using all parameters determined in this study. An excellent agreement between prediction and experimental data was found verifying the approach. Thus, it can be concluded that RoboColumns with a bed volume of 200 μL can well be used to determine isotherm parameters for predictions of larger scale columns. Overall, this approach offers a new way to determine crucial model input parameters for mechanistic modelling of chromatography for complex biological feedstocks.

Keywords: chromatography, high-throughput process development (HTPD), downstream processing (DSP), mechanistic modelling

Contents

4.1.   Introduction

Detailed models to predict chromatographic behavior are available nowadays. However, accurate model input parameters are needed to simulate chromatograms with little uncertainties. Some of these, for instance packing and mass transfer parameters, can be easily determined [1]. Others such as adsorption parameters pose a bigger challenge especially for complex biological feedstocks.

A commonly applied approach to determine such adsorption parameters is the inverse method [2-4]. Using such an approach that minimizes the difference between experimental chromatograms and the mechanistic model can give erroneous parameters in case the experimental conditions are not determined accurately even if the found residual is small [5]. Additionally, impurities eluting at almost identical conditions can hardly be identified with distinctive parameters. Another approach is the determination via batch uptake experiments, which can be performed in a high-throughput format [6,7]. However, the obtained parameters might not be as reliable as the ones determined in chromatography columns, since sufficient mixing cannot be ascertained in case of very low protein concentrations and/or large biomolecules [7]. In such cases, isocratic and linear gradient experiments on columns might be preferable.

Previously, such approaches involving column experiments have even been applied to complex feedstocks by performing multiple fractionation steps [8]. Subsequently, in efforts to save precious sample, Hanke et al. developed a 3D liquid chromatography approach that consists of: a pH gradient prefractionation as a first dimension to reduce sample complexity; a second dimension with gradient experiments to obtain isotherm parameters on RoboColumns, which have a bed volume of only 200 µL, and a final dimension of size exclusion chromatography to increase the resolution [9].

The aim of this article is to develop an improved high-throughput strategy for the determination of model input parameters for complex biological feedstocks. This article extends the approach by Hanke et al. to its use on robotic liquid handling systems to allow parallelization and time savings. The approach is also expanded to obtain parameters describing adsorption at the full range of protein concentrations, at which industrial processes are normally operated. For that, maximal binding capacities of the resin of interest are determined from fractions of the first dimension in batch-uptake

experiments in a high-throughput format. To see if protein-protein interactions have a significant impact on the adsorption behavior, the second virial coefficient of the main product, a monoclonal antibody, is determined. The second virial coefficient is commonly used to describe protein aggregation behavior [10,11]. Moreover, it has once been used in the formulation of a chromatography isotherm [12]. In this study, it is introduced as an alternative to the protein interaction parameter in Mollerup's thermodynamic framework [13] by reformulating the isotherm. Finally, the chromatography model with the newly determined parameters from crude clarified cell harvest is compared to experimental chromatographic results to show the validity of the overall approach.

4.2. Mechanistic chromatography model

The equilibrium transport dispersive model can describe the behavior inside a chromatography column with the following mass balance for the mobile phase (Equation 1):

$$\frac{\partial c_i}{\partial t} + \frac{1-\varepsilon_b}{\varepsilon_b}\frac{\partial q_i}{\partial t} = -v\frac{\partial c_i}{\partial x} + D_{L,i}\frac{\partial^2 c_i}{\partial x^2} \tag{1}$$

where c_i is the concentration in the bulk phase of protein i, ε_b is the bed porosity, v is the interstitial velocity of the mobile phase and can be calculated as $v = u/\varepsilon_b$ with u, the superficial velocity. $D_{L,i}$ is the axial dispersion coefficient. The concentration distributions inside the particles are not being considered in this model. This model is typically chosen for its simplicity and often sufficiently high accuracy [14].

The linear driving force approach for the mass transfer in the liquid phase was used to approximate the change in q_i, the concentration of protein i in the stationary phase, over time (Equation 2).

$$\frac{\partial q_i}{\partial t} = k_{ov,i}\left(c_i - c_{p,i}{}^*\right) \tag{2}$$

where $k_{ov,i}$ is the overall mass transfer coefficient. To calculate $c_{p,i}{}^*$, the concentration in the particle pores, an appropriate adsorption isotherm can be used. One example is the following mixed-mode isotherm developed within Mollerup's thermodynamic framework [13], which is valid for mixed-mode chromatography, ion-exchange chromatography and hydrophobic interaction in a nonlinear concentration range [15].

$$\frac{q_{p,i}}{c_{p,i}} = A_i \left(1 - \sum_{j=1}^{m} \frac{q_{p,j}}{q_{p,j}^{max}} \right)^{v_i + n_i} \tag{3}$$

The fraction of free ligands is shown in the term $1 - \sum_{j=1}^{m} \frac{q_{p,j}}{q_{p,j}^{max}}$, where q_p^{max} represents the maximum binding capacity; m stands for the number of proteins and j for the protein species. n_i is the stoichiometric coefficient in hydrophobic interaction chromatography. v_i is the stoichiometric coefficient for ion exchange chromatography, which can be calculated as z_p/z_s with z_p, the effective binding charge of the protein, and z_s, the charge on the salt counter ion.

The initial slope of the isotherm or partition coefficient, A_i, can be calculated by:

$$A_i = K_{eq,i} \Lambda^{(v_i + n_i)} (z_s c_s)^{-v_i} c_v^{-n_i} \gamma_i \tag{4}$$

where K_{eq} is the thermodynamic equilibrium constant, Λ the ligand density, c_s the salt concentration and c_v the molarity of the solution in the pore volume. The activity coefficient can be calculated as $\gamma_i = e^{K_{s,i}c_s + K_{p,i}c_{p,i}}$ given K_s, the salt-protein interaction coefficient or salting-out constant, and K_p, the protein-protein interaction coefficient. If salts with small salting out effects such as chlorides are used, K_s becomes negligible [16]. At very low protein concentrations, the contributions of protein-protein interactions are expected to be minimal, which is why K_p can be considered negligible. At these conditions A_i can be simplified to:

$$A_i = K_{eq,i} \Lambda^{(v_i + n_i)} (z_s c_s)^{-v_i} c_v^{-n_i} \tag{5}$$

The retention of a protein is determined by its size exclusion as well as its thermodynamic properties as described by the partition coefficient. The retention factor can, thus, be related to the partition coefficient with the following equation [17]:

$$k_i = \frac{(1-\varepsilon_b)\varepsilon_p K_{D,i}}{\varepsilon_b} (1 + A_i) \tag{6}$$

where the distribution coefficient $K_{D,i}$ describes the accessibility of the resin for each protein i.

At higher protein concentrations, however, the influence of protein-protein interactions should be taken into account. In the case of complex mixtures where one protein species is predominant, it can be assumed that protein-protein interactions are

solely of importance between proteins of this single protein species i. Then, the molar activity coefficient can be approximated by [18,19]:

$$\ln \gamma_i = 2B_{ii}c_{p,i} + \dots \tag{7}$$

where B_{ii}, or B_{22}, is the second osmotic virial coefficient, which takes into account deviations from ideal behavior that stem from interactions of two protein molecules of the same species [20]. It was assumed that interactions of more than two molecules are negligible. With that and due to the low salting-out effect of chloride, the activity coefficient for the predominant protein species was simply defined as:

$$\gamma_i = e^{2B_{22}c_{p,i}} \tag{8}$$

4.3. Material & methods

4.3.1. Gradient chromatofocussing prefractionation

The prefractionation was performed as described by Hanke et al. [9,21]. The complex sample used for this study is a clarified CHO cell culture supernatant containing a monoclonal immunoglobulin G (IgG1) with a concentration of 1.3 mg/mL. The pI of IgG1 was determined to be 8.6 by capillary isoelectric focusing. Prior to use, the samples were rebuffered using disposable PD-10 columns, following the manufacturers protocol (GE Healthcare, Sweden). As a first separation dimension, the samples were fractionated by linear pH-gradient chromatography on a Mono Q 4.6/100 strong anion exchange column (GE Healthcare, Sweden) or a Mono S 4.6/100 strong cation exchange column (GE Healthcare, Sweden).

4.3.2. High-throughput isocratic chromatography

Parts of this section have been taken and adapted from Hanke et al. [9,21,22].

Column characterization

The columns used were 200 µl RoboColumns (Repligen, Germany), packed with two different resins as described in Table 1. An Äkta Explorer 10 (GE Healthcare, Sweden) with a custom made adaptor was used to analyze the porosity and pore accessibility of these columns. A 1100 series refractive index detector (Agilent, CA, US) allowed to

measure the retention volumes of dextrans with varying sizes (180 – 6 300 000 Da). The distribution coefficient K_D was calculated as in [23]:

$$K_D = \frac{\frac{\mu_1}{V_{col}} - \varepsilon_b}{1 - \varepsilon_b} \tag{9}$$

where μ_1 is the mean retention volume or first moment of the peak corrected for the system dead volume, which is usually determined with a tracer without having a column attached, and the dead volume in the column itself. The column dead volume is very important in miniature columns such as the RoboColumns, since the ratio of column volume (V_{col}) to column dead volume is smaller. In previous studies, it was found to be 30 µL [9]. The bed porosity ε_b generally lies in between 0.3 and 0.4 for packed chromatography columns.

The intraparticle porosities, $\varepsilon_{p,n}$, and pore radii, $r_{pore,n}$, were determined by fitting the following equations (10 and 11) [24] to the K_D data using MATLAB's function *lsqcurvefit*:

$$K_{D,n} = \left(1 - \frac{r_h}{r_{pore,n}}\right)^2 \tag{10}$$

The amount of different pore types, n, is two for a resin with bidisperse pores such as POROS 50 HS. The hydrodynamic radii r_h for the dextranes were calculated with their molecular mass M according to an empirical correlation reported in [25] ($r_h = 0.0271\,M^{0.498}$). The total intraparticle porosity for a resin with two pore types was than calculated as $\varepsilon_p = \varepsilon_{p,1} + \varepsilon_{p,2}$ where $n = 1$ represents the macropores and $n = 2$ the micropores. The overall K_D for both pores is defined as [26]:

$$K_D = \varepsilon_{p,1} K_{D,1} + \varepsilon_{p,2} K_{D,2} \tag{11}$$

Isocratic chromatography

The high-throughput liquid chromatography experiments were performed on a Freedom Evo 200 liquid handling workstation equipped with an 8-channel liquid handling arm fitted with 1 ml syringes and Te-Chrom station (Tecan Switzerland). These systems are neither equipped with dual-piston pumps, nor with inline detectors. Instead single piston pumps apply a liquid flow, fractions are collected at the column outlet by a 96 well plate placed on a motorized shuttle, and analysis takes place offline. These mechanical simplifications require some adaptions to the experimental

approach, to allow generation of data that is straightforward comparable to experiments performed on traditional systems.

Prior to each chromatographic experiment, a sufficient volume of buffer for both column equilibration and elution was mixed from stock solutions by the liquid handling system. The two stock solutions were prepared with MiliQ at a low salt and a high salt concentration. The mixing ratios were chosen to result in eight different final salt concentrations in the desired ranges. Specifications for each resin and the respective buffers are given in Table 1.

Table 1: Resin and corresponding buffer specifications

Resin	Supplier	Type	dp [µm]	pH	Buffer type	Buffer [mM]	Salt type	Salt range [mM]
Poros 50HS	Applied Biosystems	Strong CEX	50 [27]	4.5	Acetic acid	25	Sodium chloride	0 - 500
Capto MMC	GE Healthcare	MMC	85 [26]	6.75	MOPS	25	Sodium chloride	0 - 350

Samples collected from the prefractionation gradient were transferred into a low salt buffer through at least 3 buffer exchange cycles in Amicon spin filters with a nominal molecular weight cut-off of 3 kDa (Millipore, USA) following the protocol recommended by the manufacturer. After rebuffering, each sample was split into eight aliquots and appropriate volumes of low and high salt buffer were added to result in eight samples of equal protein content and pH, but with salt concentrations corresponding to the eight prepared elution buffers.

Prior to injection each column was equilibrated with 5 column volumes (CV) of elution buffer. The injection volume to each column was 20 µl. The samples were eluted with a total of 15 CV of elution buffer at a flowrate of 0.15 ml/min per column. During the isocratic elution a total of 22 samples were collected from each column. The first twelve fractions had a target volume of 75 µl and were collected in a half area UV-star plate (Greiner-Bio One, the Netherlands). Afterwards six additional fractions with a target volume of 150 µl were collected in a full area UV-Star plate (Greiner Bio-One, the Netherlands), followed by four more with a target volume of 300 µl. This staggered fractionation strategy was chosen as a compromise between high resolution at the beginning of the experiment where sharp and narrow peaks were expected and a low

total number of fractions. The columns were subsequently cleaned with 5 CV of washing buffer of which the first 600 µl were collected in two fractions with a target volume of 300 µl each. Once this step had been completed both fractionation plates were passed on to the plate reader for analysis. Prior to the next experiment each column was sanitized with 5 CV of sanitation buffer.

Fraction volume estimation

One of the main technical challenges in the operation of RoboColumns on a conventional liquid handling system, is that the fractionation intervals, the moments at which the collection plate shuttle moves from one column of wells to the next, are defined in relation to the syringe motor position that applies flow to the columns. As there is no reliable mechanism to synchronize the falling of drops from the column outlet, and the size of the drops themselves may vary with changes in buffer composition and protein content, the volume that actually ends up in each well may vary significantly, especially when the target fraction volume is small. It is therefore necessary to measure the volume of each well in order to reduce the experimental noise that would be caused by assuming a constant fraction volume [28]. The method is described in detail in [22].

Reconstruction of high-throughput chromatograms

As high-throughput chromatography systems, such as the Te-Chrom used in this study, do not possess in-line detection systems, chromatograms need to be reconstructed from the measurements performed on the collected fractions. The transmission path and total well volume of each collected fraction were calculated as according to the approach outlined in the preceding section. To reduce the noise in the absorption signals each value is corrected for the absorption at 330 nm and normalized against the estimated transmission path. To determine the position of each normalized absorption in the reconstructed chromatogram, the volume of all preceding fractions is summed up and added to half the volume of the corresponding fraction.

Deconvolution and peak moment calculations

To estimate the number of peaks in each chromatogram, each data set was scanned for data points fulfilling the following criteria: they had to have a normalized 230 nm absorption of at least 0.1 mAU/cm and this value needed to be larger than both the neighboring fractions. For practical purposes related to the small number of available

data points per chromatogram only the largest four points fulfilling these criteria were considered for further analysis. The heights and positions of the local maxima identified by this algorithm were used as initial guesses for a least-squares based fitting of peak model to the reconstructed chromatogram. To estimate good parameters for components with much lower concentrations than the IgG1, parameter fitting was carried out several times for different ranges of the size exclusion chromatogram. This also reduced the time needed for the parameter fitting in general, since much less peaks were included each time.

The function chosen for fitting was based on a one-dimensional adaption of the model for multiple superimposed exponentially modified Gaussian peaks described in a previous study [21]. Instead of minimizing the squares between the measured data point and the curve described by the peak model, the average of the model curve was calculated over each fraction interval, and the squares between this value and the measurement were minimized. The fitting was carried out in MATLAB using the built-in *lsqcurvefit* function. All parameters were normalized for the regression. Computation was performed in parallel on four cores using MATLAB's Parallel Computing Toolbox[TM]. The areas and first moments of the fitted peaks were calculated together with their standard errors of regression following the same principles as in [21].

Parameter fitting

The resulting peak moments were used to calculate the retention factors, k_i, defined by [23]:

$$k_i = \frac{\mu_{1,i} - V_0}{V_0} \tag{16}$$

V_0 is the column void volume ($\varepsilon_b V_{col}$). With that, the combination of equation 5 and 6 allows the regression of relevant isotherm parameters based on the peak moments at the used experimental conditions. For the cation exchange resin POROS 50 HS, the stoichiometric coefficient for HIC, n, can be set to 0. At the investigated pH and salt type, chromatographic behavior seemed to be sufficiently well described on Capto MMC using only the ion exchange part of the adsorption isotherm, although Capto MMC is a mixed mode resin. Therefore, also here n was set to 0 simplifying the isotherm.

The regression was performed with MATLAB's *lsqcurvefit function.* The termination tolerance for the objective function value (*FunTol*) and the parameter (*TolX*) were set to 10^{-12} and the maximum number of iterations allowed to 1000.

4.3.3.   Batch uptake experiments

Additionally, the fractions containing the IgG1 were analyzed further to determine the maximal capacity. For that, batch uptake experiments were performed in 96 well filter plates. The resin volume of 7.8 µL was dispensed with help of the MediaScout Resiquot (Repligen, Germany) as described in [29]. Even though the volume dispensed by the Resiquot is quite accurate, less particles might be present than in a packed column because of a smaller packing density [30,31]. In this study, a factor of 1.06 was applied as suggested by the supplier for POROS 50 HS [32]. For Capto MMC, no packing factor was used.

For each resin, the residual amount of liquid staying inside the resin after centrifugation, the liquid hold-up volume, was determined according to a protocol described by Nfor et al [15]. Before usage, the resin plaques were equilibrated with 300 µL of the respective buffer. For that, they were incubated at 1300 rpm for 5 min and afterwards centrifuged at 4000g. The equilibration procedure was repeated once. The corresponding buffer solutions are shown in Table 1. The salt concentration for Capto MMC and Poros 50 HS was 0 M. The plates were incubated for two hours at 1300 rpm at room temperature. To minimize evaporation, they were covered with a self-adhesive foil. In order to verify the maximal capacities, additional batch uptake experiments were performed with a sample of the product that was purified with a protein A column.

The regression was performed with MATLAB's *nlinfit function*, because it allows weighted regression. Weights were proportional to the standard error attached to each data point. Otherwise, the same settings as in the previous section were applied. The fitting function here was Equation 3 with only q_p^{max} as variable.

4.3.4.   Self-interaction chromatography

In the clarified cell harvest, IgG1 has a much greater concentration than any other protein. Therefore, it was assumed that only the activity coefficient for IgG1 needs to be known and thus, its second osmotic virial coefficient B_{22}. The B_{22} was determined

by self-interaction chromatography using prepacked HiTrap NHS-activated HP columns (GE Healthcare, Sweden) on an Äkta Avant 25 chromatography system (GE Healthcare, Sweden). The HiTrap columns were flushed with 6 ml of an ice-cold 1 mM HCl solution to wash out the storage solution, isopropanol, as suggested by the manufacturer. A buffer of 0.2 M NaHCO3 and 0.5 M NaCl at pH 8.5 was used as a coupling buffer. The IgG1 sample, which was purified with a Protein A column, was supplied by Synthon. The coupling buffer was exchanged with Amicon Ultra-4 Centrifugal filters (Merck Millipore, the Netherlands) by centrifuging multiple times for 15 min at 4000xg. Each time, the sample was diluted 2:1 with the coupling buffer to prevent aggregation. The final solution contained 3 g/L IgG1. For coupling, it was recirculated with a flowrate of 1 ml/min over the column for 4 h at around 4°C to ensure uniform coupling [33]. The coupling solution was washed out with 3 CV of coupling buffer. The concentration of the eluent containing the IgG1 was measured at UV 280 nm to determine the amount of IgG1 that was immobilized onto the column. Subsequently, the surface coverage was calculated as described by [11] to be 12.3 %, which falls in the range of recommended surface coverage [33]. Finally, any excess active groups were deactivated according to the protocol by the manufacturer of the columns.

According to the approach described by Ahamed et al [11], the retention volume of the IgG1 without protein-protein interactions was measured in an additional HiTrap column without immobilized antibody. It was generated according to the same deactivation protocol. This column assumedly acts only as a size exclusion column. For each solution condition, experiments were performed in the blocked column and adjusted with the following correlation to account for integrity differences:

$$V_0 = aV_{0,b} + b \tag{17}$$

where a and b are determined from the retention data of acetone and dextran in the immobilized column as a function of their retention in the blocked column ($V_{0,b}$). For that, 50 μL of a 1% acetone solution and a solution of 2 g/L blue dextran in a 50 mM Tris-HCl and 100 mM KCl buffer at pH 7.5 were injected and eluted at 1 mL/min; in case of blue dextran, 1 M NaCl was added for the elution. Here, a was found to be 0.25 and b 0.32.

The retention volumes were measured for IgG1 in both buffers (25 mM of MOPS or acetate buffer) with salt concentrations ranging from 0 to 1 M and from pH 4.5 to 7.5

on each column in duplicate. For that, the columns were first equilibrated with 10 CV of the respective buffer with a flowrate of 0.5 mL/min. The protein in the correct buffer with a concentration of 1.5 g/L was then injected and flushed with 5 CV of the respective buffer. Afterwards, the column was washed with 3 CV of 0.5 M NaCl.

A second order polynomial function was fitted to the determined B_{22} values using MATLAB's *fit* function with the robust bisquare weights method. The polynomial was defined as following:

$$B_{22} = b_1 + b_2\ pH + b_3\ c_s + b_4\ pH\ c_s + b_5\ pH^2 + b_6\ c_s^2 \qquad (18)$$

The resulting B_{22} was in the units (mol mL)/g^2. To use the determined B_{22} in the mechanistic model as shown in equation 8, the units needed to be changed to L/mol by multiplying with the squared molecular weight and dividing by 1000.

4.3.5. Validation experiments

Validation experiments were performed on OPUS® ValiChrom 11.3/100 columns prepacked with the respective resins by Repligen (Germany) on an Äkta Avant 25 (GE Healthcare, Sweden). The flowrate was 400 cm/h. An additional validation run was performed with a column with a bed volume of 14.8 mL packed with POROS 50HS. The flowrate was 400 cm/h. Linear gradients of 12 CV were used during the elution in all validation experiments. All columns were stored in 20% Ethanol. Absorption was recorded at 210, 230 and 280 nm.

4.3.6. Protein quantification by size exclusion chromatography

All protein concentrations were determined in a UHPLC$^+$ (Thermo Fisher Scientific, MA, USA) system as described by Hanke et al. [9].

4.3.7. Modelling techniques

Mechanistic modelling was applied as described in [34]. All correlations to determine relevant parameters are shown in Table 2.

Table 2: Mass transfer correlations

Parameter	Correlations
Free Diffusivity	Young [35]
Film Mass Transfer Coefficient	Wilson & Geankoplis [36]
Pore Tortuosity	Suzuki & Smith [37]
Pore Diffusivity	Brenner & Gaydos [38]
Axial Dispersion Coefficient	Gunn [39]
Hydrodynamic radius	Stokes Einstein [40]

4.4.   Results & discussion

4.4.1.   Prefractionation and reference chromatogram

The prefractionation experiments and the corresponding two-dimensional reference maps are shown in Figure 1 and Figure 2. For the anion exchange prefractionation (Figure 1a and b), Peak 2 corresponds to IgG1, the product. The proteins, whose peaks are identified with the IDs 1-8, have very similar charge properties. This includes a high molecular weight protein marked with ID 5. The large difference in elution-pH of peaks 9-17 in relation to the product, indicates that these impurities could easily be removed and, thus, they will be considered as non-critical impurities further on. Consequently, only the fractions of interest as marked in the prefractionation chromatogram (Figure 1 a) were analyzed in detail. In the cation exchange prefractionation (Figure 2), IgG1 is represented by ID 1. Here, much fewer contaminants were found to elute in the gradient indicating it to be a better mode of separation than anion exchange. Only one critical impurity, Peak 2, was identified. Therefore, only the two fractions as shown in Figure 2 a were analyzed further.

(a)

(b)
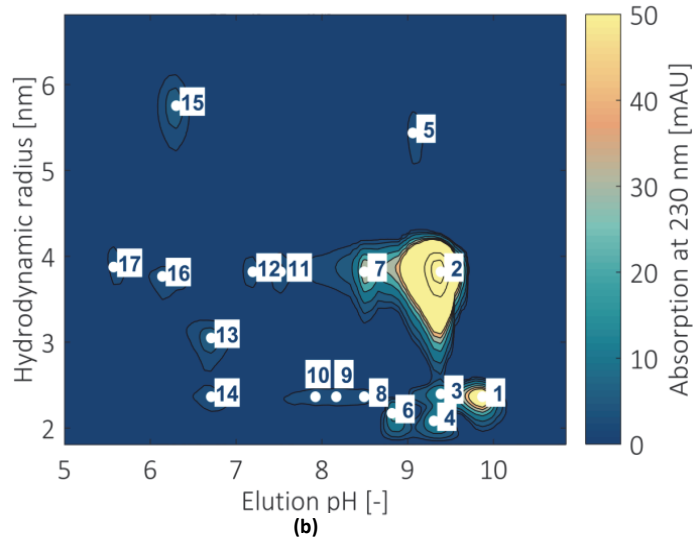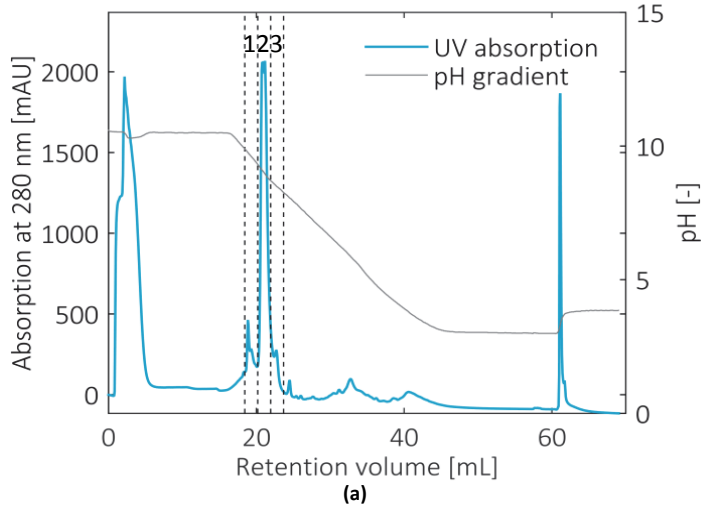
Figure 1: Prefractionation step on the AEX

Fractions of interest are marked by 1, 2, 3; b: Two-dimensional reference chromatogram generated by an additional SEC analysis of the fractions from (a). Proteins are marked at their peak maximum according to the peak finding algorithm. The ones with the IDs 1-8 (b) are contained in the fractions of interest. The absorption scale was cut at 50 mAU to also show contaminants at low concentrations. (b) was adapted from [22].

(a)

(b)
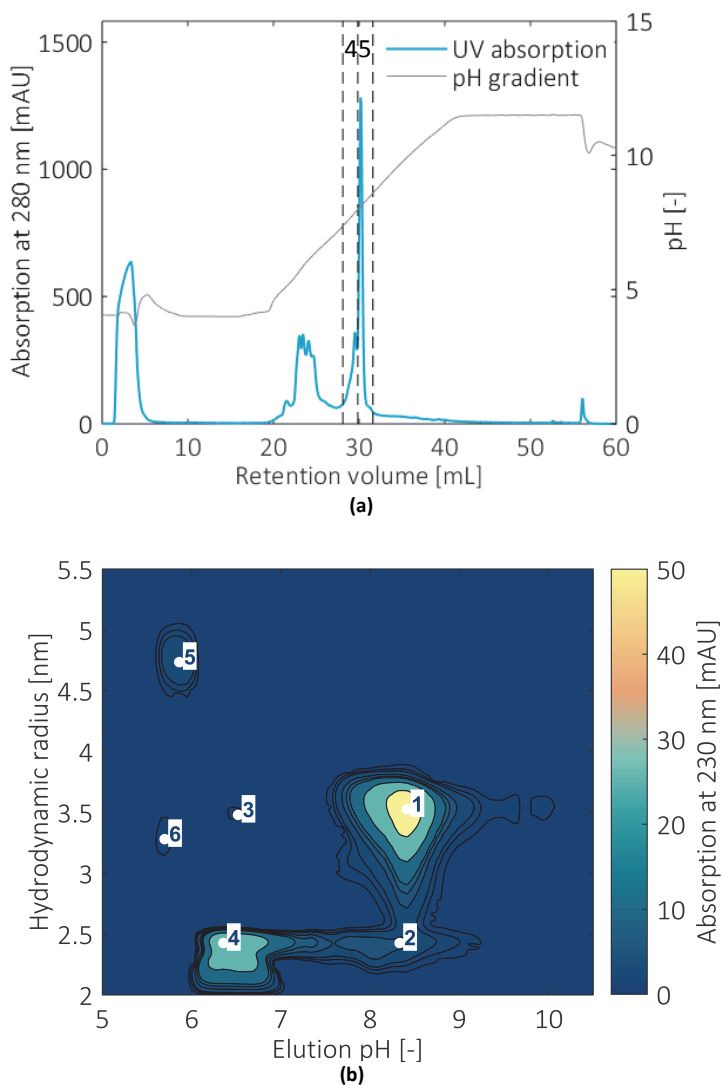
Figure 2 Prefractionation step on the CEX (a) column

Fractions of interest are marked by 4 and 5; b: Two-dimensional reference chromatogram generated by an additional SEC analysis of the fractions from (a). Proteins are marked at their peak maximum according to the peak finding algorithm. The ones with the IDs 1-2 (b) are contained in the fractions of interest. The absorption scale was cut at 50 mAU to also show contaminants at low concentrations. (b) was adapted from [21].

4.4.2. High-throughput isocratic experiments

Resin and column characteristics

The RoboColumns were characterized by pulse injections of dextran standards. The distribution coefficients, K_D, as calculated by Equation 9 are shown in Figure 3. The observed trend is typical for particles with bidisperse pores: First, K_D decreases with increasing hydrodynamic radius, which means that the bigger the particles the less access to the micropores they have; after around 10 nm, the curve starts levelling off, since now the access to the macropores is determining the behavior of the curve. Due to the big macropores, not even the largest dextrans are fully excluded from the particle pore volume. This is why the bed porosity cannot be calculated from the retention volume of the biggest dextran. For the RoboColumns, the bed porosity was assumed to be identical for all RoboColumns with the same resin (0.3 for POROS 50 HS and 0.35 for Capto MMC). For the validation columns, the bed porosity was determined to be 0.34 for POROS 50 HS and 0.36 for Capto MMC solving the Blake-Kozeny equation, which describes the change in pressure drop with linear flow.

Fitting Equation 10 and 11 to the data resulted in the pore radii and porosities with their 95 % confidence interval as presented in Table 3. The smaller pores (8.2 nm) are hardly accessible for IgG1 with its calculated hydrodynamic radius of 4.3 nm. The parameters as determined here mostly lie within the standard error of the parameters determined in [41] for POROS 50 HS although the porosity of the micropores is slightly
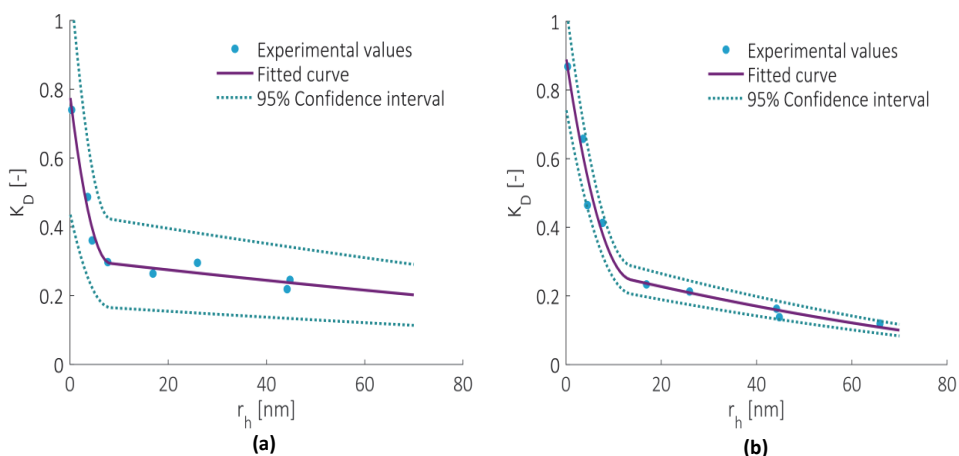

Figure 3: Calculated K_D values of the Dextran standards, the fitted K_D curve and its 95% confidence interval for POROS 50 HS (a) and Capto MMC (b)

higher, which might be explained by batch to batch variation. The total particle porosity varies more drastically, because it was calculated with a different equation than in [41]. Overall, this shows that RoboColumns can well be used to determine resin properties such as porosities and pore sizes despite their small bed volume.

The same procedure was applied to RoboColumns filled with Capto MMC. In [26], it was assumed that the pore distribution in this resin is monodisperse and a good fit with the data was shown. However, only dextrans with a hydrodynamic radius of up to around 8 nm were used. Our data, which is very similar for smaller hydrodynamic radii, clearly shows with higher hydrodynamic radii that also Capto MMC has a bidisperse pore distribution. The behavior is very similar to POROS 50 HS, although the micropores have a slightly bigger radius and a higher porosity. Additionally, the macropores are smaller.

During the modelling, the pore diffusion was simply calculated as a combination of the diffusion in the macro- and the micropores taking into account their respective porosities:

$$D_p = \varepsilon_{p,1} D_{p,1} + \varepsilon_{p,2} D_{p,2} \tag{18}$$

The pore diffusion in the macro- and micropores was calculated as suggested in [23]. Based on the findings in [41], intraparticle convection is assumed to be negligible at the comparably low flow rates applied in this study regardless of the big pore radius of the macropores.

Table 3: Resin characteristics in POROS 50 HS and Capto MMC; values are given with their standard error

	POROS 50 HS [41]	POROS 50 HS, this study	Capto MMC, this study
macropore radius [nm]	470 ± 10.0	370.5 ± 78.00	168.8 ± 21.60
macropore porosity [-]	0.32 ± 0.01	0.31 ± 0.01	0.29 ± 0.02
micropore radius [nm]	11 ± 4.00	8.2 ± 0.40	13.6 ± 0.80
micropore porosity [-]	0.41 ± 0.01	0.48 ± 0.02	0.61 ± 0.03
total particle porosity [-]	0.60 ± 0.01	0.79 ± 0.02	0.90 ± 0.03

The ligand density Λ is another critical parameter that defines the adsorption of the compounds to the resin and is thus needed for the calculation of the isotherm (Equation 4 and 5). Data for it is available in literature: For POROS 50 HS, the ligand density per adsorber skeleton was reported to be 0.276 M with acid-base titration [30]; for Capto MMC, the ligand density per particle volume was reported as 0.128 M [26].

Isocratic chromatography

Each fraction of interest was analyzed with isocratic experiments at different salt concentrations on RoboColumns containing the respective resin (1, 2 and 3 on POROS 50HS; 4 and 5 on Capto MMC). Fractions collected here were further analyzed with size exclusion measurements, to increase resolution and sensitivity [9], and UV measurements, to determine the well volume. Typical results of these experiments are shown in Figure 4. In the shown example, fraction 2 as marked in Figure 1 a) was subjected to different salt concentrations. With increasing salt concentration, the proteins (ID 3 and ID 4 detected in the shown range of hydrodynamic radii) elute
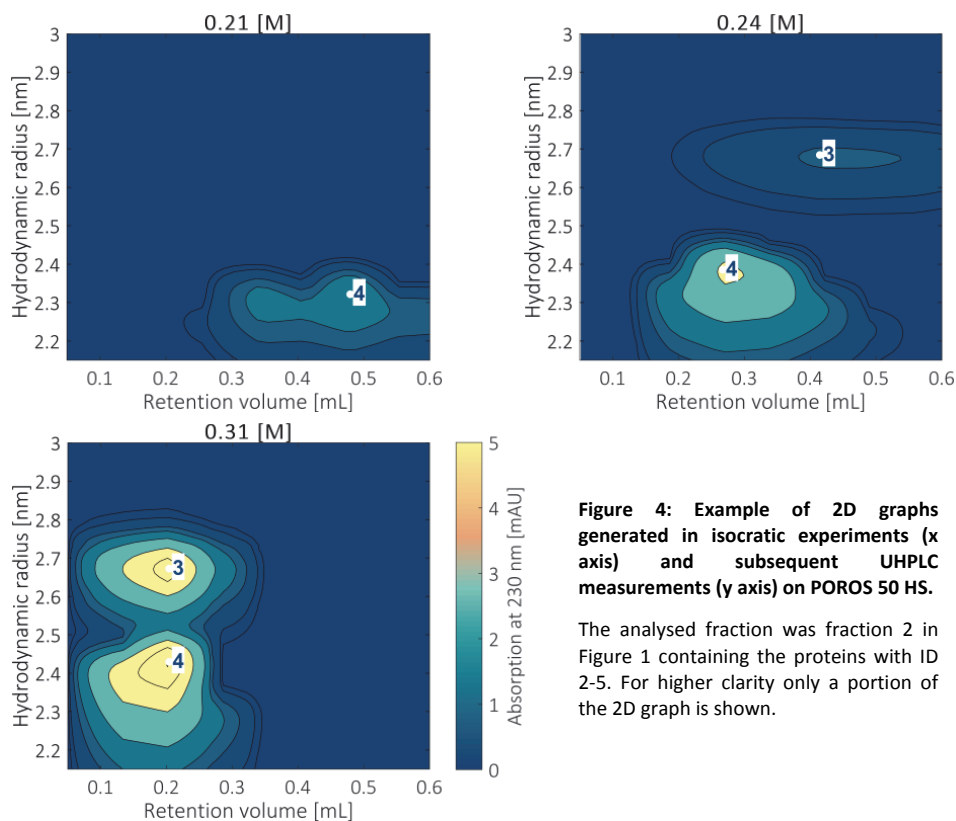

Figure 4: Example of 2D graphs generated in isocratic experiments (x axis) and subsequent UHPLC measurements (y axis) on POROS 50 HS.

The analysed fraction was fraction 2 in Figure 1 containing the proteins with ID 2-5. For higher clarity only a portion of the 2D graph is shown.

earlier, which is typically expected in ion exchange chromatography. The additional UHPLC measurements resulting in the y axis make a clear distinction between the two proteins possible. Moreover, they allow the sequential regression of isotherm parameters for different ranges of hydrodynamic radii, which greatly improves the quality of parameters regressed for low concentrated proteins.

Figure 5 summarizes the results for all proteins of interest by plotting their first moments depending on the salt concentration. For Capto MMC, both proteins were present in fraction 4 and 5. Different retention volumes were found especially for the IgG1 (here shown with ID 1) depending on the fraction it was contained in. Since the protein concentrations were low in all RoboColumn experiments, this is most likely not due to competition or interaction effects between the proteins. Thus, it is unclear what causes this difference in behavior. These first moments were then used to fit the relevant isotherm parameters K_{eq} and ν as reported in Table 4. For Capto MMC, the final parameters are the average of the parameters fitted for each fraction. The curves shown in Figure 5 were created with the fitted parameters. The protein with ID 5 could not be eluted under the salt concentrations applied during the experiments. Thus, no isotherm parameters could be fitted.

Table 4: Isotherm parameters regressed from retention volume curves determined in RoboColumns with their standard deviation

Resin	Protein	rh [nm]	K_{eq} [-]	ν [-]
POROS 50 HS	ID 1	2.4	12.6 ± 0.54	2.9 ± 0.5
POROS 50 HS	ID 2	4.2	34.6 ± 1.7	9.8 ± 1.3
POROS 50 HS	ID 3	2.7	2.2 ± 0.2	7.4 ± 0.7
POROS 50 HS	ID 4	2.2	177.1 ± 16.1	5.4 ± 1.1
POROS 50 HS	ID 6	2.2	0.9 ± 0.8	7.0 ± 0.3
POROS 50 HS	ID 7	4.2	2.0 ± 0.2	2.5 ± 0.2
POROS 50 HS	ID 8	2.4	0.2 ± 0.1	16.9 ± 6.4
Capto MMC	ID 1	4.2	51.5 ± 2.1	3.6 ± 0.4
Capto MMC	ID 2	2.8	16.6 ± 5.8	4.7 ± 1.6

rh: hydrodynamic radius; K_{eq}: equilibrium constant; ν: stoichiometric coefficient

4.4.3.   Batch-uptake experiments

Isotherms were determined under maximum binding conditions for both, an antibody purified with a Protein A step and the fractions from the prefractionation that contain mostly the antibody. Both sample types were chosen to understand if the small amounts of impurities present would influence the maximum binding capacity. For the modelling shown in section 4.4.5, the maximum capacities were used that were determined with the fractions from the prefractionation as sample type. For all impurities, the resin capacity was assumed to be non-limiting, since their smaller size allows them access to pore space not available for IgG1 [42]. Therefore, the maximal capacity of the resin was only analyzed for IgG1; results are shown in Figure 6 for both
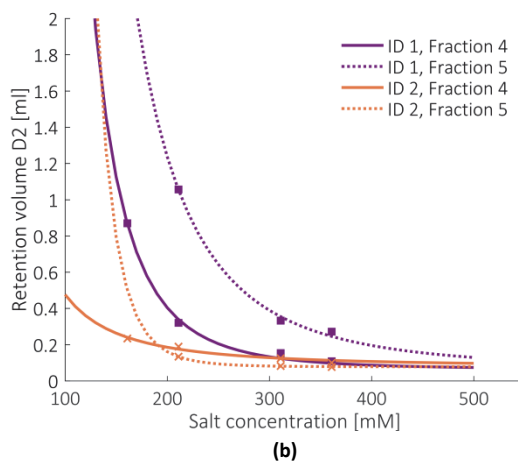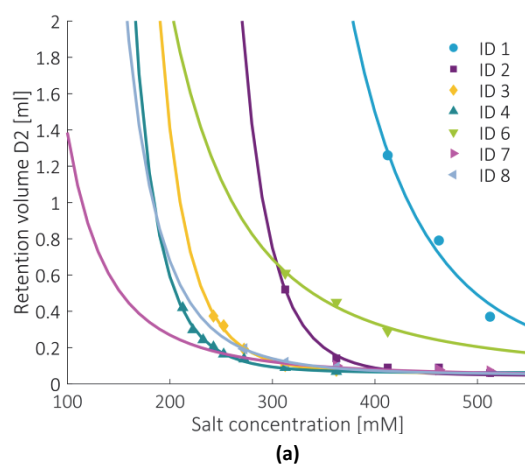
4

(a)

(b)

Figure 5: Experimental retention volumes (marker) and the respective fitted curves (lines) for all critical proteins on POROS 50HS (a) and Capto MMC (b)

resins.

On POROS 50 HS, a maximum capacity of 49.0 $\pm$ 0.7 g/L was found for the purified mAb, while a maximum capacity of 44.2 $\pm$ 0.2 g/L was determined for the antibody contained in the fractions. This might be due to competition in the fractions between other impurities and IgG1. In literature, a slightly higher value of 58 g/L is reported for a different IgG [27]. One possible reason could be that the packing factor might be higher than 1.06 as stated by the supplier [32] when applying the resin with the ResiQuot, as was already observed previously [30]. Moreover, it could likely be caused by a difference in the antibody itself, the ionic strength of the solution or resin lot variability.

On Capto MMC, a maximum capacity of 66.4 $\pm$ 3.1 g/L was regressed for purified IgG1 and 77.4 $\pm$ 2.1 g/L for IgG1 in the fractions. The determined capacities fall into similar ranges as reported for another IgG in the literature on Capto MMC [43]. The disparities between both values might be explained by the poor fit of the experimental values for the purified antibody with the predicted slope determined in the RoboColumn experiments. If a smaller slope was used during parameter regression, a higher maximal capacity would have been regressed. Still, the predicted slopes fit well with all other experimental data sets. A slight change of ionic strength in the buffer solution might be an explanation for the experiments with purified antibody on Capto MMC, since it was not measured in this study. Thus, it would be recommended to measure the ionic
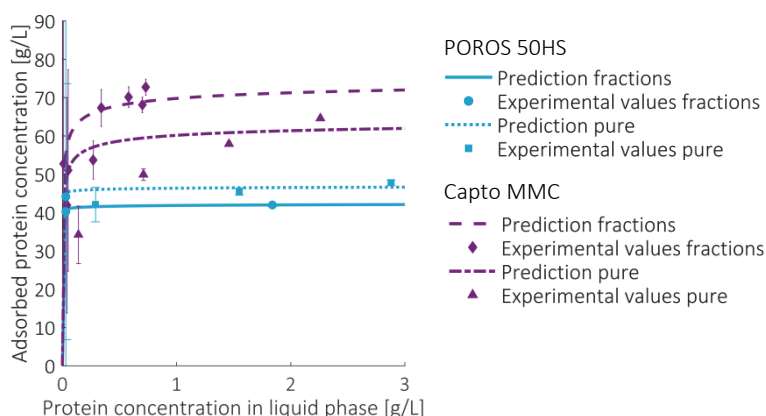

Figure 6: Determination of the maximal capacity for mAb on POROS 50 HS and Capto MMC

The predicted lines were created by using the isotherm slope determined in the RoboColumn experiments with the maximum capacity as a fitting parameter. Values determined above 3 g/L are not shown.

strength in each well directly in future studies.

4.4.4.   Protein-protein interactions

Figure 7 summarises the B_{22} values that were determined for IgG1 with varying salt concentrations and pH. The resulting second order polynomial functions were plotted for each buffer in the investigated range. The constants for both polynomials can be found in Table 5. In the acetate buffer (a), all B_{22} values fall into the so-called 'crystallization slot', which covers B_{22} values between -1×10^{-4} and -8×10^{-4} $mol*ml/g^2$ and is characterised by weak attractive protein interactions [44]. Also in the MOPS buffer (b), the B_{22} values are always negative indicating attraction. Here, however, the attraction is even weaker than in the acetate buffer suggesting higher protein stability. This difference might be explained by the zwitterionic nature of MOPS, since zwitterions do not contribute to the ionic strength of a solution [45].

Additionally, pH and salt concentration seem to have an almost negligible influence on the B_{22} values obtained in the MOPS buffer. Such comparably small changes for B_{22} values of monoclonal antibodies were already reported previously and explained with the ionic strength of the buffer system [46]. In that explanation, buffer and salt ions are shielding protein charges and, therefore, limit electrostatic interactions as well as the resulting changes in the B_{22} values.

Table 5: All constants for the second order polynomial as defined in equation 18. They need to be multiplied with 10-4.

	b1	b2	b3	b4	b5	b6
Acetate buffer	6.791	-2.794	1.249	-0.575	0.237	1.474
MOPS buffer	2.119	-0.807	-0.199	0.222	0.046	-1.013

This theory might be true, since the change of pH has its strongest influence at the lowest salt concentration. Nevertheless, the influence of salt concentration and pH on B_{22} values is stronger in the acetate buffer, which has a higher ionic strength. Compared to literature data, however, where B_{22} data was shown to vary for instance between 10×10^{-4} and -15×10^{-4} $mol*ml/g^2$ for lysozyme with changing pH and NaCl concentration [47], even the values reported here for the acetate buffer vary only slightly (1.5×10^{-4} $mol*ml/g^2$).

A minimum of B_{22} values can be found at the highest salt concentration and the highest pH. This is logical, since salting out is typically strongest at the highest salt concentration. Additionally, the charge of IgG1 is lower the closer the pH is to its pI (for IgG1, the pI is typically between 8 and 9). The higher positive charge at lower pH values will result in increased repulsive interactions and, thus, an inreased B_{22}.

In Figure 8, experimental values are compared with the values predicted by the fitted second order polynomial function. In general a good correlation was found between predicted and experimental data. Since there was a higher variation in the B_{22} values of the acetate buffer, two additional experimental data points were determined that were
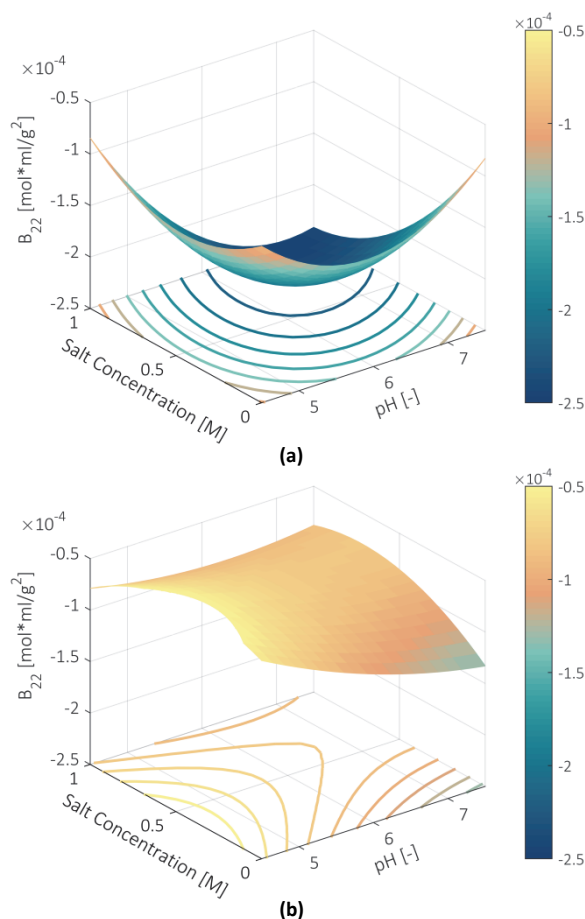

(a)

(b)

Figure 7: B_{22} values of IgG1 as a function of salt concentration and pH

Second order polynomial functions that were fitted on experimental data determined with the acetate buffer (a) and the MOPS buffer (b)
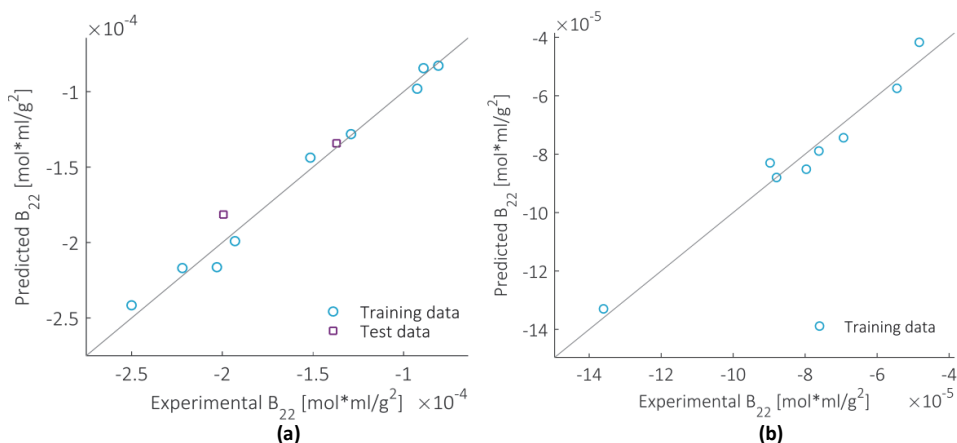
Figure 8: Comparison of experimentally obtained B$_{22}$ values with values given by the polynomial function for the acetate buffer (a) and the MOPS buffer (b)

not included in the data set used to fit the polynomial. As can be seen in Figure 8 b, these two test data points were as well predicted by the polynomial as the data points used for the fitting.

4.4.5. Model validation

Finally, all determined parameters were used as model input parameters for the mechanistic model to simulate the critical proteins. Experiments were performed at identical conditions at lab scale with the clarified cell harvest to evaluate the accuracy of the model predictions.

In Figure 10 a, b and c, results can be seen for POROS 50 HS and Capto MMC under low loading conditions. The applied sample is the clarified cell harvest after a buffer exchange. In both predictions, tailing of IgG1 is underestimated, which becomes especially obvious in the zoomed chromatogram shown in Figure 10 b. UHPLC analysis showed that this tailing was caused by dimerization or higher levels of aggregation. Besides that, an overall good agreement between predictions and experimental data can be observed. This can lead us to two conclusions. First, the critical impurities were defined well in the prefractionation. If these critical impurities were to be removed by the respective chromatographic step, the purification step would be successful. Second, isotherm parameters for low protein concentrations can be determined in RoboColumns without any extra modifications during scale-up. This was expected, because isotherm parameters cover the thermodynamics of protein adsorption in resin

beads, which should be identical at an increased scale. Packing parameters and flow behavior are of course changed.

Additionally, the model was tested at different high protein loadings. The sample was purified with a Protein A column prior to sample application. One example is shown for a protein load of 20 g/L of resin on POROS 50HS in Figure 9. The predicted peak elutes slightly later than the experimental one. This can be caused by a small difference in ligand density, which can vary for example due to resin lot variation [48]. Another possibility could be that protein-protein interactions are not only taking place between two molecules, but even more. In that case, higher virial coefficients would need to be determined as well. The tailing of the peak was expected to be caused by a dimer or higher level of aggregates of the monoclonal antibody as in the experiment with low loading conditions. There was no isotherm data available for the dimer itself, since it did not form under the conditions applied in our parameter determination approach. Therefore, retention data of IgG1 was fitted again but with a K_D based on the doubled molecular weight (K_{eq}: 50.7 $\pm$ 2.6; v: 8.3 $\pm$ 1.4) . The simulations show that this seems to be a reasonable approximation.

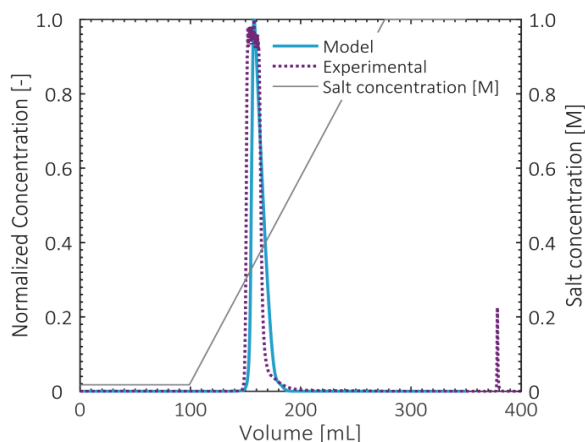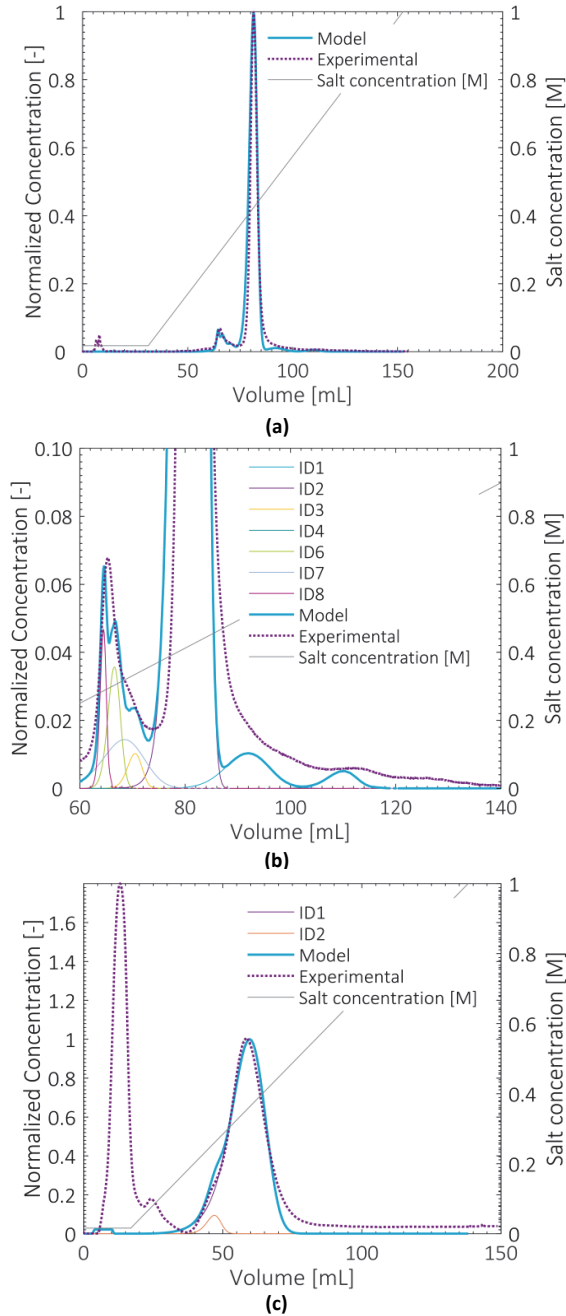**Figure 9: Load of 20 g/L of POROS 50HS on a 14.8 mL lab scale column**

Figure 10: Model prediction versus experimental data

a, b and c: At low loading conditions on POROS 50HS for the complete chromatogram (a) and a zoom-in (b) as well as on Capto MMC (c) The critical proteins were simulated (POROS 50HS: ID 1-8; Capto MMC: ID 1-2). The buffer of the clarified cell harvest was exchanged before sample application.

4.5.   Conclusion

This paper presented an extensive approach to determine isotherm parameters for a clarified cell harvest containing a monoclonal antibody with a high-throughput workstation. First, the clarified cell harvest was prefractionated to simplify the mixture and define critical proteins. Second, the obtained fractions were analyzed with isocratic column experiments on RoboColumns, which led to isotherm parameters in the linear protein concentration range of the isotherm. Third, the maximal capacity of the resin was determined in batch uptake experiments. Fourth, the second osmotic virial coefficient was measured for IgG1 with self-interaction chromatography to describe protein-protein interactions. As a last step, the mechanistic model was tested at lab scale using all parameters obtained in this study. Results showed a high agreement between modelled and predicted chromatograms. Thus, the most obvious finding to emerge from this study is that RoboColumn data can indeed be used to model larger scale columns. Additionally, it verifies our assumption that it is sufficient to only focus on critical compounds.

Nevertheless, certain assumptions are only valid for a mixture like the one studied, where one protein, like the IgG1 in this study, is present in a much higher concentration than the others. If this was not the case, maximum capacities would need to be determined for other proteins as well. In that case, however, this would not be a problem, since these proteins would occur in higher quantities. Additionally, the assumptions made regarding the second virial coefficient would not be valid. Here, the B_{22} of a mixture would need to be calculated as for instance explained in [20].

An improvement that could be made to the current study is to move all experiments (excluding the prefractionation) on a high-throughput workstation to drive automation even further and decrease sample usage. For that, only self-interaction chromatography and size-exclusion chromatography would need to be adapted or exchanged, which would need further research.

Overall, the presented approach delivers reliable parameters for mechanistic modelling of chromatography. With that, it can aid the model-based development of processes, which promises reduced costs and time until a product can reach the market.

Acknowledgment

References

1. Osberghaus A, Hepbildikler S, Nath S, Haindl M, von Lieres E, Hubbuch J. Determination of parameters for the steric mass action model--a comparison between two approaches. *J Chromatogr A.* 2012;1233(0):54-65.

2. Kumar V, Leweke S, von Lieres E, Rathore AS. Mechanistic modeling of ion-exchange process chromatography of charge variants of monoclonal antibody products. *Journal of Chromatography A.* 2015;1426:140-153.

3. Osberghaus A, Hepbildikler S, Nath S, Haindl M, von Lieres E, Hubbuch J. Determination of parameters for the steric mass action model—A comparison between two approaches. *Journal of Chromatography A.* 2012;1233(0):54-65.

4. Marchetti N, Cavazzini A, Pasti L, Dondi F. Determination of adsorption isotherms by means of HPLC: adsorption mechanism elucidation and separation optimization. *J Sep Sci.* 2009;32(5-6):727-741.

5. Borg N, Westerberg K, Andersson N, von Lieres E, Nilsson B. Effects of uncertainties in experimental conditions on the estimation of adsorption model parameters in preparative chromatography. *Computers & Chemical Engineering.* 2013;55(0):148-157.

6. Lacki KM, Brekkan E. High throughput screening techniques in protein purification. *Methods Biochem Anal.* 2011;54:489-506.

7. Bergander T, Nilsson-Välimaa K, Öberg K, Lacki KM. High-Throughput Process Development: Determination of Dynamic Binding Capacity Using Microtiter Filter Plates Filled with Chromatography Resin. *Biotechnology Progress.* 2008;24(3):632-639.

8. Nfor BK, Ahamed T, Pinkse MW, et al. Multi-dimensional fractionation and characterization of crude protein mixtures: toward establishment of a database of protein purification process development parameters. *Biotechnol Bioeng.* 2012;109(12):3070-3083.

9. Hanke AT, Tsintavi E, Ramirez Vazquez MD, et al. 3D-liquid chromatography as a complex mixture characterization tool for knowledge-based downstream process development. *Biotechnol Prog.* 2016;32(5):1283-1291.

4

10. Quigley A, Williams DR. The second virial coefficient as a predictor of protein aggregation propensity: A self-interaction chromatography study. *Eur J Pharm Biopharm.* 2015;96:282-290.

11. Ahamed T, Ottens M, van Dedem GWK, van der Wielen LAM. Design of self-interaction chromatography as an analytical tool for predicting protein phase behavior. *Journal of Chromatography A.* 2005;1089(1-2):111-124.

12. Xu X, Lenhoff AM. A predictive approach to correlating protein adsorption isotherms on ion-exchange media. *J Phys Chem B.* 2008;112(3):1028-1040.

13. Mollerup JM. Applied thermodynamics: A new frontier for biotechnology. *Fluid Phase Equilibria.* 2006;241(1-2):205-215.

14. Nfor BK, Ahamed T, van Dedem GWK, et al. Model-based rational methodology for protein purification process synthesis. *Chem Eng Sci.* 2013;89(0):185-195.

15. Nfor BK, Noverraz M, Chilamkurthi S, Verhaert PD, van der Wielen LA, Ottens M. High-throughput isotherm determination and thermodynamic modeling of protein adsorption on mixed mode adsorbents. *J Chromatogr A.* 2010;1217(44):6829-6850.

16. Mollerup JM, Hansen TB, Kidal S, Staby A. Quality by design--thermodynamic modelling of chromatographic separation of proteins. *J Chromatogr A.* 2008;1177(2):200-206.

17. Mollerup JM. The thermodynamic principles of ligand binding in chromatography and biology. *J Biotechnol.* 2007;132(2):187-195.

18. Hill TL. Thermodynamics for chemists and biologists. 1968.

19. Winzor DJ, Carrington LE, Harding SE. Analysis of thermodynamic non-ideality in terms of protein solvation. *Biophys Chem.* 2001;93(2-3):231-240.

20. Prausnitz JM, Lichtenthaler RN, de Azevedo EG. *Molecular thermodynamics of fluid-phase equilibria.* Pearson Education; 1998.

21. Hanke AT, Verhaert PD, van der Wielen LA, Eppink MH, van de Sandt EJ, Ottens M. Fourier transform assisted deconvolution of skewed peaks in complex multi-dimensional chromatograms. *J Chromatogr A.* 2015;1394:54-61.

22. Hanke AT. *Technologies to accelerate protein purification process development* [Doctoral Dissertation]. Delft, TU Delft; 2016.

23. Carta G, Jungbauer A. *Protein Chromatography: Process Development and Scale-Up.* Weinheim: Wiley-VCH Verlag GmbH & Co; 2010.

24. Zhang S, Iskra T, Daniels W, et al. Structural and performance characteristics of representative anion exchange resins used for weak partitioning chromatography. *Biotechnol Prog.* 2017;33(2):425-434.

25. Hagel L. Pore size distributions. In: Dubin PL, ed. *Aqueous Size-Exclusion Chromatography*. Amsterdam: Elsevier; 1988.

26. Zhu M, Carta G. Protein adsorption equilibrium and kinetics in multimodal cation exchange resins. *Adsorption.* 2016;22(2):165-179.

27. Staby A, Sand MB, Hansen RG, et al. Comparison of chromatographic ion-exchange resins. III. Strong cation-exchange resins. *J Chromatogr A.* 2004;1034(1-2):85-97.

28. Wiendahl M, Wierling PS, Nielsen J, et al. High throughput screening for the design and optimization of chromatographic processes - Miniaturization, automation and parallelization of breakthrough and elution studies. *Chem Eng Technol.* 2008;31(6):893-903.

29. Herrmann T, Schröder M, Hubbuch J. Generation of Equally Sized Particle Plaques Using Solid-Liquid Suspensions. *Biotechnology progress.* 2006;22(3):914-918.

30. Huuk TC, Briskot T, Hahn T, Hubbuch J. A versatile noninvasive method for adsorber quantification in batch and column chromatography based on the ionic capacity. *Biotechnol Prog.* 2016;32(3):666-677.

31. Bergander T, Lacki KM. High-throughput process development: Chromatography media volume definition. *Engineering in Life Sciences.* 2016;16(2):185-189.

32. ThermoFisher Scientific. POROS™ Strong Cation Exchange Resins: XS and 50 HS. https://assets.thermofisher.com/TFS-Assets/LSG/manuals/100031321_POROS_StrongCationExchResins_PI.pdf. Accessed 01.11.2017.

33. Rakel N, Schleining K, Dismer F, Hubbuch J. Self-interaction chromatography in pre-packed columns: a critical evaluation of self-interaction chromatography methodology to determine the second virial coefficient. *J Chromatogr A.* 2013;1293:75-84.

34. Pirrung SM, van der Wielen LAM, van Beckhoven R, van de Sandt E, Eppink MHM, Ottens M. Optimization of biopharmaceutical downstream processes supported by mechanistic models and artificial neural networks. *Biotechnol Prog.* 2017;33(3):696-707.

35. Young M, Carroad P, Bell R. Estimation of diffusion coefficients of proteins. *Biotechnology and Bioengineering.* 1980;22(5):947-955.

36. Wilson EJ, Geankoplis CJ. Liquid Mass Transfer at Very Low Reynolds Numbers in Packed Beds. *Industrial & Engineering Chemistry Fundamentals.* 1966;5(1):9-+.

37. Suzuki M, Smith JM. Axial dispersion in beds of small particles. *The Chemical Engineering Journal.* 1972;3(Supplement C):256-264.

38. Brenner H, Gaydos LJ. The constrained brownian movement of spherical particles in cylindrical pores of comparable radius: Models of the diffusive and convective transport of solute molecules in membranes and porous media. *Journal of Colloid and Interface Science.* 1977;58(2):312-356.

39. Gunn DJ. Axial and radial dispersion in fixed beds. *Chemical Engineering Science.* 1987;42(2):363-373.

40. LeVan MD, Carta G, Yon CM. Adsorption and Ion Exchange. In: Green DW, ed. *Perry's Chemical Engineers' Handbook.*

4

New York: McGraw-Hill Companies Inc.; 1999:16-19.

41. Wu Y, Simons J, Hooson S, Abraham D, Carta G. Protein and virus-like particle adsorption on perfusion chromatography media. *J Chromatogr A.* 2013;1297:96-105.

42. Garke G, Hartmann R, Papamichael N, Deckwer WD, Anspach FB. The influence of protein size on adsorption kinetics and equilibria in ion-exchange chromatography. *Separation Science and Technology.* 1999;34(13):2521-2538.

43. Hofer S, Ronacher A, Horak J, Graalfs H, Lindner W. Static and dynamic binding capacities of human immunoglobulin G on polymethacrylate based mixed-modal, thiophilic and hydrophobic cation exchangers. *J Chromatogr A.* 2011;1218(49):8925-8936.

44. George A. Predicting protein crystallization from a dilute solution property. *Acta Crystallographica Section A: Foundations and Advances.* 1994;50(4):361.

45. Stellwagen E, Prantner JD, Stellwagen NC. Do zwitterions contribute to the ionic strength of a solution? *Anal Biochem.* 2008;373(2):407-409.

46. Le Brun V, Friess W, Bassarab S, Muhlau S, Garidel P. A critical evaluation of self-interaction chromatography as a predictive tool for the assessment of protein-protein interactions in protein formulation development: a case study of a therapeutic monoclonal antibody. *Eur J Pharm Biopharm.* 2010;75(1):16-25.

47. Tessier PM, Lenhoff AM, Sandler SI. Rapid measurement of protein osmotic second virial coefficients by self-interaction chromatography. *Biophys J.* 2002;82(3):1620-1631.

48. Susanto A, Knieps-Grünhagen E, von Lieres E, Hubbuch J. High Throughput Screening for the Design and Optimization of Chromatographic Processes: Assessment of Model Parameter Determination from High Throughput Compatible Data. *Chemical Engineering & Technology.* 2008;31(12):1846-1855.

5

Model-based optimization of integrated purification sequences for biopharmaceuticals

Abstract

Chromatography is the most important purification unit in downstream processing of biopharmaceuticals, which makes the design and optimization of chromatographic steps an area of great interest. Recently, mechanistic models that can accelerate the development of chromatographic unit operations became widely available. In previous work, several chromatographic models have been linked together to simulate and optimize integrated chromatographic processes. However, considering only chromatographic steps may lead to a suboptimal process. Consequently, the aim of this study was to include models for ultra- and diafiltration units into the optimization approach to account for buffer exchange steps. Thus, entire purification sequences could be described. This approach was applied to an industrial case, the purification of a monoclonal antibody. The 'best' in silico purification process was found based on the performance criteria yield, purity and solvent usage.

Submitted for publication.

Contents

5.1.   Introduction

The purification of biopharmaceuticals is an area of great interest for current research in academia and industry alike. High quality assurances are generally required for pharmaceutical products, which puts pressure on the downstream process. Moreover, costs of downstream purification units such as chromatography columns typically do not benefit much from economies of scale but instead scale at least linearly. Thus, the more is produced upstream, the higher will be the proportional cost of the downstream process. Therefore, purification processes might even be the bottleneck of the whole production process [1]. This increasing importance of the downstream process clearly shows the need for better development and optimization approaches.

One way to achieve that, is the use of detailed mechanistic models based on first principles. Currently, these type of models are widely used for instance for the simulation and design of chromatography units [2-4] and allow an easy exploration of the design space for a specific unit. Prior work has dealt with linking such chromatography models together and optimizing the resulting sequences [5,6]. In a recent study [7], this was even done simultaneously using a combination of detailed mechanistic models and speed-enhancing artificial neural networks (ANNs). This novel approach opened up the way for more complex optimization problems. However, a downside in all these studies was that only chromatographic separation units were considered and not ultra/diafiltration (UF/DF) units, which can be placed between chromatography columns to adjust the buffer conditions and, thus, could alter the resulting optimal process [6,7].

Thus, the aim of this work is to integrate filtration units into the latter approach, which would extend the general applicability of the approach greatly. To achieve that, filtration models are implemented and applied in the optimization approach. The purification of a monoclonal antibody, IgG1, from clarified cell harvest is used as a test case. Parameters for two resins, a cation exchange (CEX) resin and a mixed mode chromatography (MMC) resin, were already available [8]. Therefore, additional model parameters are only determined for one extra hydrophobic interaction (HIC) resin as well as the UF/DF units. Subsequently, the optimization approach is applied to sequences of filtration and chromatography units to find the best purification sequence.

5

5.2. Material & Methods

5.2.1. Modelling and Optimization

Optimization problem definition

The optimization problem was defined and treated in a similar manner as described in a prior study [7]. A general constrained optimization problem can be described as:

$$\max \quad f(x, y) \tag{1a}$$

$$s.t. \quad \begin{aligned} &\mathrm{h}(x) = 0 \\ &g(x, y) \leq 0 \\ &\mathrm{lb} \leq x \leq \mathrm{ub}, \; y \in \{0, 1\} \end{aligned} \tag{1b}$$

where f is the objective function. The objective function depends on two type of variables: continuous x variables, which reflect either operating conditions or design parameters for each unit, and binary y variables, which define the investigated process sequences. In this study, the objective function includes the overall process yield and the overall solvent use, since solvent use is affected by chromatography and filtration units. The equality constraints $\mathrm{h}(x)$ include for instance mass balances. Other constraints can be defined using the inequalities $g(x, y)$. Here, the final product purity was defined to be at least above 99.9 %.

This overall problem was split up into smaller problems twice. First, it was divided into a master problem and subproblems. The master problem is responsible for generating all possible process sequences, which is shown by the binary y variables. These variables tell, which unit operations are in a sequence and their order. The master problem here was formulated as:

$$\max \quad f(y_{m,s}) \tag{2a}$$

$$s.t. \quad \begin{aligned} &\sum_m y_{m,s} \leq 1 \\ &\sum_s \sum_{m=1}^{3} y_{m,s} \leq 2 \\ &\sum_s y_{m,s} \leq 1 \qquad\qquad \text{for } 1 \leq m \leq 3 \\ &1 - y_{4,s} + \sum_{m=1}^{3} y_{m,s+1} \geq 1 \\ &1 - \sum_m y_{m,2} + \sum_m y_{m,1} \geq 1 \\ &1 - \sum_m y_{m,3} + \sum_m y_{m,2} \geq 1 \end{aligned} \tag{2b}$$

$$1 - \sum_m y_{m,4} + \sum_m y_{m,3} \geq 1$$
$$y_{m,s} \epsilon \{0,1\}$$

where subscript m indicates the mode used, $m \epsilon \{1,2,3,4\}$ meaning CEX, HIC, MMC and UF/DF. The number of purification steps is given by s, $s \epsilon \{1,2,3,4\}$. The first constraint defines that maximal one unit can be used per purification step. The second constraint shows that only a maximum of two chromatography units can be in a process sequence. The third constraint then defines that each chromatography mode can only be included once. Filtration units can be used more often. However, they can only occur before a chromatography unit shown in the next constraint. Finally, the last constraints mean that a unit has to be chosen for all earlier occurring steps. A scheme with all resulting process alternatives is shown in Figure 1.
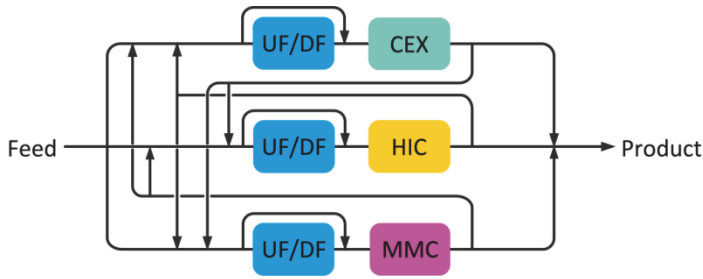
Figure 1: Scheme with all considered process options
A maximum of two chromatographic units are allowed as defined by the second constraint in Equation 2b.

Each generated process sequence than forms its own subproblem. In each subproblem, the operating variables x for each purification unit in the specific sequence are optimised simultaneously. Since this is still a rather complex optimization, the problem was divided again into a local search and a global search problem. The global search was performed to generate good starting points for the subsequent local search increasing the chance to find a global optimum. In this study, the global search problem was defined as

$$max \quad f = yield + 2 * \text{purity} \tag{3a}$$

$$s.t. \quad h(x) = 0 \tag{3b}$$
$$0 \leq x \leq 1$$

All variables were normalized, so that their lower boundary is zero and their upper boundary one. For an easier solution, no nonlinear constraints were included in the global search problem. Thus, the purity after the final purification unit was treated as an additional objective. Its importance over the other objectives was set higher to increase the likelihood of already feasible starting points for the local search, where purity is used as constraint. The solvent volume was not yet included in the objective, since this first optimization is primarily performed to find feasible starting points for the next optimisation. Potential yield loss in UF/DF was not taken into account, since the considered product, IgG1, cannot pass the membrane.

The global optimisation was run 40 times for each process sequence with random starting points, which were created with MATLAB's function *lhsdesign* (criterion set to correlation)*.* As optimisation algorithm *patternsearch* was used with *searchlhs* as search method performing a complete search. The maximum number of function evaluations was set to 1000 and an output function was used, which could stop the search early, if the starting point was not promising.

The x variabels that were optimised for each chromatography unit were the length of the gradient elution, the length of the extra elution volume with the final eluent composition, the product pool cut points and the final salt concentration as shown in Figure 2. The starting salt concentration as well as the pH are determined by the prior processing unit. For the filtration units, it was investigated in section 5.3.1 which variables to include.

During the global optimization, ANNs were used as surrogate models for the mechanistic models. This allows a faster evaluation of purity and yield at specific
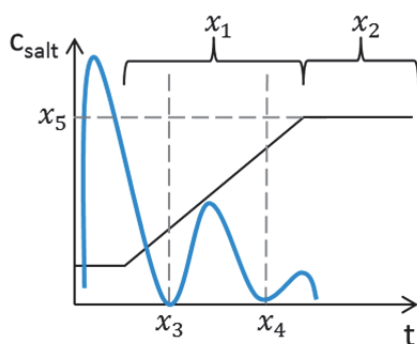
Figure 2: Optimization variables for chromatography units

variable values. Since the ANNs sometimes find solutions that only exist due to inaccuracies in their own predictions [7], all starting points were checked with the mechanistic models. This is also why ANNs were only used during the global optimization. If the objective function value was below a specified value they were fed to the next optimizer.

The local search problem was then defined with the final purity as constraint and the solvent volume included in the objective:

$$\max \quad f = -V_{solvent} + yield \tag{4a}$$

$$s.t. \quad h(x) = 0$$
$$purity(x) > 99.9\,\% \tag{4b}$$
$$0 \le x \le 1$$

The solvent volume, $V_{solvent}$, is the sum of solvent used per unit operation. Both objectives were normalized to give them a similar importance. The local search algorithm used was *fmincon*. The sequential quadratic programming algorithm was used for its higher robustness compared to the other available algorithms. The objective and constraint function are approximated by finite differences. Since the values of these functions are numerical solutions of ordinary and partial differential equations, the relative step of the finite difference should not be too small or too big. If it is too small, it might be for instance that there is no change in the objective function yet. If it is too big, nonlinearity might influence the finite difference. A value of 1e-3 was chosen as recommended by MATLAB for optimization problems including ordinary differential equations.

Filtration modelling

The ultrafiltration/diafiltration (UF/DF) process can be described by a set of ordinary differential equations (ODE) for a variable volume diafiltration process [9]:

$$\frac{dV}{dt} = (\alpha - 1)\,JA \tag{5}$$

$$\frac{dc_i}{dt} = \frac{c_i}{V}\left(\sigma_i - \alpha\right) JA \tag{6}$$

$$\frac{dV_{diluent}}{dt} = \alpha JA \tag{7}$$

where α is the ratio between diluent inflow and outflow over the membrane, $\alpha = Q/JA$ with Q the volumetric flowrate of the diluent, J the flux over the membrane and A the membrane area. V is the volume of the solution and c_i is the concentration for a compound i. The rejection coefficient σ_i defines how well compounds are being retained by the membrane. For instance for the salt, the rejection coefficient is 0, because it can freely pass the membrane. If the added diluent buffer already contains salt ($c_{s,diluent}$), Equation 6 needs to be adjusted as follows to describe the change in salt concentration ($i = s$):

$$\frac{dc_s}{dt} = \frac{c_s}{V}\left(\sigma_s - \alpha\right)JA + \frac{c_{s,diluent}}{V}\alpha JA \tag{8}$$

The flux J can be calculated with the osmotic pressure model:

$$J = \frac{\Delta P - \Delta \pi}{\mu R_m} \tag{9}$$

where μ is the viscosity of the permeate stream, $\Delta \pi$ is the osmotic pressure and ΔP the transmembrane pressure (TMP), which is defined as:

$$\Delta P = \frac{P_{feed} + P_{retentate}}{2} - P_{permeate} \tag{10}$$

The osmotic pressure can be expressed by a virial expansion. An expansion with two virial coefficients was chosen; the third coefficient can be negligible in low concentration ranges [10]. In case of a final formulation step, where much higher concentration ranges occur, the third coefficient would need to be included. Additionally, the spatial variation in transmembrane pressure would need to be taken into account. This situation was extensively studied by Binabaji [11].

$$\frac{\pi}{c_{i,wall}RT} = \frac{1}{M} + B_{22}c_{i,wall} + \cdots \tag{11}$$

where $c_{i,wall}$ is the concentration of protein at the wall or membrane surface. B_{22} is the second osmotic virial coefficient. In UF/DF processes, a layer forms almost immediately as a result of concentration polarization, when a solution with macromolecules is to be filtered [12]. Assuming the instantaneous formation of this layer, $c_{i,wall}$ can be calculated by the stagnant film model [13]:

$$J = k \ln \frac{c_{i,wall} - c_{i,permeate}}{c_{i,bulk} - c_{i,permeate}} \tag{12}$$

where $c_{i,bulk}$ is the protein concentration in the bulk solution assuming that it is well mixed and $c_{i,permeate}$ is the concentration in the permeate. The mass transfer coefficient k is defined as the ratio of diffusivity D to the thickness of the boundary layer. It can be described depending on the Sherwood number, a commonly used dimensionless number [14]:

$$Sh = \frac{k\,d_h}{D} = aRe^b Sc^c \left(\frac{d_h}{l}\right)^d \tag{13}$$

where Re is the Reynolds number defined with the density ρ and the cross membrane velocity v as $Re = \rho v d_h/\mu$. The Schmidt number Sc can be calculated as $Sc = \mu/\rho D$. The diffusivity D was calculated using the Young correlation valid for globular proteins [15].

The characteristic length of the system is shown as l. The membrane cassette used here is a flat channel with spacers enhancing mass transfer. For this module geometry, the characteristic length is the size of one mesh [14], which can be calculated as the sum of the mesh opening and twice the wire diameter. For the C screen type membrane cassettes, these parameters can be found in recent literature [16]. The mesh opening is thus 350 µm, the wire diameter 270 µm resulting in a total characteristic length of 890 µm. The empirical constants a, b, c and d are dependent of the specific geometry of the system as well and can be found in literature for most systems. Here, a is 0.664, b 0.5, c 0.33 and d 0.5 respectively [14]. Additionally, the hydraulic diameter d_h is defined as $4 * cross\ section/wetted\ perimeter$ and, thus, depends on the system used. In this case, it can be defined as [17]:

$$d_h = 4h \frac{\varepsilon_s}{1 + \frac{2(1-\varepsilon_s)h}{r}} \tag{14}$$

where ε_s is the porosity of the spacer, h is the half-height of the channel and r is the fibre radius. Furthermore, the cross-membrane velocity can be calculated as $v = J/(a_c\varepsilon_s)$, where a_c is the ratio of feed channel area to membrane area. The spacers in the membrane cassette used were Screen C type ($\varepsilon_s = 0.63$; $h = 0.026$ cm; $r = 0.014$ cm; $a_c = 0.0018$) [17].

With increasing protein concentration, the viscosity of the solution changes, which is why the dependence of the mass transfer coefficient on viscosity was incorporated. An exponential relationship between viscosity and protein concentration, c_i, can often be

assumed: $\mu = \mu_0 e^{\vartheta c_i}$, where ϑ is a constant depending on the molecule and μ_0 the solvent viscosity. In this study, ϑ was found to be 0.017 ± 0.001 L/g. It was determined by measuring the viscosity of the IgG solution at different protein concentrations using a viscometer. Subsequently, a least square fit was performed using MATLAB's *lsqcurvefit* function. The relationship between mass transfer coefficient and viscosity was derived from Equation 13 with the module specific constants b and c:

$$k = k_0 \left(\frac{\mu}{\mu_0}\right)^{-\frac{1}{6}} = k_0 \, e^{-\frac{1}{6}\vartheta c_i} \tag{15}$$

The initial mass transfer coefficient, k_0, was calculated using Equation 13. Assuming that the boundary layer is sufficiently thin, the viscosity was evaluated using the bulk concentration $c_{i,bulk}$.

At initial conditions, it was assumed that the flux predicted by the osmotic pressure model is identical to the flux due to the immediately formed concentration polarization. Another assumption made was that the antibody has by far the most impact due to its higher molecular mass and concentration ($i = mAb$). Additionally, the antibody is completely retained by the membrane. Based on these assumptions, Equations 9 and 12 could be equated as follows:

$$k \ln\frac{c_{mAb,wall}}{c_{mAb,bulk}} - \frac{\Delta P - \Delta \pi}{\mu R_m} = 0 \tag{16}$$

This function was solved by the MATLAB function *fsolve* for finding the initial wall concentration.

The change of wall concentration over time was found by implicit differentiation of Equation 16 as shown for a similar case in detail by [9] and incorporated in the ODE system comprised of Equation 5, 6, 7 and 8. An additional ODE described the fraction of diluent in the system at a specific time. The ODE system was solved using the ODE solver *ode15s* from MATLAB.

Filtration optimization

Different objectives can be defined in the optimization of UF/DF units such as processing time [18,19], economic factors [20], minimum amount of diluent [21], product loss, if the product is not fully rejected by the membrane, or a combination of all of these factors [22]. For the optimization of only the filtration step, the minimum amount of

diluent was chosen as single objective, since the results can be easily evaluated experimentally. Therefore, the optimization problem was formulated as:

$$max \quad f = \min_{\alpha(t)} \int_{t_0}^{t_{end}} \alpha(t) AJ(t) \, dt \tag{17a}$$

$$s.t. \quad V(t_0) = V_0; \; c_i(t_0) = c_{i,0}; \; c_i(t_{end}) = c_{i,end} \tag{17b}$$
$$0 \leq \alpha(t) \leq 1$$
$$\alpha(t) = \sum_{k=1}^{N} \alpha_k$$

where $\alpha(t)$ is described as a piecewise constant for N time intervals. α_k is then the value α assumes during a specific step k. The duration of each step k, the value of α_k during the step and the overall duration of the ultrafiltration/diafiltration process were used as variables. To define constraints for an easier comparison, a simple base case was simulated with only one step and a constant α (α = 0.75). The final concentrations experienced during the base case were used as constraints, $c_{i,end}$. In this base case, the diafiltration was performed for 20 min, the concentration of the antibody was increased from 1.0 to 5.6 g/L and the salt concentration was decreased from 58.4 to 0.4 g/L. In total, 123 mL of diluent were consumed.

The optimizations were performed with MATLAB's function *fmincon*. The same settings as described above were used. Each optimization was performed with 20 different starting points, which were generated with the function *lhsdesign* and the criterion set to correlation.

Chromatography modelling

The equilibrium transport dispersive model can be applied to model chromatography columns [23]. The following mass balance is used to describe the mobile phase (Equation 18):

$$\frac{\partial c_i}{\partial t} + \frac{1 - \varepsilon_b}{\varepsilon_b} \frac{\partial q_i}{\partial t} = -v \frac{\partial c_i}{\partial x} + D_{L,i} \frac{\partial^2 c_i}{\partial x^2} \tag{18}$$

where c_i is the concentration of protein i in the bulk phase, ε_b is the bed porosity and $D_{L,i}$ is the axial dispersion coefficient. The interstitial velocity of the mobile phase v is defined as $v = u/\varepsilon_b$ with u, the superficial velocity of the mobile phase.

The change in q_i, the concentration in the stationary phase, over time was approximated with the linear driving force approach for the mass transfer in the liquid phase (Equation 19).

$$\frac{\partial q_i}{\partial t} = k_{ov,i}(c_i - c_i^*) \tag{19}$$

where $k_{ov,i}$ is the overall mass transfer coefficient. An appropriate adsorption isotherm needs to be used to calculate c_i^*, the protein concentration inside the particle pores. One possible option is the mixed-mode isotherm developed based on thermodynamic principles by Nfor et al [24]:

$$\frac{q_i}{c_i^*} = A_i \left(1 - \sum_{j=1}^{m} \frac{q_j}{q_j^{max}}\right)^{\nu_i + n_i} \tag{20}$$

Its validity range spans mixed-mode chromatography, ion-exchange chromatography and hydrophobic interaction. m stands for the number of proteins, q^{max} for the maximum binding capacity and j for the protein species. The stoichiometric coefficient in hydrophobic interaction chromatography is n_i and in ion exchange chromatography ν_i respectively. ν_i can be calculated as z_p/z_s with z_p, the effective binding charge of the protein, and z_s, the charge on the salt counter ion.

The initial slope of the isotherm A_i is defined as:

$$A_i = K_{eq,i} \Lambda^{(\nu_i + n_i)} (z_s c_s)^{-\nu_i} c_v^{-n_i} \gamma_i \tag{21}$$

where K_{eq} is the thermodynamic equilibrium constant, c_s the salt concentration, c_v the molarity of the solution in the pore volume and Λ the ligand density. The activity coefficient can be expressed as

$$\gamma_i = e^{2B_{22}c_i} \tag{22}$$

assuming that protein-protein interactions are only of importance between one protein species and that these interactions mostly occur between two molecules [8]. Additionally, it is assumed that salt protein interactions are negligible, which is valid when salts with a low salting-out effect are used such as chlorides [25]. For hydrophobic interaction chromatography, however, sulphates are commonly used, which makes this assumption invalid. Therefore, the salting-out constant K_s and the salt concentration were included in the definition of the activity coefficient in case sulphates are used:

$$\gamma_i = e^{K_{s,i}c_s + 2B_{22}c_i} \tag{23}$$

The mechanistic model was solved as described in [7] employing the mass transfer correlations as shown in [8].

Artificial neural networks Artificial neural networks (ANNs) were generated and trained with the Neural Network Toolbox™ by MATLAB as described previously [7]. Here, seven variables were used: the gradient length, the length of the extra elution volume after the end of the gradient, both product pool cut points, the injection volume, the starting and final salt concentration as well as the pH. Different ANNs were trained to predict the protein concentration for all proteins in the product pool, the volume of the product pool, the solvent volume as well as the salt concentration of the product pool. The neural networks were trained for different number of sample points (1000 or 2000), hidden layer sizes (10 to 40) as well as different amounts of hidden layers (1 or 2); networks with the best R^2 were chosen further. Typically an R^2 above 0.8 indicates sufficient predictive power [26].

Computations

All computations were performed on an Intel® Xeon® Processor E5-1620 v2 with 3.7 GHz. MATLAB's Parallel Computing Toolbox™ was used to compute in parallel on four cores whenever possible.

5.2.2. Materials

Sample Preparation

A clarified CHO cell culture supernatant containing a monoclonal immunoglobulin G (IgG1) was used as sample with a concentration of 1.3 mg/mL of IgG1 and a pH pf 7.72. The pI of IgG1 was determined to be 8.6 by capillary isoelectric focusing. Additionally, a sample of the same antibody after Protein A purification was used.

Buffers and Chromatography Resins

The buffers used in this study are shown in Table 1. In the chromatographic steps, the acetic acid buffer was mainly used for the cation exchange resin Poros 50 HS (Thermo Fisher Scientific Breda, Breda, The Netherlands), the MOPS buffer for the mixed mode resin Capto MMC (GE Healthcare, Eindhoven, The Netherlands) and the Tris-HCl buffer

for the hydrophobic interaction resin Cellufine Phenyl (AMS Biotechnology, Abingdon, United Kingdom). All buffers were purchased in buffer grade.

Table 1: Buffer specifications

Buffer type	Supplier	pH	Buffer [mM]	Salt type	Salt range [mM]
Acetic acid	Sigma Aldrich, Zwijndrecht, The Netherlands	4.5	25	Sodium chloride	0 - 1000
MOPS	Applichem GmbH Darmstadt, Germany	6.75	25	Sodium chloride	0 - 1000
Tris-HCl	Sigma Aldrich, Zwijndrecht, The Netherlands	7.5	25	Ammonium sulphate	0 - 750

5.2.3. Experimental Techniques

Filtration

Figure 3 shows a scheme of the experimental set-up used for all UF/DF experiments. The sample solution was added to the feed tank, from where it was continuously circulated over an 88 cm^2 Pellicon 3 Ultracel 30 kDa membrane cassette placed in a cassette holder (Merck Millipore, Amsterdam, The Netherlands) by a peristaltic
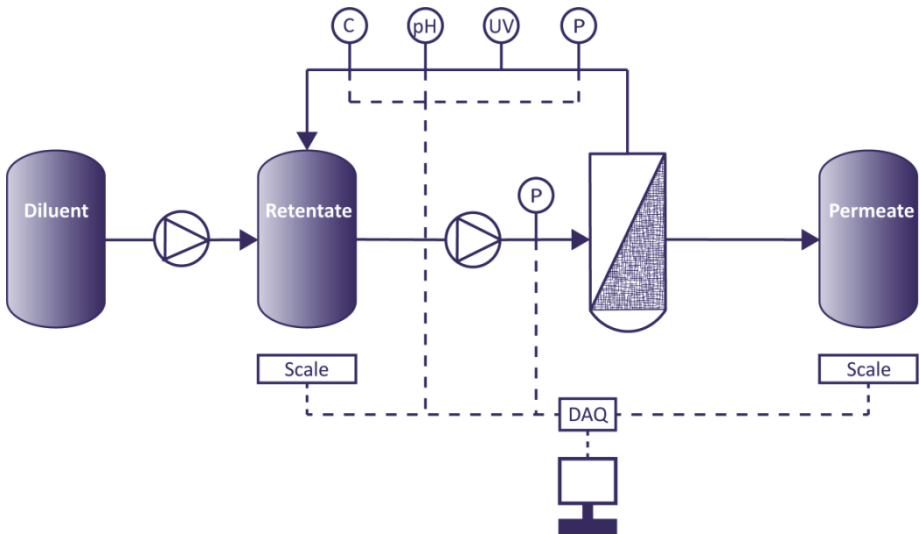

Figure 3: Scheme of the experimental setup with the ultrafiltration/diafiltration membrane

Masterflex L/S pump (Metrohm Netherlands B.V., Barendrecht, The Netherlands). If desired, diluent solution was added with a LC-8A HPLC pump (Shimadzu, s'Hertogenbosch, The Netherlands). The mass of permeate and retentate was constantly recorded with the help of PG 3001-S scales (Mettler Toledo, Tiel, The Netherlands). Signals from all other sensors were sent as an analogous signal to the data acquisition device DAQ USB 6009 (National Instruments Netherlands BV, Woerden, The Netherlands), which converts them to digital signals. The program SignalExpress (National Instruments Netherlands BV, Woerden, The Netherlands) was then used to process the data.

Initial membrane resistance The flux of a pure water stream J was measured at a flowrate of 20 mL/ min. Subsequently, the initial membrane resistance was calculated to be $7.92 \pm 0.44 * 1012$ 1/m using the following equation and the viscosity of water:

$$R_m = \frac{\Delta P}{\mu J} \tag{24}$$

Rejection coefficient A relation for the rejection coefficient, which describes how well proteins are retained by the membrane, was found based on model molecules as listed in Table 2. Model proteins were used instead of dextrans, which are linear polymers, since not only molecular weight but also molecule structure influences retention behavior [12]. For each experiment, the protein concentration was 0.2 g/L.

Table 2: Model proteins used to determine the rejection coefficient

Name	Molecular weight (kDa)	Stokes radius (nm)
Lysozyme	14.3	1.86
α-Chymotrypsin	25.0	2.09
Albumin from hen egg white	44.3	2.93
Albumin from bovine serum	66.5	3.48

Second virial coefficient The second virial osmotic coefficient was determined and fitted for the Tris-HCl buffer as described in detail elsewhere using self-interaction chromatography [8]. In that study, data for IgG1 in the acetate and MOPS buffer can also be found as shown in Table 3.

Table 3: Parameters to calculate the B_{22} for IgG1 in the acetate and MOPS buffer taken from [8]. They need to be multiplied with 10^{-4}.

	b_1	b_2	b_3	b_4	b_5	b_6
Acetate buffer	6.791	-2.794	1.249	-0.575	0.237	1.474
MOPS buffer	2.119	-0.807	-0.199	0.222	0.046	-1.013

A second order polynomial function was fitted to the determined B_{22} values using MATLAB's *fit* function:

$$B_{22} = b_1 + b_2\ pH + b_3\ c_s + b_4\ pH\ c_s + b_5\ pH^2 + b_6\ c_s^2 \qquad (25)$$

The salt concentration is shown as c_s. The resulting B_{22} was in the units (mol mL)/g^2 as required for Equation 11. To use the determined B_{22} in the chromatographic mechanistic model as shown in Equation 22 and 23, the units need to be changed to L/mol with the squared molecular weight.

The pH during the diafiltration was assumed to be a sum of the pH of each buffer multiplied with its fraction of the total solution. This assumption was proven to be applicable through mixing experiments (data not shown).

Validation experiments Experiments were performed at least in duplicates. The TMP was kept constant during the experiments. The starting concentration of IgG1 was 1 g/L. Modelling results were compared with experimental data with help of the coefficient of determination (R^2), which was calculated from the correlation coefficients given by MATLAB's *corrcoef* function.

Cleaning After each use, the membrane was cleaned according to the manufacturer's instructions.

Chromatography

Ion exchange and mixed mode chromatography Model input parameters for the cation exchange resin, POROS 50 HS, and the mixed mode resin, Capto MMC, were taken from literature [8].

Hydrophobic interaction chromatography Parameters for the hydrophobic interaction resin, Cellufine Phenyl, were determined by a 3D liquid chromatography method as

described in [27,28]. The first dimension, which is mainly to reduce the complexity of the mixture and to allow a focus on critical impurities, is identical to the one shown in [8]. Here, the mixture was prefractioned twice, once on a cation exchange resin and once on an anion exchange resin. However, more fractions were analysed further, since the adsorption behavior on cation or anion exchange resins is quite different from the adsorption behavior due to hydrophobic interaction. To avoid correlation errors during the regression, several parameters, which can be assumed as constant in the investigated range, were combined with the equilibrium constant to form one parameter $(K_{comb,i} = K_{eq,i}(\Lambda/c_v)^n)$[27]. The isotherm parameters $\mathrm{K_{comb}}$ and $\mathrm{K_s}$ for proteins contained in these fractions were determined on RoboColumns with a volume of 200 µL prefilled with the resin of interest, Cellufine Phenyl, by Repligen (Weingarten, Germany). For that, three types of gradient elution experiments (12, 24 and 36 CV gradient length) were performed for each fraction. The salt concentration in the beginning of the gradient, $\boldsymbol{c_{s,in}}$, was 1 M ammonium sulphate and the salt concentration in the end, $\boldsymbol{c_{s,f}}$, 0 M respectively. The following equation as derived in [27] was used to fit the resulting data:

$$V_{R,g,i} =$$

$$\frac{V_G}{-K_{s,i}(c_{s,f}-c_{s,in})} \ln \left(1 + V_{column}(1-\varepsilon_b)\varepsilon_p K_{D,i} \frac{-K_{s,i}(c_{s,f}-c_{s,in})}{V_G} K_{comb,i} e^{K_{s,i}c_{s,in}} \right) \quad (26)$$

As determined in [27], the bed porosity of the RoboColumns filled with Cellufine Phenyl was 0.3 and the particle porosity 0.93. The other isotherm parameters q_{max} and n were determined in batch uptake experiments as described in [8]. Different to the method described there, the salt concentration to perform these experiments was set to 0.75 M of ammonium sulphate, since binding capacities are typically higher in HIC at higher salt concentrations.

Validation experiments Validation experiments were performed on OPUS® ValiChrom 11.3/100 columns prepacked with the resin Cellufine Phenyl by Repligen (Weingarten, Germany) on an Äkta Avant 25 (GE Healthcare, Uppsala, Sweden). The bed porosity was determined with the help of the Blake-Kozeny equation that correlates pressure drop and applied flowrate. The flowrate was 182 cm/h. Linear salt gradients of 12 CV were

used during the elution. 20% Ethanol was used as storage solution. Absorption was recorded at 210, 230 and 280 nm.

Quantification

If not defined otherwise, protein concentrations were determined in a UHPLC+ (Thermo Fisher Scientific, Waltham, USA) system as described by Hanke et al. [27].

Protein Identification

A mass spectrometric (MS) analysis was performed for the fractions of the cation exchange prefractionation. The samples were desalted and concentrated prior to a proteolytic digestion, which was based on literature [29]. They were then analysed with liquid chromatography followed by mass spectrometry (LC-MS). Protein names of all proteins and their intensity in each fraction were determined with the help of UniProt. After that, they were matched with the tracked proteins. Additionally, the isoelectric point for the antibody was measured externally with capillary isoelectric focusing (CIEF). Isoelectric points for the impurities were estimated using ExPASy.

5.3. Results & Discussion

The first section focusses on UF/DF units. Here, parameter determination, modelling and subsequent validation of the model is shown. Additionally, a short section on the optimization of UF/DF units is included. The second section is about chromatography units. It starts by describing the chromatographic model input parameters and then shows the mechanistic model together with its validation. This section finishes with a short discussion on the training of ANNs to predict the chromatography units. The last section shows the results of the process optimisation including the best found process option.

5.3.1. Filtration

Model parameters

Rejection coefficient To understand how well differently sized proteins are retained by the membrane, sieving experiments were performed. The rejection coefficient was approximated with a logistic function and the molecular weight, MW, in kDa as:
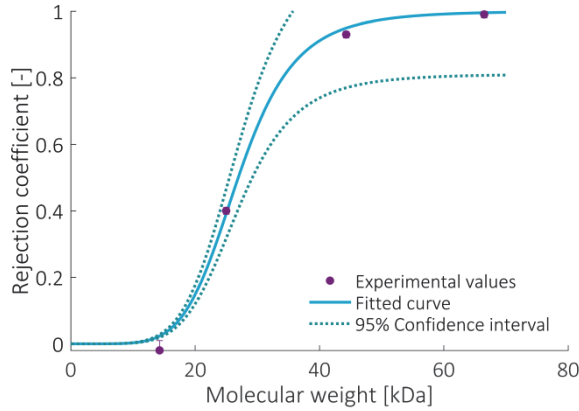
Figure 4: Rejection coefficient

$$\sigma_i = \frac{1}{1+(a_1*MW_i)^{a_2}} \qquad (27)$$

The experimental results together with the fitted curve can be found in Figure 4. As expected, smaller proteins up to 15 kDa can easily pass the 30 kDa membrane. Above 50 kDa, proteins are almost fully retained. The fitted parameter a_1 was found to be 0.037 ± 0.001 and a_2 -5.9 $\pm$ 1.1. For an improved description of the retention of impurities, the dependence of the rejection coefficient on the flux should be taken into account additionally.

Second virial coefficient All B_{22} results for the Tris-HCl buffer are summarized in Figure 5. Figure 5 a shows the second order polynomial function. It was fitted to the experimentally determined B_{22} values resulting in the following constants x 10^{-4}: b_1 -7.016; b_2 2.145; b_3 2.431; b_4 -0.226; b_5 -0.187 and b_6 -1.407. Ammonium sulfate concentrations greater than 0.75 were not investigated due to stability issues such as aggregation. Two general trends can be observed from the results: First, the B_{22} values decrease with increasing pH. Second, salt concentration only has a strong influence on protein-protein interactions at high pH values. Both trends can well be explained by the fact that the IgG is getting closer to its pI (around 8.6) and therefore is less charged. With a decrease in protein charge, repulsive interactions between IgGs decrease as shown by the decrease in B_{22}.

(a)

(b)
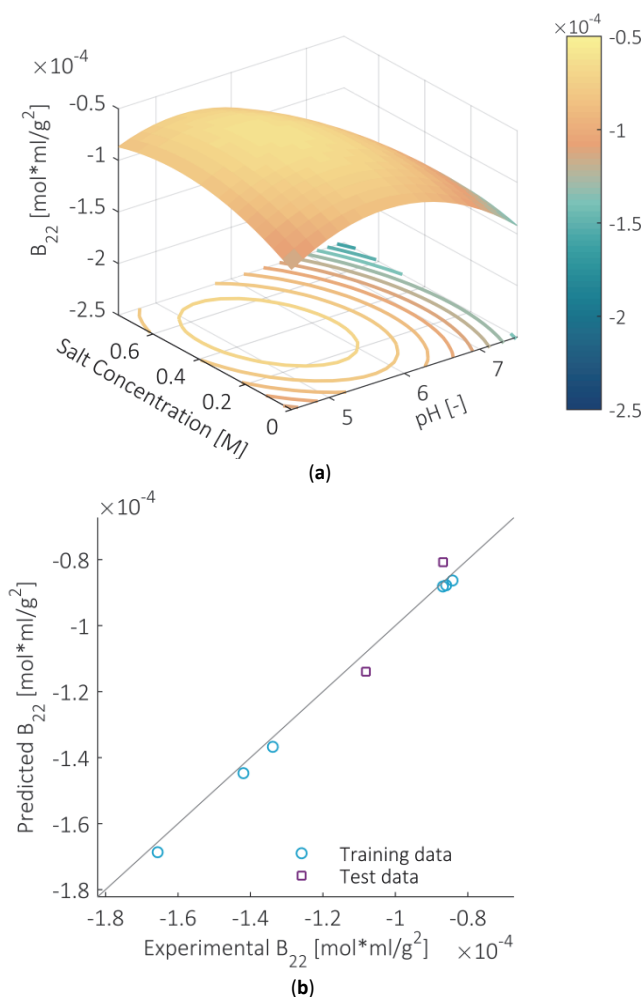
Figure 5: B_{22} values of IgG1 as a function of salt concentration and pH for the Tris-HCl buffer
a: Second order polynomial function that was fitted on experimental data; **b:** Comparison of experimentally obtained B_{22} values with values given by the polynomial function

The correlation between B_{22} values predicted by the polynomial and the experimentally determined ones is plotted in Figure 5 b. A good correlation was also found for two test data points, that were not included in the data set used for fitting.

Modelling & Validation

Figure 6 compares model predictions for UF/DF processes with experimental data. An excellent agreement (R^2 of at least 0.99) was found in all cases supporting the validity of the model approach employed. In the ultrafiltration experiment in Figure 6 a, only a

small deviation between experimental values and model predictions was found indicating that the third virial coefficient as well as fouling of the membrane are indeed negligible in the investigated concentration range of up to around 15 g/L. This was not clear beforehand considering the high wall concentrations, which were predicted to be around 5 g/L at the start of the experiment and around 85 g/L at the end.

Figure 6 b and c show different dilution strategies; even the results for the most complex dilution strategy was well predicted as is shown in Figure 6 b. Here a random trajectory with ten different steps was chosen. In conclusion, the UF/DF model can well
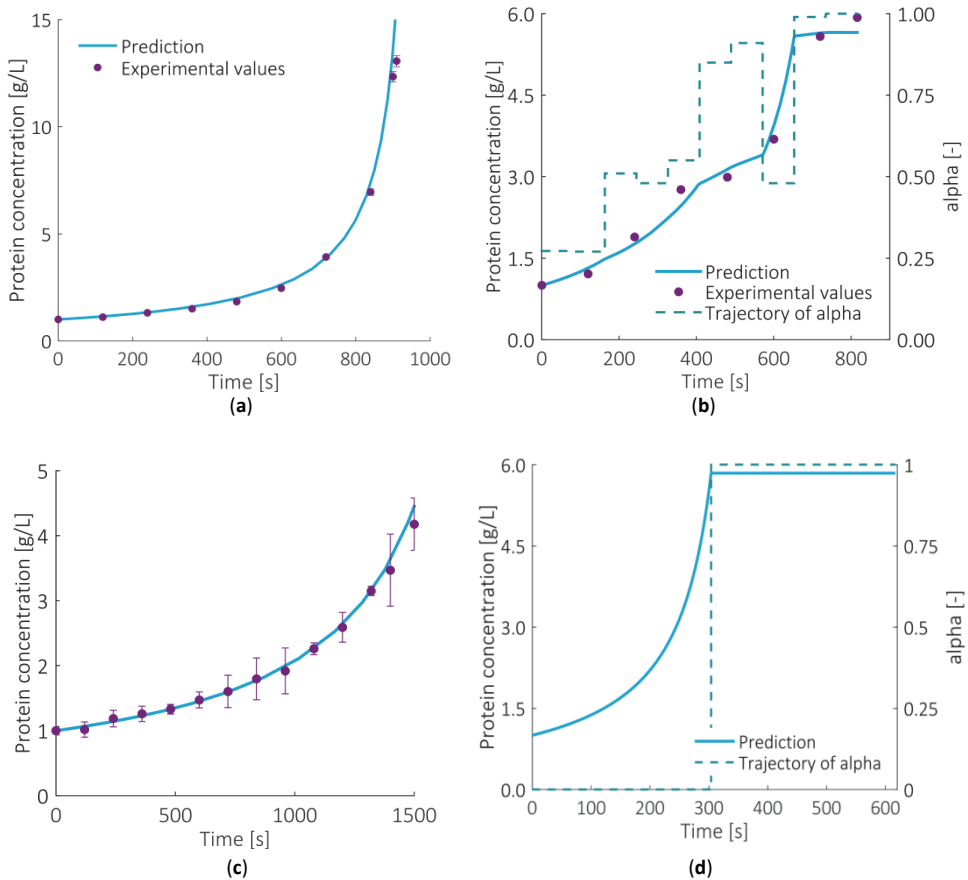
Figure 6: Model predictions for comparison with ultrafiltration/diafiltration experiments (a), (b) and (c) and the optimization result (d)
a: Compared with experimental values for an ultrafiltration experiment. The TMP was kept constant at 93 kPa. b: For a diafiltration experiment with alpha as a piece wise constant following the shown trajectory and a constant TMP of 93 kPa; c: For a diafiltration experiment with constant alpha of 0.75. The TMP was constant at 123 kPa; d: Regardless of the number of steps.

be used in the investigated concentration range.

These validation experiments were performed with a purified solution of IgG1. To see, if other proteins have an additional impact on the flux, experiments with the clarified cell harvest were performed at different salt concentrations, buffer compositions and pH values. Fluxes predicted fell in the range of experimental error (1.3 10^{-6} m/s) of experimentally determined fluxes, which is why the prediction with only osmotic data of IgG1 was declared sufficient.

Experiments, where buffer was exchanged from initial clarified cell harvest, resulted in unexpected aggregation. Therefore, the final protein concentration for the initial diafiltration step was constrained to stay below 5 g/L. For filtration units that were placed between chromatography units it was constrained to stay below 10 g/L. If higher protein concentrations are being used, as would be needed for instance for a final formulation step, the influence of fouling on the ultra/diafiltration needs to be investigated in more detail.

Optimization

The purpose of the optimization as described in Equation 17 was the reduction of diluent volume. Typically, an ultrafiltration/diafiltration process is performed as follows: First step, the volume is reduced until the product concentration reaches the desired value ($\alpha = 0$); second step, the diafiltration is performed until the desired salt concentration or pH is achieved ($\alpha = 1$). It was investigated if a higher flexibility in α, meaning more steps with variable α and variable duration, would lead to a further reduction in diluent volume. Consequently, optimizations were performed with two, five, ten and forty steps.

In all cases, the same optimal result was found, which is shown in Figure 6 d. The minimal diluent volume needed was 43 mL which is a great reduction of 65 % compared to the base case. This result shows that the traditional way of operating is indeed optimal in regards to diluent usage confirming the finding by Paulen et al. [21]. However, the same group showed in a later study that more complex control strategies for α can be beneficial in certain cases [30]. Since no benefits were found by using more complex profiles for α in this case, the typical two step profile was chosen as described above in all further studies. Thus, only the total length of the ultrafiltration/diafiltration process and the duration of the ultrafiltration step were used as variables further on,

which greatly reduces the complexity of the optimization problem. The duration of the diafiltration step was calculated as difference between total length of the filtration step and the ultrafiltration step.

In general, this is a sensible approach. First the volume is reduced until the desired product concentration is reached leading to a smaller amount of diluent that is needed to exchange the buffer. However, it should be kept in mind that this way of processing means that the buffer is exchanged at the highest protein concentration. This might cause stability problems, which should be investigated first.

Speed The time needed to evaluate the filtration model is very fast compared to the chromatography model. It only takes in between 0.01 and 0.05 seconds, when the relative tolerance is set to 10^{-4} and the absolute tolerance to 10^{-6}. Thus, the speed increase due to artificial neural networks (around 0.005 s per evaluation) would not compensate for the initial time needed to train them and the general loss of accuracy. The complete optimization for a two-step process with five variables took with 20 different starting points around 200 s for a parallel computation on four cores. In 14 of these optimizations, the constraints could be fulfilled and the same minimal diluent was found.

5.3.2. Chromatography

Model parameters

The parameters regressed from all linear gradient experiments with the HIC resin Cellufine Phenyl are summarized in Table 4 together with the results taken from previous work for the other two resins [8]. There it was shown that proteins can be given an ID and tracked through different experiments by knowing, which proteins are in each fraction and what their hydrodynamic radius is. In the case of Cellufine Phenyl, two prefractionations were performed with an anion exchange and a cation exchange resin. Many fractions were taken during the prefractionations, so that all impurities with a high abundancy could be characterised by their hydrophobicity.

Determining hydrophobic interaction parameters for fractions of both prefractionations allowed the matching of protein ID's from the different prefractionations to each other. Since the hydrodynamic radius of proteins, which were known to be identical, varied in the different experiments on Cellufine Phenyl, the peak volume as well as the elution

behaviour were used in addition for this protein matching. Nonetheless, the varying hydrodynamic radii made the ID matching less conclusive. Therefore, the worst case scenario, which means the most challenging separation, was considered: if a protein showed near identical behaviour on HIC even though the hydrodynamic radius was different, it was assumed to be the same protein.

Table 4: Isotherm parameters regressed from retention volume curves determined in RoboColumns with their standard deviation as taken from [8] for POROS 50 HS and Capto MMC or determined in this study for Cellufine Phenyl

Resin	Protein ID		rh [nm]	Keq or Kcomb [-]	v [-]	Ks [L/mol]
	AEX	CEX				
POROS 50 HS	1		2.4	12.6 ± 0.54	2.9 ± 0.5	-
POROS 50 HS	2	1	4.2	34.6 ± 1.7	9.8 ± 1.3	-
POROS 50 HS	3		2.7	2.2 ± 0.2	7.4 ± 0.7	-
POROS 50 HS	4	2	2.2	177.1 ± 16.1	5.4 ± 1.1	-
POROS 50 HS	6	4	2.2	0.9 ± 0.8	7.0 ± 0.3	-
POROS 50 HS	7	3	4.2	2.0 ± 0.2	2.5 ± 0.2	-
POROS 50 HS	8		2.4	0.2 ± 0.1	16.9 ± 6.4	-
Capto MMC	2	1	4.2	51.5 ± 2.1	3.6 ± 0.4	-
Capto MMC	4	2	2.8	16.6 ± 5.8	4.7 ± 1.6	-
Cellufine Phenyl	2	1	3.5	13.9 ± 6.4	-	4.7 ± 2.0
Cellufine Phenyl	4	2	2.2	6.4 ± 3.2	-	3.3 ± 1.0
Cellufine Phenyl	6	4	2.2	11.3 ± 3.9	-	6.4 ± 6.2
Cellufine Phenyl	7	3	3.5	17.0 ± 2.4	-	3.8 ± 0.5

MW: molecular weight; Keq or Kcomb: equilibrium constant; v: stoichiometric coefficient; Ks: Salting out constant;

Even so, it was difficult to assess if any protein of the AEX prefractionation is equivalent to the protein with ID 2 from the CEX prefractionation (ID2 CEX). It was assigned to be the same protein as ID4 AEX but it might also be equivalent to ID3 AEX. To eliminate any ambiguity in future studies, it would be recommended to perform all parameter determination studies with fractions of both prefractionations. Another option would be to analyse all fractions of the prefractionations by MS.
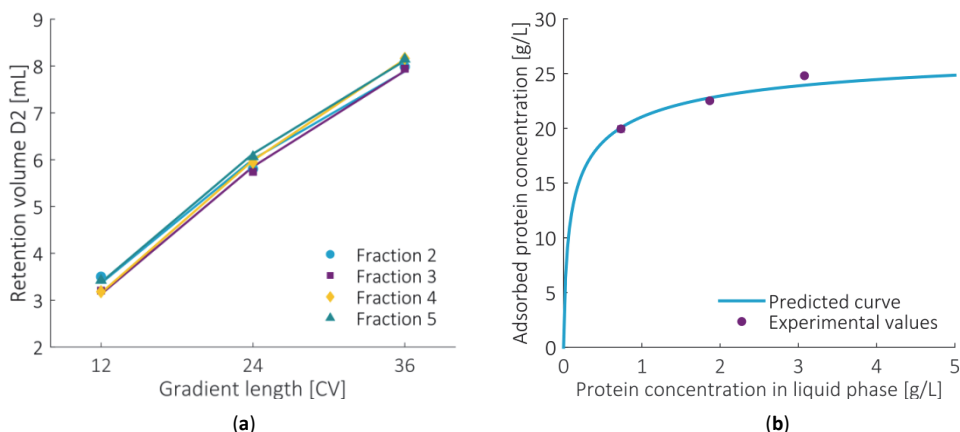
Figure 7: Results of the linear gradient RoboColumn experiments (a) and the batch uptake experiments (b) for IgG1 on the hydrophobic interaction resin

How the model parameters for the hydrophobic interaction resin were determined is shown in Figure 7 taking the product as example. The product IgG1 was assigned ID 2 during the anion exchange prefractionation (ID2 AEX) and ID 1 during the cation exchange prefractionation (ID1 CEX). In Figure 7 a), experimental retention volumes for IgG1 (ID2 AEX & ID1 CEX) at different gradient lengths are shown with markers; the curves resulted from the parameter fitting using Equation 26. Fraction 2 and 3 were taken during the AEX prefractionation, while fraction 4 and 5 were taken during the CEX prefractionation. In all other fractions, the concentrations of IgG1 were too small to be analysed. The retention volumes found for IgG1 in the different fractions were quite similar to each other, showing that the prefractionation method does not change the hydrophobicity of the protein.

The maximal capacity of the resin for IgG1 was determined with batch uptake experiments as shown in Figure 7 b. It was found to be 31.8 ± 4.7 g/L. This capacity is in the range reported for other types of proteins on the same resin [31]. The hydrophobic stoichiometric coefficient was regressed to be 2.8 ± 0.9. The particle size average (85 µm) was taken from the technical data sheet supplied by the manufacturer [31]. The pore size was estimated to be 45 nm based on a published pore size accessibility curve [27].

pH dependence of the stoichiometric ion exchange coefficient Hydrophobic interactions are almost not influenced by pH changes. However, electrostatic interactions are highly depending on pH. The variance of the stoichiometric ion

exchange coefficient, which is in this case identical to the effective binding charge, with pH was assumed to follow this relationship [32]:

$$\nu_i = g_{1,i} + g_{2,i} \ln pH \tag{28}$$

However, this trend is only valid at pH values that are not too close to the pKa of the ligand [24]. Since the pKa of Capto MMC is 3.3 [33] and the pKa of the functional group of POROS 50 HS is 1.2, this is given in the investigated pH range. Additionally, the isoelectric points (pI) for the proteins were used assuming that net charge and binding charge are identical at that point. The pI's for the impurities were estimated with ExPASy, while the pI for IgG1 was determined experimentally. This partly explains the much smaller standard deviation found for the fitting parameters of the monoclonal antibody as shown in Table 5.

Table 5: pH dependence of the stoichiometric coefficient for ion exchange

Protein ID AEX	pI	g_1	g_2
1	7.1 [b]	12.4 [c]	-6.3 [c]
2	8.6 [a]	32.6 ± 0.2	-15.1 ± 0.11
3	5.6 [b]	58.3 [c]	-33.8 [c]
4	8.7 [b]	17.5 ± 8.6	-7.6 ± 4.6
6	7.6 [b]	26.9 [c]	-13.2 [c]
7	4.7 [b]	89.0 [c]	-57.5 [c]
8	7.5 [b]	66.4 [c]	-32.9 [c]

a: Experimentally determined with capillary isoelectric focusing; b: Estimated with ExPASy; c: Not enough data points available to calculate the standard deviation

Generally protein charge does not follow a strict relationship as given in Equation 28, as can be seen for instance in published protein net charge data [34]. Therefore, Equation 28 and the fitted parameters shown in Table 5 should be seen as estimates. The influence of the stoichiometric coefficient on the equilibrium constant was not taken into account.

Modelling & Validation

Validation of the mechanistic chromatography model with experimental data was shown previously for POROS 50 HS and Capto MMC [8]. Therefore, validation experiments were only performed with the hydrophobic interaction resin, Cellufine Phenyl. Unfortunately, IgG1 (ID1 CEX) did not show the expected behaviour in experiments on the lab scale column packed with this resin. It did not elute with ammonium sulphate as an eluent even though the elution was predicted by a simulation, which is depicted in Figure 8 a. A potential reason for this might be varying ligand density caused by a different resin lot used in the lab scale columns than in the
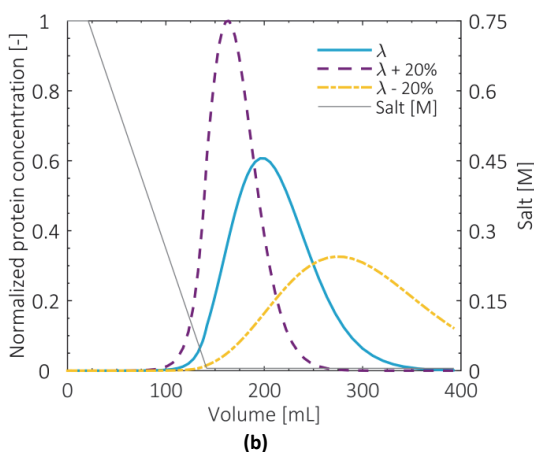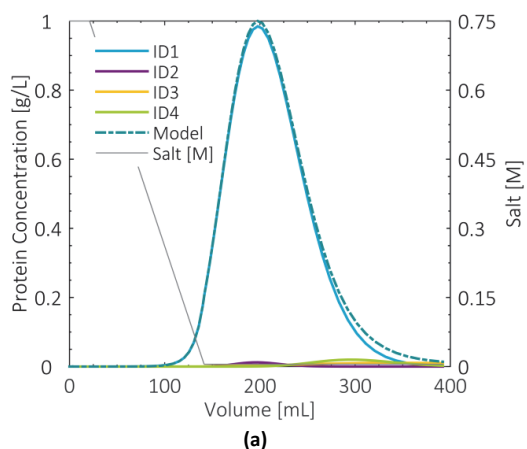

(a)

(b)

Figure 8: Modelling of a chromatographic separation in a column filled with the hydrophobic interaction resin Cellufine Phenyl
a: The behaviour of all proteins of interest was simulated. The ID's are from the cation exchange prefractionation; b: The behaviour of IgG1 was simulated at varying ligand densities.

RoboColumns. This difference in ligand density might be up to 20 % [35], which could explain this observation in part. As investigated by Deitcher et al.[36], a change in the ligand density of 7.5 % could already lead up to a change in the retention factor of 50 - 100 %. Therefore, simulations were performed at varying ligand densities, which is shown for IgG1 in Figure 8 b. As can be seen, even a 20 % difference in ligand density would lead to the elution of IgG1 with the salt buffer at the end of the gradient.

In our experimental approach, the ligand density was lumped together with another parameter. Since it appears to be an important parameter, however, this would not be recommended for future work. An experimental determination of the ligand density for each used resin batch is highly recommendable [37].

Generally, the purification capability of this resin is quite poor for IgG1, since IgG1 as well as critical impurities elute in the very end or even after the ammonium sulphate gradient. To avoid this problem, a less hydrophobic resin such as for instance one with a butyl group as functional group should be investigated instead. Another option to improve this step would be the use of a different salt with a smaller salting-out capacity such as sodium chloride. Nevertheless, Cellufine Phenyl was used during the process optimisation later; it can still show how the approach works.

Artificial neural networks

Since more variables were included compared with a previous study [7], the number of hidden layers, the amount of neurons in them and the needed starting points were reevaluated. It was found that two hidden layers increased the predictive quality of the ANNs considerably. The amount of neurons were varied from 10 to 20 in each layer during training; the networks with the best R^2 were used further. For the cation exchange and hydrophobic interaction resins, 1000 sample points were sufficient, while for the mixed mode resin the sample points had to be increased to 2000 to obtain ANNs with an R^2 above 0.8 for yield.

5.3.3. Optimization of process sequences

Finally, an overall optimization of all process sequences was performed. The scheme to generate process sequences, which was previously described in Equation 2, employs y variables that tell which unit is in a sequence and at which position. Having the duration of the UF/DF process as one of the x variables, greatly simplifies this scheme. With that,

the filtration units can be included as fixed units before each chromatography unit without having y variables attached to it, because the optimizer can simply change the duration of the UF/DF to zero if a filtration unit was not needed in that position. Thus, only the chromatographic units needed to be taken into account for generating all process alternatives. The amount of process sequence variants was therefore reduced from 30 to 9 while still taking all possibilities into account:

max $\quad f(y_{m,s})$ $\hspace{6cm}$ (29a)

s.t. $\quad \sum_m y_{m,s} \leq 1$
$\quad\quad \sum_s y_{m,s} \leq 1$ $\hspace{5cm}$ (29b)
$\quad\quad 1 - \sum_m y_{m,2} + \sum_m y_{m,1} \geq 1$
$\quad\quad y_{m,s} \epsilon \{0,1\}; \; m \, \epsilon \, \{1,2,3\}; \; s \, \epsilon \, \{1,2\}$

The optimization of all resulting process sequences took about 9.5 h with the local optimization taking around 80 % of the total time.

Table 6: Best results for each possible process sequence fulfilling the constraint of 99.9 % purity

Sequence	CEX	HIC	MMC	CEX - HIC	CEX - MMC	HIC - CEX	HIC - MMC	MMC - CEX	MMC -HIC
Filtration steps	**1**	-	1	2	2	2	2	2	2
Solvent use [mL]	**63.6**	-	106.9	297.2	133.2	259.3	257.7	196.0	260.3
Yield [-]	**96.8**	-	95.7	94.7	95.5	84.7	89.8	95.8	75.1

The best process option is highlighted in bold. UF/DF units were added by the optimizer before each chromatography unit in every shown process sequence; CEX: cation exchange chromatography; HIC: hydrophobic interaction chromatography; MMC: mixed-mode chromatography

Table 6 summarizes the best results for each process sequence; the nonlinear constraint of at least 99.9% purity was fulfilled for all shown options. The solvent use includes the solvent used in filtration and chromatography units alike. As can be seen, all sequences including the hydrophobic interaction resin show a much higher solvent use, which is due to the very late elution of the product. Thus, the resulting peaks are very broad and the elution is more time and solvent consuming. Moreover, this complicates the separation of product and impurities resulting in a trade-off between solvent use and yield. It was the only resin that would not be expected to purify the solution when applied as single chromatography column in the process sequence.

The best process option found, which consists of a UF/DF step and a subsequent cation exchange column, is shown in Figure 9. During the first step, the bigger molecules such as the product (ID2 AEX) and the biggest impurity (ID7 AEX) are being concentrated.

Smaller molecules, which are able to pass the membrane such as the salt and the smallest impurity (ID4 AEX), are being diluted. Additionally, this step adjusts the pH for the following chromatographic step. The cation exchange chromatography is able to separate the product from the impurities reaching the wanted purity while still having a
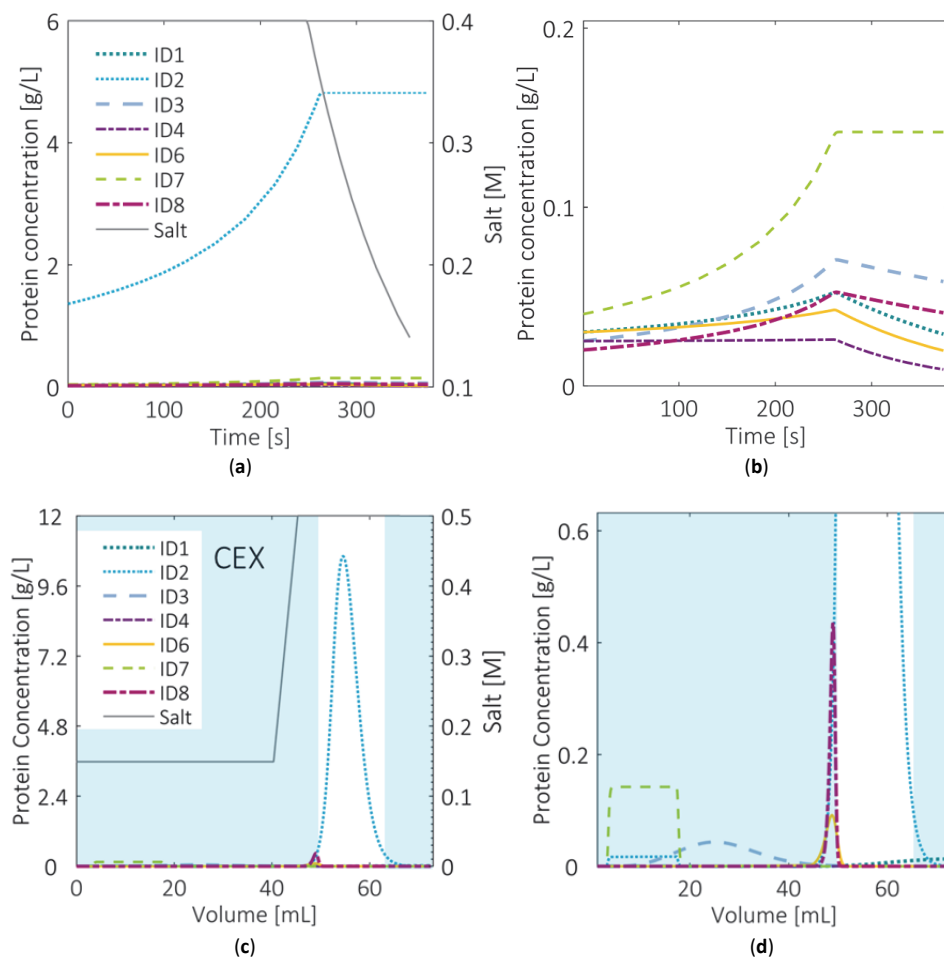

Figure 9: Best process option
a and b: First step is a UF/DF unit to adjust salt level and pH shown in full (a) and as zoom-in (b). 50 mL of clarified cell harvest was used. The TMP was set to 123 kPa.
c and d: Second and final step is a cation exchange column at pH 5.6 with the full chromatogram (c) and the zoom-in (d). The white area is the product pool.
The ID's are the ones according to the anion exchange prefractionation.

generally high yield.

To test the robustness of this process, a simulation was performed with four times spiked impurity levels. Under these conditions, a purity of only 99.6 % could be reached, which is below the defined constraint of 99.9 %. This could be counteracted by moving the product pool cut points accordingly leading to a great loss of yield. Another option would be to add more processing units such as suggested in the process sequence CEX-MMC. This would lead to a more robust process that could easily remove higher concentrations of impurities.

Even though some of the influences of pH were already included in this study, it would be very interesting to see them implemented in more detail. Chromatography units could for instance use pH or dual gradients (a combination of salt and pH) [38] as eluents, which could definitely change the result of the optimization.

5.4.   Conclusion

This paper presented an improved approach for the development and optimization of process sequences to purify a monoclonal antibody from clarified cell harvest. The main improvement is the addition of ultra/diafiltration units. To add new unit operations into the optimization approach, the following steps needed to be carried out: First, mechanistic models describing the considered unit operations were developed. Next, the needed model input parameters were determined. After that, optimizations of only the respective unit were performed to decide, which variables need to be included in further optimizations. For the ultra/diafiltration unit, it was found that only two of the investigated variables are crucial: The duration of the total filtration step and the duration of the ultrafiltration step.

Then, the simulation time was evaluated to see, if it is necessary to train fast artificial neural networks, which can be used instead of the more detailed mechanistic models during optimization. Since the simulation time of the UF/DF only takes in between 0.01 and 0.05 seconds, this was deemed unnecessary. For unit operation models that take a longer time to simulate such as the chromatography units, however, this step needed to be performed. Finally, the unit operations were included into the process sequences for an overall optimization.

By adding new unit operations and objectives, this paper showed the flexibility of the optimization approach. The approach could easily be extended to include more unit operations. Also the objectives and constraints can be changed as long as they can be simulated by the used mechanistic models. Additionally, the number of variables used as inputs for ANNs was doubled, which showed that more complex problems can be tackled with only few adjustments. By looking at other recent publications, a further surge of new applications including ANNs or other surrogate models for chromatography is expected due to their ease of use and great applicability.

Furthermore, it should be kept in mind that only high molecular weight contaminants were considered as impurities in this study. The removal of other impurities such as viruses, DNA or endotoxins was not yet investigated with this method. However, this could be a very interesting addition in the future making the results more realistic.

In conclusion, the presented approach can greatly influence the way purification processes are being developed. It is especially useful in early process development stages when little is known about the sample material and availability is limited.

Acknowledgment

References

1. Gronemeyer P, Ditz R, Strube J. Trends in Upstream and Downstream Process Development for Antibody Manufacturing. *Bioengineering.* 2014;1(4):188-212.

2. Meyer K, Huusom JK, Abildskov J. High-order approximation of chromatographic models using a nodal discontinuous Galerkin approach. *Comput Chem Eng.* 2018;109(Supplement C):68-76.

3. Wang G, Hahn T, Hubbuch J. Water on hydrophobic surfaces: Mechanistic modeling of hydrophobic interaction chromatography. *J Chromatogr A.* 2016.

4. Sellberg A, Ojala F, Nilsson B. Model-Based Comparison of Antibody Dimerization in Continuous and Batch-Wise Downstream Processing. *Antibodies.* 2015;4(3):157-169.

5. Nfor BK, Ahamed T, van Dedem GWK, et al. Model-based rational

methodology for protein purification process synthesis. *Chem Eng Sci.* 2013;89(0):185-195.

6. Huuk TC, Hahn T, Osberghaus A, Hubbuch J. Model-based integrated optimization and evaluation of a multi-step ion exchange chromatography. *Sep Purif Technol.* 2014;136(0):207-222.

7. Pirrung SM, van der Wielen LAM, van Beckhoven R, van de Sandt E, Eppink MHM, Ottens M. Optimization of biopharmaceutical downstream processes supported by mechanistic models and artificial neural networks. *Biotechnol Prog.* 2017;33(3):696-707.

8. Pirrung SM, Parruca da Cruz D, Hanke AT, et al. Chromatographic parameter determination for complex biological feedstocks. *Biotechnol Prog.* 2018.

9. Foley G. *Membrane Filtration: A Problem Solving Approach with MATLAB®.* Cambridge, UK: Cambridge University Press; 2013.

10. van Reis R, Goodrich EM, Yson CL, Frautschy LN, Whiteley R, Zydney AL. Constant Cwall ultrafiltration process control. *Journal of Membrane Science.* 1997;130(1):123-140.

11. Binabaji E. *Ultrafiltration of highly concentrated monoclonal antibody solutions* [Doctoral Dissertation]. Ann Arbor, The Pennsylvania State University; 2015.

12. Baker RW. Ultrafiltration. *Membrane Technology and Applications*. Chichester, UK: John Wiley & Sons, Ltd; 2004:237-274.

13. Zydney AL. Stagnant film model for concentration polarization in

membrane systems. *J Membr Sci.* 1997;130(1-2):275-281.

14. Da Costa AR, Fane AG, Wiley DE. Spacer characterization and pressure drop modelling in spacer-filled channels for ultrafiltration. *J Membr Sci.* 1994;87(1-2):79-98.

15. Young M, Carroad P, Bell R. Estimation of diffusion coefficients of proteins. *Biotechnology and Bioengineering.* 1980;22(5):947-955.

16. Lutz H, Arias J, Zou Y. High concentration biotherapeutic formulation and ultrafiltration: Part 1 pressure limits. *Biotechnol Prog.* 2017;33(1):113-124.

17. Lutz H. *Ultrafiltration for Bioprocessing.* Oxford, UK: Woodhead Publishing; 2015.

18. Foley G. Minimisation of process time in ultrafiltration and continuous diafiltration: the effect of incomplete macrosolute rejection. *J Membr Sci.* 1999;163(2):349-355.

19. Paulen R, Foley G, Fikar M, Kovacs Z, Czermak P. Minimizing the process time for ultrafiltration/diafiltration under gel polarization conditions. *J Membr Sci.* 2011;380(1-2):148-154.

20. Fikar M, Kovacs Z, Czermak P. Dynamic optimization of batch diafiltration processes. *J Membr Sci.* 2010;355(1-2):168-174.

21. Paulen R, Fikar M, Kovacs Z, Czermak P. Process optimization of diafiltration with time-dependent water adding for albumin production. *Chem Eng Process.* 2011;50(8):815-821.

5

22. Fikar M. Modelling, control, and optimisation of membrane processes. Paper presented at: Control Conference (ICCC), 2014 15th International Carpathian; 28-30 May 2014, 2014.

23. Guiochon G, Felinger A, Shirazi DG, Katti AM. *Fundamentals of Preparative and Nonlinear Chromatography.* Elsevier Inc.; 2006.

24. Nfor BK, Noverraz M, Chilamkurthi S, Verhaert PD, van der Wielen LA, Ottens M. High-throughput isotherm determination and thermodynamic modeling of protein adsorption on mixed mode adsorbents. *J Chromatogr A.* 2010;1217(44):6829-6850.

25. Mollerup JM, Hansen TB, Kidal S, Staby A. Quality by design--thermodynamic modelling of chromatographic separation of proteins. *J Chromatogr A.* 2008;1177(2):200-206.

26. Forrester A, Sobester A, Keane A. *Engineering design via surrogate modelling: a practical guide.* Chichester, UK: John Wiley & Sons; 2008.

27. Hanke AT, Tsintavi E, Ramirez Vazquez MD, et al. 3D-liquid chromatography as a complex mixture characterization tool for knowledge-based downstream process development. *Biotechnol Prog.* 2016;32(5):1283-1291.

28. Tsintavi E. Multidimensional Crude Feedstock Profiling. 2015.

29. Wang Y, Li X, Liu Y-H, et al. Simultaneous monitoring of oxidation, deamidation, isomerization, and glycosylation of monoclonal antibodies by liquid chromatography-mass spectrometry method with ultrafast tryptic digestion. Paper presented at: mAbs2016.

30. Paulen R, Fikar M, Foley G, Kovacs Z, Czermak P. Optimal feeding strategy of diafiltration buffer in batch membrane processes. *J Membr Sci.* 2012;411:160-172.

31. Corporation J. Hydrophobic Interaction Chromatography Media Cellufine® Butyl Cellufine® Phenyl. http://www.jnc-corp.co.jp/fine/en/cellufine/guide/pdf/hydrophobic/TD_HIC_DF013015_V3_1_EN_20140711.pdf. Accessed 19.12.2017.

32. Mollerup JM. A review of the thermodynamics of protein association to ligands, protein adsorption, and adsorption isotherms. *Chem Eng Technol.* 2008;31(6):864-874.

33. Pinto IF, Aires-Barros MR, Azevedo AM. Multimodal chromatography: debottlenecking the downstream processing of monoclonal antibodies. *Pharm Bioprocess.* 2015;3(3):263-279.

34. Lehermayr C, Mahler HC, Mader K, Fischer S. Assessment of net charge and protein-protein interactions of different monoclonal antibodies. *J Pharm Sci.* 2011;100(7):2551-2562.

35. Susanto A, Knieps-Grünhagen E, von Lieres E, Hubbuch J. High Throughput Screening for the Design and Optimization of Chromatographic Processes: Assessment of Model Parameter Determination from High Throughput Compatible Data. *Chem Eng Technol.* 2008;31(12):1846-1855.

36. Deitcher RW, Rome JE, Gildea PA, O'Connell JP, Fernandez EJ. A new thermodynamic model describes the effects of ligand density and type, salt concentration and protein species in hydrophobic interaction

chromatography. *J Chromatogr A.* 2010;1217(2):199-208.

37. Huuk TC, Briskot T, Hahn T, Hubbuch J. A versatile noninvasive method for adsorber quantification in batch and column chromatography based on the ionic capacity. *Biotechnol Prog.* 2016;32(3):666-677.

38. Lee YF, Schmidt M, Graalfs H, Hafner M, Frech C. Modeling of dual gradient elution in ion exchange and mixed-mode chromatography. *J Chromatogr A.* 2015;1417(Supplement C):64-72.

5

6

Conclusions & Outlook

All sorts of things can happen when you're open to new ideas and playing around with things.

Stephanie Kwolek

Contents

6.   Conclusions & Outlook

The development of biopurification processes is an area that saw major changes in recent years. Especially the rise of high-throughput experimental techniques and mechanistic modelling have influenced the playing field. By now the interest has shifted towards the best applications of these techniques.

This thesis presented an overall approach combining these techniques: High-throughput experimental techniques were used to obtain input parameters for more detailed mechanistic models, which were then able to simulate different purification unit operations. These were connected in sequences that could be optimized towards specified performance metrics such as yield or purity. Since computational speed was limiting, ANNs were trained to substitute slower mechanistic models when needed and where less information was still sufficient such as for instance during the global optimization. The final local optimization was than performed on starting points found during the global optimization with the mechanistic models.

One of the main conclusions of this thesis is that ANNs can well be used to predict the behaviour of proteins in chromatography columns. Such ANNs will be a great asset for many different applications. Their use can already be seen in other recent publications, where they were for instance used to investigate root causes of product and impurity level deviations [1] and to estimate model input parameters [2].

Of course, there are also other surrogate models available such as Gaussian process regression models, which were also used in an optimization context with chromatography columns recently [3,4]. These are especially useful, if no mechanistic model is available but instead (fewer) experimental data points. Moreover, the predictability of these models can be improved by generating additional experimental data points, where the likelihood of improvement is biggest. This type of method could also be applied to experimental data sets, which are typically already available in industry circumventing the need for a detailed parameter determination as required for mechanistic models. However, mechanistic knowledge, and the process understanding that comes along with that, would not be created in such an approach.

Another important conclusion is that RoboColumns with a 200 µL bed volume are indeed able to determine trust-worthy model input parameters for the prediction of

larger columns. However, extra analytical steps like the size exclusion chromatography as employed in Chapter 4 and 5 need to be used. Additionally, if a liquid handling station is to be used for parameter determination, parameters are more accurately determined with isocratic elution as was performed in Chapter 4, which requires more experiments than linear gradient elution. Linear gradient experiments are easier implemented, when attaching the RoboColumns to a conventional liquid chromatography system (Chapter 5). New methods for generating gradients on liquid handling stations exist [5] and could be implemented in this approach. Another option could be the use and adaption of a recently published new method developed on MiniColumns by Keller and coworkers [6,7].

Platform processes for monoclonal antibodies typically target the more constant region, called Fc region, which is the same for all antibodies in a class. This is most typically done with the very selective Protein A resin. With new types of antibodies and other types of pharmaceutical proteins being developed, new process options need to be found. This area is exactly where a novel process development approach such as the one developed in this work can be of great use.

Furthermore, there is a current trend towards more and more personalized medicine. This type of medicine requires flexible production facilities that can easily be optimized for production of a new product. Thus, small and flexible multi-product facilities are being favoured. These often include continuous processing units [8-10] due to their reduced size. Mathematical descriptions are already available for continuous units such as simulated moving bed [11,12] and crystallization [13] or semi-continuous units such as multi-column counter-current solvent gradient purification [14]. These models could be added, which would allow to use this approach e.g. to design new multi-product facilities or adjust an existing one for the production of a new product.

What could also be very interesting as well as challenging is the inclusion of the upstream part into the optimization approach. With that, the complete production process could be simulated and optimized simultaneously. Looking at the upstream and downstream process at the same time might change the favoured processing units: An upstream processing step up with a high yield could generate impurities, which are very difficult to remove in the downstream process, leading to an overall lower yield

compared with another upstream option with a lower yield and easily removable impurities.

In conclusion, an extensive toolbox for the development and optimization of connected biopurification sequences has been presented. This approach will hopefully inspire future works improving it further that will lead to even better downstream purification processes for biopharmaceuticals.

References

1. Wang G, Briskot T, Hahn T, Baumann P, Hubbuch J. Root cause investigation of deviations in protein chromatography based on mechanistic models and artificial neural networks. *J Chromatogr A.* 2017;1515(Supplement C):146-153.

2. Wang G, Briskot T, Hahn T, Baumann P, Hubbuch J. Estimation of adsorption isotherm and mass transfer parameters in protein chromatography using artificial neural networks. *J Chromatogr A.* 2017;1487:211-217.

3. Freier L, von Lieres E. Multi-objective global optimization (MOGO): Algorithm and case study in gradient elution chromatography. *Biotechnol J.* 2017;12(7):1600613-n/a.

4. Freier L, von Lieres E. Robust Multi-Objective Global Optimization of Stochastic Processes With a Case Study in Gradient Elution Chromatography. *Biotechnol J.* 2017:1700257-n/a.

5. Kiesewetter A, Menstell P, Peeck LH, Stein A. Development of pseudo-linear gradient elution for high-throughput resin selectivity screening in RoboColumn((R)) Format. *Biotechnol Prog.* 2016;32(6):1503-1519.

6. Keller WR, Evans ST, Ferreira G, Robbins D, Cramer SM. Understanding operational system differences for transfer of miniaturized chromatography column data using simulations. *J Chromatogr A.* 2017;1515:154-163.

7. Keller WR, Evans ST, Ferreira G, Robbins D, Cramer SM. Use of MiniColumns for linear isotherm parameter estimation and prediction of benchtop column performance. *J Chromatogr A.* 2015;1418(Supplement C):94-102.

8. Jungbauer A. Continuous downstream processing of biopharmaceuticals. *Trends Biotechnol.* 2013;31(8):479-492.

9. Rathore AS, Agarwal H, Sharma AK, Pathak M, Muthukumar S. Continuous processing for production of biopharmaceuticals. *Prep Biochem Biotechnol.* 2015;45(8):836-849.

10. Jungbauer A, Hammerschmidt N. Integrated Continuous Manufacturing of Biopharmaceuticals. In: Kleinebudde P, Khinast J, Rantanen J, eds. *Continuous Manufacturing of Pharmaceuticals*: John Wiley & Sons Ltd.; 2017:247-281.

11. Freydell EJ, Bulsink Y, van Hateren S, van der Wielen L, Eppink M, Ottens M. Size-exclusion simulated moving bed chromatographic protein refolding. *Chem Eng Sci.* 2010;65(16):4701-4713.

6

12. Santos da Silva FV, Seidel-Morgenstern A. Evaluation of center-cut separations applying simulated moving bed chromatography with 8 zones. *J Chromatogr A.* 2016;1456:123-136.

13. Kwon JSI, Nayhouse M, Christofides PD, Orkoulas G. Modeling and control of crystal shape in continuous protein crystallization. *Chem Eng Sci.* 2014;107:47-57.

14. Sellberg A, Andersson N, Holmqvist A, Nilsson B. Development and Optimization of a Single Column Analog Model for a Multi-Column Counter-Current Solvent Gradient Purification Process. In: Espuña A, Graells M, Puigjaner L, eds. *Computer Aided Chemical Engineering.* Vol 40: Elsevier; 2017:187-192.

A
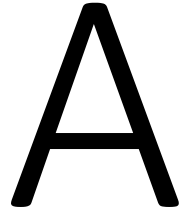
Acknowledgments, List of publications & Curriculum Vitae

Contents

A.1. Acknowledgements

Who knew four years could fly by like that. I would like to take a moment and thank everyone that was part of this work and made time fly even faster.

First of all, a big thanks to Marcel. Without you and your belief in my abilities, this thesis would not have been possible. I really appreciated your hands off guidance throughout my PhD that gave me creative freedom and room to grow. Thanks for all the amazing opportunities you gave me during my PhD!

Of course, I would also like to thank Luuk for our meetings together, your input throughout my thesis and your challenging thoughts.

I'm grateful to Alex for showing me everything about being a PhD student in the beginning. Without you, I might have quit one memorable day after 6 months of PhD and I am really glad I kept going. And thanks for still being a good friend even across borders!

Another big thanks goes to my master students: Lutz, Antoon, Carme and Carmen. I hope you learned a lot working with me, I certainly learned a lot working with you! Here, I also want to acknowledge Renske, it was fun helping you out during your internship.

Thanks to Diogo for working in this project during his individual design project. You were a great help and you are a good friend!

Next, I would like to thank all other people involved in my project: Michel, Xiaonan, Ruud, Emile, Han, Hoon, Jürgen and Marieke. Thanks for all those nice meetings together and the constructive input all of you gave me during the last four years!

Special thanks are due to my two paranymphs:
Thanks to Debbi, for giving me German support against all the Portuguese and Spanish PhDs and just generally for being there for me! It was a pleasure to try all your home brews!
And thanks to Marcelo, it was really fun working with you from the beginning of our PhDs until the end. We always went through the same stages in our PhDs at pretty much the same time, which meant we always had someone that understands the problems the other is having. Keep on singing!
To all the other Portuguese: Man, did I earn that honorary Portuguese citizenship..

A

Many thanks to all members of the BPE group! That includes all the permanent staff members Kawieta, Maria, Adrie, Stef, Max and Song and all the PhD students and master students I met during this time. I really appreciated the time we spent together at our countless lunches and coffee breaks. Especially our group bonding trips to Lille, Nice, Dublin, Barcelona and - of course - the love boat will always be great memories.

I'm honestly not sure what I will do without our talks and crazy discussions…
Alexenstein: Beer, networking and life – Arjan: The art of baking, but this was more about me trying the delicious cakes you made – Bianca: Everything cheerful, I still cannot believe how optimistic you are. I hope you'll always be that way! – Carlos: Grapes, grapes, grapes (sorry, this never gets old), dancing and politics – Chema: The concept of fruit break and the other crazy things you constantly come up with ;) – David: Stuff and things – Debbi: Beer yoga, poke and the power of holding hands – Diogenstark: Portuguese inventions, Portuguese Wikipedia and German dialects – Floor: Chilly and crazy boarding school stories – Joana: Alpacas, making the world a better place and just about everything – Lisette: Bob Ross, the Veluwe and Disney – Marcelo: Your favorite TV shows Master Chef and Shark Tank, Benfica & of course Portugal – Monica: Mexican food, the super bowl and happiness – Rafael & Renato: Football and the history of the world – Rita: Joaninha, weddings and PhD life – Sara: Catalonia and being an expat in The Netherlands – Shima: Iranian culture and cousine, a pity we never made it to that Iranian restaurant in Den Haag – Song: Technology and travelling, especially to my favourite city Hong Kong – Susana: Feminism and the best soap opera ever, Game of Thrones. I love how opinionated you are! – Victor: Modelling, drinking and 'The Subtle Art of Not Giving a F*ck'.

Additionally, I would like to thank the other members of BT – Hugo, Simon, Mihir, Robin, Danny, Leonor, and so many others – for our nice conversations especially during the times of keldertje.

Thanks also to my other Delft friends during this time! Here I want to thank especially Sara, MJ and Jil. Thanks for always getting a beer with me, when I needed it!

Vielen Dank auch an meine liebe Familie. Ohne eure Liebe und euren Glauben an mich und meine Fähigkeiten während der letzten 30 Jahre hätte ich es nie so weit gebracht!

Sist men inte minst, tack vare min kärlek Pontus. Jag är så tacksam för att du gav mig en känsla av hem, när du flyttade hit för tre år sedan – du gör mig glad varje dag och stöder mig oändligt!

A.2. List of publications

A.2.1. Book chapter

Pirrung SM, Ottens M. *High Throughput Process Development*. In: Arne Staby ASR, Satinder Ahuja, ed. Preparative Chromatography for Separation of Proteins. Hoboken, New Jersey: John Wiley & Sons, Inc.; 2017:269-292.

A.2.2. Journal Publications

Pirrung SM, Parruca da Cruz D, Hanke AT, Berends C, van Beckhoven RFWC, Eppink MHM, Ottens M, *Chromatographic parameter determination for complex biological feedstocks*. Biotechnol Prog. 2018.

Pirrung SM, van der Wielen LAM, van Beckhoven RFWC, van de Sandt EJAX, Eppink MHM, Ottens M, *Optimization of biopharmaceutical downstream processes supported by mechanistic models and artificial neural networks*. Biotechnol Prog, 2017. 33(3): p. 696-707.

A.2.3. Oral Presentations

Pirrung SM, van der Wielen LAM, van Beckhoven RFWC, Eppink MHM, Ottens M, *Towards Efficient Chromatographic Processes for Complex Biological Feedstocks*, 2017, HTPD 4th International Meeting, Toledo, Spain

Pirrung SM, Berends C, Pons Royo MDC, van der Wielen LAM, van Beckhoven RFWC, Eppink MHM, Ottens M, *Integrated optimization of purification processes for biopharmaceuticals*, 2017, 10th World Congress of Chemical Engineering, Barcelona, Spain

Pirrung SM, Pons Royo MDC, Parruca da Cruz DE, van der Wielen LAM, van Beckhoven RFWC, Eppink MHM, Ottens M, *Chromatographic process development for complex biological feedstocks,* 2017, 13th International PhD Seminar on Chromatographic Separation Science, Annweiler am Trifels, Germany

Pirrung SM, Parruca da Cruz DE, Hanke AT, van der Wielen LAM, van de Sandt EJAX, Eppink MHM, Ottens M, *Model-based optimization of a non-affinity chromatographic*

mAb purification process, 2016, 11th European Symposium on Biochemical Engineering Sciences, Dublin, Ireland

Pirrung SM, Hanke AT, van der Wielen LAM, van de Sandt EJAX, Eppink MHM, Ottens M, *Model-based process development for biopharmaceuticals*, 2016, 12th International PhD Seminar on Chromatographic Separation Science, Schleiden, Germany

Pirrung SM, Ottens M, *Hybrid HTPD – Combining models and experiments for rational process development* [Keynote], 2015, 3rd European Congress of Applied Biotechnology, Nice, France

Pirrung SM, *Affinity separations by process modeling/synthesis*, 2015, Dutch industrial separation consortium NL GUTS, Nijmegen, The Netherlands

Pirrung SM, Hanke AT, van der Wielen LAM, Verhaert PDEM, van de Sandt EJAX, Eppink MHM, Ottens M, *A new Paradigm in Bio Purification Process Development*, 2015, 11th International PhD Seminar on Chromatographic Separation Science, Sorpesee, Germany

A.3. Curriculum vitae

Silvia Pirrung was born on the 9th of May 1988 in Karlsruhe, Germany. After finishing her Abitur at Bismarck-Gymnasium Karlsruhe in 2007, she started studying Molecular Biotechnology at the Technical University of Munich, where she realized her passion for engineering.

Thus, the new master's program in Industrial Biotechnology, where she could focus on bioprocess engineering as well as bio separation engineering, was the perfect fit for her. In 2013, she received her master's degree which included an exchange semester on business at the Hong Kong University of Science and Technology. During her master thesis at the Technical University of Denmark in the group of John Woodley, she developed a great interest in process engineering, which convinced her to pursue a PhD degree in that field.

In 2014, she became a PhD candidate in the bioprocess engineering group at Delft University of Technology with Luuk van der Wielen and Marcel Ottens as her promotors. Her PhD focused on modelling and optimization of downstream processes. In her research, she applied various tools including mechanistic modelling and artificial neural networks.

A